

THE UNIVERSITY OF CALGARY

SOLITARY WAVES IN FLUID-FILLED ELASTIC TUBES

by

CLIFTON REED JOHNSTON

A DISSERTATION

**SUBMITTED TO THE FACULTY OF GRADUATE STUDIES
IN PARTIAL FULFILLMENT OF THE REQUIREMENTS FOR THE
DEGREE OF DOCTOR OF PHILOSOPHY**

**DEPARTMENT OF MECHANICAL AND MANUFACTURING
ENGINEERING**

CALGARY, ALBERTA

AUGUST, 2001

© CLIFTON REED JOHNSTON 2001



National Library
of Canada

Acquisitions and
Bibliographic Services

395 Wellington Street
Ottawa ON K1A 0N4
Canada

Bibliothèque nationale
du Canada

Acquisitions et
services bibliographiques

395, rue Wellington
Ottawa ON K1A 0N4
Canada

Your file Votre référence

Our file Notre référence

The author has granted a non-exclusive licence allowing the National Library of Canada to reproduce, loan, distribute or sell copies of this thesis in microform, paper or electronic formats.

The author retains ownership of the copyright in this thesis. Neither the thesis nor substantial extracts from it may be printed or otherwise reproduced without the author's permission.

L'auteur a accordé une licence non exclusive permettant à la Bibliothèque nationale du Canada de reproduire, prêter, distribuer ou vendre des copies de cette thèse sous la forme de microfiche/film, de reproduction sur papier ou sur format électronique.

L'auteur conserve la propriété du droit d'auteur qui protège cette thèse. Ni la thèse ni des extraits substantiels de celle-ci ne doivent être imprimés ou autrement reproduits sans son autorisation.

0-612-64866-4

Canada

Abstract

The propagation of solitary waves in fluid-filled elastic tubes was investigated by direct analysis of the governing field equations. The primary advantage of this approach over the widely used asymptotic techniques is that, for a specified wave speed, the solution of the ‘exact’ amplitude of the solitary waves only requires the roots of an algebraic equation. The shape of the wave can be found to any required degree of accuracy numerically. This approach can be applied beyond the long-wave approximation for any amplitude of wave.

The presented direct approach was used to consider a fluid-filled elastic thin-walled tube where axial displacements were neglected and the velocity of the fluid was averaged over the tube radius. It was shown that errors can become as large as 20% for displacements up to 25% of the tube radius when the reductive perturbation technique is used. The direct approach was also used to investigate a problem in plasma physics, specifically ion-acoustic waves, to illustrate a broader application of the proposed technique.

The kinematically exact shell equations for the tube, including both axial and radial displacements were considered and it was shown that, by casting the problem in a variational framework, it becomes possible to find explicit first integrals of the governing equations. The first integrals then allowed the speed, amplitude and shape of the resulting solitary wave to be determined ‘exactly’ using the proposed direct approach. The results showed that the wave amplitude calculated using the exact displacements were an order of magnitude greater than found when axial displacements were neglected. It was subsequently shown that the axial strain was of the

same order as the magnitude of the radial strain and that in the prestressed reference configuration their relationship was approximately linear.

Exploiting this approximate linear relationship, a linear function was found from the axial first integral, permitting the reduction of the governing equations to a problem of one equation in one dependent variable, while still retaining a contribution for the axial displacement. The amplitude predicted using this approximate approach was found to differ from the exact value by as little as 3%.

Finally, the tube wall pressure predicted from our inviscid, incompressible one-dimensional fluid model was compared to a two-dimensional flow, simulated using a modified discrete-vortex method. The tube geometries examined corresponded to the solitary wave profiles for four representative wave speeds. It was shown that the predicted pressures from the existing one-dimensional model compared well with the two-dimensional flow. Based upon this, it should be expected that solitary waves predicted using a two-dimensional fluid model will be in close agreement with the results presented in this dissertation.

Acknowledgements

I begin by thanking my supervisor Dr. Marcelo Epstein. He took on a supervisorless student with no project and became a mentor, collaborator and friend. It was never so much working for him as it was working with him, and that made all the difference. He is also too smart for his own good, which challenges you work even harder just to keep up. My education with Dr. Epstein has included mechanical engineering, but was not limited to it. For all his support, enthusiasm and encouragement, gratia!

I would also like to thank Dr. Ron Hugo for his initial suggestion and continued guidance on the development of the fluid modelling technique developed in this dissertation. Despite his many other responsibilities, he always made time to talk to me about all problems I was facing and provided clear suggestions to get me back on the right track.

I would be remiss if I did not tip my hat to Dr. Daryl Caswell and Dr. Rod Fauvel. They have been very strong contributors to my education, both as a researcher and as an individual. While I may have been here sooner had I not gotten mixed up with them, I would have been much poorer for it.

I owe a debt to both Dan Forre and Khee Tech Wong for answering my never ending questions. Long live Linux! Much thanks for all the administrative support provided to me in the department from Maria, Karen, Nareeza, Marion, Lois, and Rhonda. Too many times my bad planning became your emergency, yet I was never turned away. I would also like to thank Doug Phillips for the assistance in getting my fluid model run on the MACI Cluster. Without his help that part of my work would not have been possible.

As all good acknowledgements go, I must especially thank my parents, Bill and Carol Johnston. I have been blessed with unlimited support and encouragement over the years. There is no way I could have gotten where I am, professionally or personally, without my parents pushing and prodding and most of all reminding me that being smart does not get you out of mowing the lawn.

Finally, I would like to thank my ever supportive wife, Amy McEvoy. She has never once wavered from her dedication to seeing me achieve this goal, despite signing on after the decision had been made. I can never thank her enough for her support, but look forward to a lifetime trying.

Table of Contents

Approval Page	ii
Abstract	iii
Acknowledgements	v
Table of Contents	vii
List of Tables	ix
List of Figures	x
List of Symbols, Abbreviations, Nomenclature	xii
1 Introduction	1
1.1 What is a Wave?	1
1.1.1 Dispersion	2
1.1.2 Nonlinearity	4
1.2 Background	11
1.2.1 Solitary Waves	12
1.2.2 Waves in Fluid-Filled Elastic Tubes	15
1.2.3 Solitary Waves Meet Fluid-Filled Tubes	17
2 A Direct Approach for Solitary Waves in Fluid-Filled Elastic Tubes	20
2.1 Introduction	20
2.2 Mathematical Preliminaries	23
2.3 Analysis of the equations of motion	28
2.4 Sample calculations	33
2.5 Comparative results	38
2.6 Extension of the theory	40
2.7 Conclusions	43
3 Example of Direct Approach in Plasma Physics	44
3.1 Introduction	44
3.2 The Governing Equations and their Reduction	47
3.3 Solitary Wave Solution	50
3.4 Numerical Example	51
3.5 Discussion	54

3.6	Conclusions	56
4	Two Dimensional Considerations for Solitary Waves in Fluid-Filled Elastic Tubes	58
4.1	Introduction	58
4.2	Derivation of the equations of motion	60
4.3	Fluid-solid Interaction	65
4.4	Solitary Waves and Variational Formulation	67
4.5	Noether's Theorem, first integrals and numeric solvability	70
4.6	Numerical Example	76
4.7	Discussion	84
4.8	Conclusions	87
5	Approximation of Axial Displacement	90
5.1	Introduction	90
5.2	Derivation of First Integral	91
5.3	Approximation of u'	95
5.4	Example of Approximate Solution	96
5.5	Conclusions	103
6	Consideration of the Fluid Model	104
6.1	Introduction	104
6.2	Modified Discrete Axisymmetric-Vortex Model	106
6.3	Application of Modified Discrete-Vortex Model	115
6.3.1	Tube Geometry	115
6.3.2	Vortex Spacing & Tube Length	117
6.3.3	Bounding Vortices	121
6.4	Simulation Results	123
6.5	Conclusions	131
7	Conclusions and Recommendations	133
7.1	Conclusions Drawn from the Study	133
7.2	Recommendations for Future Work	135
	Bibliography	137

List of Tables

2.1	Comparison between 'exact' method and Demiray's approach	40
2.2	Comparison of wave amplitudes with additional slope-square terms	43
6.1	Comparison of velocities at two positions 0.006 and 0.012 below the tube wall for $c = 3.175$ tube geometry	126

List of Figures

1.1	Development of a parabolic pulse governed by Eq. (1.8) (from Bhatnagar, 1979)	6
1.2	Development of a parabolic pulse governed by Eq. (1.12) (from Bhatnagar, 1979)	8
1.3	Appearance of roots of $f(u)$ for solitary wave solution for Eq. (1.16)	10
2.1	General appearance of solitary wave	25
2.2	General appearance of F_c	26
2.3	RHS of Eq. (2.22) in numerical example	34
2.4	(a) Periodic behaviour of solution with $\bar{w}(0) = 0.0933321$, (b) Divergent behaviour of solution with $\bar{w}(0) = 0.0933322$	35
2.5	Comparison between the 'exact' and Demiray (1996) solution	38
2.6	Behaviour of F_c for limiting propagation speed	39
3.1	Evaluation of the RHS of Eq. (3.14) for a wave speed of $c = 1.25$	51
3.2	Evaluation of the RHS of Eq. (3.15) for a wave speed of $c = 1.25$	52
3.3	Solution of Eq. (3.14) for a wave speed of $c = 1.25$ showing (a) Periodic behaviour for $v_i(0) = 0.711603$ and (b) Divergent behaviour for $v_i(0) = 0.711604$	53
3.4	Comparison between the 'exact' solution (—) and the dressed solitary wave of Malfliet and Wieers (1996) (----) with $c = 1.25$ and $k = 0.30$	55
4.1	Reference and deformed configurations	61
4.2	Forces acting upon element of deformed tube in longitudinal direction	62
4.3	Hoop and longitudinal forces acting upon element of deformed tube .	63
4.4	General shape of the solitary wave	73
4.5	General appearance of Eq. (4.49)	75
4.6	Actual shape of Eq. (4.49) for $c = 3.175$	80
4.7	Comparison of solutions for initial conditions (a) $w_{max} = 0.4495390$ and (b) $w_{max} = 0.4495391$	81
4.8	Calculated shape of the solitary wave for $c = 3.175$	83
4.9	Domain of existence ($\rho = 1/8$) for simple model	86
4.10	\hat{w} and \hat{u}' in the prestressed reference configuration of for $c = 3.175$. .	88
5.1	Section of tube deformed by solitary wave	92
5.2	Plot of Eq. (5.12) (---) and the linear approximation (—) for $c = 6.05$	98

5.3	Plot of Eq. (5.12) (---) and the linear approximation (—) for $c = 7$	99
5.4	Solitary wave profiles for the approximation $\bar{u}' = K_c \bar{w}$ and the exact solution for $c = 6.05$ and $c = 7$	101
5.5	The Domain of Existence of the solitary wave solutions of Eq. (5.13)	102
6.1	Orientation of a typical vortex ring element	107
6.2	Stokes stream function for an axisymmetric vortex ring (Lamb, 1945)	108
6.3	Illustration of placement of ring vortices, bounding vortices and control points for a simple tube	110
6.4	Orientation of arbitrary tube segment	114
6.5	Tube geometries corresponding to the solitary wave solution for speeds $c = 3.175, 3.402, 3.629$ and 3.856	117
6.6	Near wall velocity at $x = 0$ for $\Delta_\kappa = 0.010, 0.004$ and 0.0025	119
6.7	Effect of bounding vortices on the calculated vortex strength near the outflow boundary using $M = 0, 2N$ and $4N$	122
6.8	Vortex strengths determined using single and double precision calculations for $c = 3.175$ tube geometry	123
6.9	Vortex strengths determined using discrete-vortex model for tube geometries corresponding to $c = 3.175, 3.402, 3.629$ and 3.856	124
6.10	Streamlines determined for tube geometries corresponding to $c = 3.175$ and 3.856	125
6.11	Velocity profiles at axial position $x = 0$ for tube geometries corresponding to $c = 3.175, 3.402, 3.629,$ and 3.856	127
6.12	Tube wall pressures predicted using Eq. (6.26) (—) and Eq. (6.27) (---)	130

List of Symbols, Abbreviations, Nomenclature

b	I-H-T material constant
c	constant wave speed
g	gravitational constant
h	tube wall thickness
I_1	first strain invariant
I_2	second strain invariant
k	wave number
K_c	ratio of axial to radial strain
ℓ_1	minimum distance to vortex ring
ℓ_2	maximum distance to vortex ring
L	Lagrangian density
L_o	characteristic length
L_t	length of tube in vortex model
m	thickness parameter
M	number of image vortex rings
n	fluctuation of ion density
n_1	Kirchhoff longitudinal-stress resultant
n_2	Kirchhoff hoop-stress resultant
n_i	ion density
N	number of vortex rings
p	total fluid pressure
p^*	incremental pressure
q	spatial coordinate in axial direction
R	initial radius of tube
S_1	total non-dimensional longitudinal stress
S_2	total non-dimensional hoop stress
t	time coordinate
T_o	characteristic time
u	axial displacement
u_T	total axial velocity induced by all vortex rings
U	axial displacement between two cylindrical references
U_{fs}	free stream velocity
v_f	fluid velocity
v_i	ion flow velocity
v_T	total radial velocity induced by all vortex rings
V	total velocity

w	radial displacement
w_κ	radial velocity induced by ring vortex
W	radial displacement between two cylindrical references
x	axial coordinate
x°	axial location of axisymmetric vortex ring
x_{fs}	axial position of free stream velocity
y	radial coordinate
y°	radial location of axisymmetric vortex ring
y_{fs}	radial position of free stream velocity
α	empirical material constant
β	I-H-T material constant
Δ_κ	vortex ring spacing
θ	angle of control point to horizontal
κ	vortex strength
λ	ratio of distances to vortex ring
λ_z	prestress in longitudinal direction
λ_θ	prestress in hoop direction
Λ_1	principal stretch in longitudinal direction
Λ_2	principal stretch in hoop direction
μ	shear modulus of tube material
ξ	travelling wave coordinate
ρ	tube material density
ρ_f	fluid density
σ_1	total longitudinal stress
σ_2	total hoop stress
Σ	strain energy density function
ϕ	slope of the deformed tube meridian
φ	electrostatic potential
Ψ	Stokes stream function for an axisymmetric vortex ring
ω	wave frequency

Subscripts

∞	conditions at infinity
max	maximum value

Chapter 1

Introduction

In this dissertation solitary waves propagating in fluid-filled elastic tubes have been examined. Solitary waves have been investigated in several physical contexts due to their characteristic of propagating with a constant speed and form. If asked to describe how solitary waves can exist, the standard answer tends to be that they exist through a balance of dispersion and nonlinearity. While mathematically and physically true, this answer provides little in tangible understanding. Therefore, for the first part of this dissertation, a brief introduction to the basic concepts used in this approach, with an emphasis on physical meaning, is provided. Having done that, a brief historical introduction to the problem considered here will also be examined.

1.1 What is a Wave?

A persons understating of waves is often influenced by their background. Someone working in acoustics likely envisions waves as periodic, while an aerodynamicist is more likely to envision a shock. Therefore, one should begin by assigning a definition to the term *wave*.

To that end, we will adopt the definition given by Whitham (1974), where a wave is defined as

any recognizable signal that is transferred from one part of the medium to another with a recognizable velocity of propagation.

The signal may take the form of a maximum or an abrupt change, so long as the position and speed may be determined at any time. This definition is very broad but is intended to encompass the wide range of physical entities called waves.

With this frame of reference, it is worthwhile for us to consider two other characteristics of waves, with implications to this work, and to examine their physical features. A more complete treatment can be found in Bhatnagar (1979), who provides an excellent introduction to topics particularly important to this dissertation and some of whose explanations and definitions are reproduced here.

1.1.1 Dispersion

The first point of interest is the effect of dispersion. The discussion of dispersion is begun through the consideration of a generic example. Let us consider a general, linear partial differential equation (PDE) for a function ϕ of two independent variables x and t , such that

$$L[\phi] = 0 \tag{1.1}$$

where L is a linear operator. In Eq. (1.1), we assume that the variables x and t do not appear explicitly and that the equation is homogeneous. Because this equation is linear its solution can be found through superposition. Assuming this, we can seek a harmonic wave type solution by substituting

$$\phi = a \exp\{i(kx - \omega t)\} \tag{1.2}$$

into Eq. (1.1). In Eq. (1.2), a is the amplitude, k is the wave number and ω is the wave frequency. In making this substitution, all the derivatives of x and t now

become

$$\frac{\partial}{\partial x} \rightarrow -ik \quad \text{and} \quad \frac{\partial}{\partial t} \rightarrow -i\omega$$

Having done this, the original differential equation reduces to the algebraic relation

$$D(\omega, k, A_i) = 0 \tag{1.3}$$

where A_i are any parameters appearing in Eq. (1.1).

Equation (1.3) is then defined as the linear dispersion relation and gives the wave frequency in terms of the wave number and any parameters. We can re-write Eq. (1.3) so that

$$\omega = \omega(k) \tag{1.4}$$

where we have assumed the dependence on the parameters A_i . This is the form of the dispersion relation most commonly considered. Now, if Eq. (1.4) determines a real value of ω for every value of $0 \leq k < \infty$ and $\frac{\partial^2 \omega}{\partial k^2} = \omega''(k) \neq 0$ the wave is said to be dispersive.

In order to provide some physical meaning to this theoretical definition of dispersion, let us consider the superposition of two harmonic waves that differ by a small amount in their frequencies and wave numbers, but are of the same amplitude. We can write this as

$$\begin{aligned} \phi_1(x, t) &= a \cos[kx - \omega t] \\ \phi_2(x, t) &= a \cos[(k + \delta k)x - (\omega + \delta \omega)t] \end{aligned} \tag{1.5}$$

where the superposition of these two waves produces

$$\phi = \phi_1 + \phi_2 = \left(2a \cos \left[\frac{1}{2}(x\delta k - t\delta \omega) \right] \right) \cos \left[\left(k + \frac{\delta k}{2} \right) x - \left(\omega + \frac{\delta \omega}{2} \right) t \right] \tag{1.6}$$

The resulting interference pattern produces a wave with the familiar appearance of repeating ‘beats’.

From Eq. (1.6), we see that the effective amplitude of the larger ‘beats’ is given by $2a \cos(\frac{1}{2}(x\delta k - t\delta\omega))$. From this we can determine that the larger ‘beats’ propagate at a velocity given by

$$\frac{dx}{dt} = \frac{\delta\omega}{\delta k} \quad (1.7)$$

which in the limit of $k \rightarrow 0$ becomes $\frac{\partial\omega}{\partial k} = \omega'(k)$ and is defined as the group velocity.

Therefore, from our definition of dispersion, if the condition $\omega''(k) \neq 0$ is true then the group velocity, $\omega'(k)$ must be a function of k . This implies that waves with different wave numbers must travel at different speeds. If we consider a disturbance which consists of a number of different wave numbers, like our example above, then each component will travel with a different speed and will, therefore, spread out over a certain length and that length increases with time. Therefore, any linear PDE that satisfies our mathematical definition will include waves that spread out as they propagate and the PDE is said to be dispersive.

1.1.2 Nonlinearity

We shall start our discussion of the effects of nonlinearity by first considering a simple linear PDE given by

$$u_t + \alpha u_x = 0 \quad (1.8)$$

where α is a constant and u is a function of x and t . We wish to consider a traveling wave solution such that

$$u(x, t) = u(x - ct) = u(\xi) \quad (1.9)$$

where $u(\xi)$ is some arbitrary function, c is the constant wave speed and $\xi = x - ct$. Therefore, if we assume that the solution of Eq. (1.8) has this form, we can rewrite it as

$$-cu' + \alpha u' = 0 \quad (1.10)$$

where the primes indicate differentiation with respect to ξ . Assuming $u' \neq 0$, we can cancel it and be left with

$$c = \alpha \quad (1.11)$$

From this we can say that for any initial conditions, Eq. (1.8) will propagate a wave undisturbed at the speed $c = \alpha$. If we assume a parabolic shaped pulse as the initial conditions, then the propagation of that linear wave will be as illustrated in Figure 1.1.

Let us now consider the corresponding nonlinear case. A nonlinear generalization of Eq. (1.8) is given by

$$u_t + uu_x = 0 \quad (1.12)$$

If we again consider a traveling wave solution and introduce Eq. (1.9) into Eq. (1.12) we can write

$$-cu' + uu' = 0 \quad (1.13)$$

If, as before, $u' \neq 0$ we can eliminate it from Eq. (1.13) and leave

$$c = u(\xi) \quad (1.14)$$

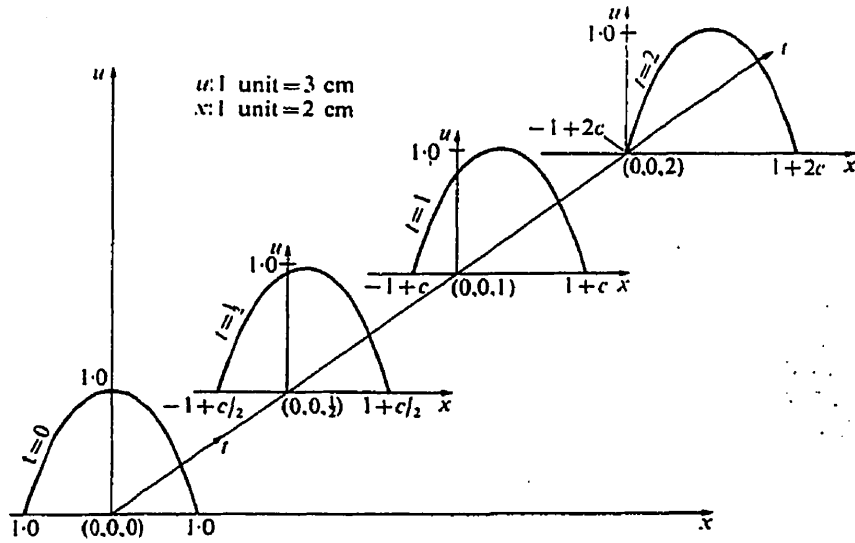


Figure 1.1: Development of a parabolic pulse governed by Eq. (1.8) (from Bhatnagar, 1979)

For a traveling wave, the speed c is a constant, and therefore Eq. (1.14) contradicts this, meaning no traveling wave solution exists for Eq. (1.12).

In order to further examine our nonlinear example, we can consider the characteristics of Eq. (1.12). We can determine that the characteristics of Eq. (1.12) are

$$\frac{dx}{dt} = u \quad (1.15)$$

In the (x, t) -plane then, on each characteristic of Eq. (1.12), the value u retains a definite constant value and the slope of each characteristic is given by Eq. (1.15).

If we interpret each characteristic in the (x, t) -plane as a moving wavelet where

the speed of each particular wavelet is the piece of information that moves with its corresponding characteristic, then Eq. (1.12) represents a series of wavelets each moving with a different velocity. The wavelet that carries a higher value of u moves faster. In broad sense, Eq. (1.14) could also be interpreted in this way. What then is the implication of this as compared to the linear case?

Let us now consider a parabolic shaped pulse as the initial conditions for the nonlinear case also. We can see the evolution of this pulse in Figure 1.2. We see that the effect of each wavelet moving with a speed u causes the initially parabolic pulse to distort, with greater distortion of the wave occurring for increasing time. We see that the points of $u = 0$ do not move at all while the point $u = u_{max}$ is distorted the most. Therefore, based upon this simple comparison, we can say that the role of nonlinearity is to produce increasing amounts of deformation in the wave profile as time progresses.

So we now have some insight into the physical meaning of dispersion and nonlinearity. The dispersion will tend to spread the wave out over time and the nonlinearity tends to deform the wave. As stated earlier, a balance in these two properties can produce a solitary wave, which propagates without change in form. Yet, waves can be governed by equations that contain both dispersion and nonlinearity, but do not exhibit a solitary wave. What characteristics do the governing equations need to exhibit in order to produce the delicate balance? For some insight we shall consider the famous Korteweg-de Vries (KdV) equation.

The nonlinear KdV equation is considered by many to be synonymous with solitary waves. When looking for solitary waves, very often the goal is to find a KdV type equation. The KdV equation (originally derived by Korteweg and de Vries,

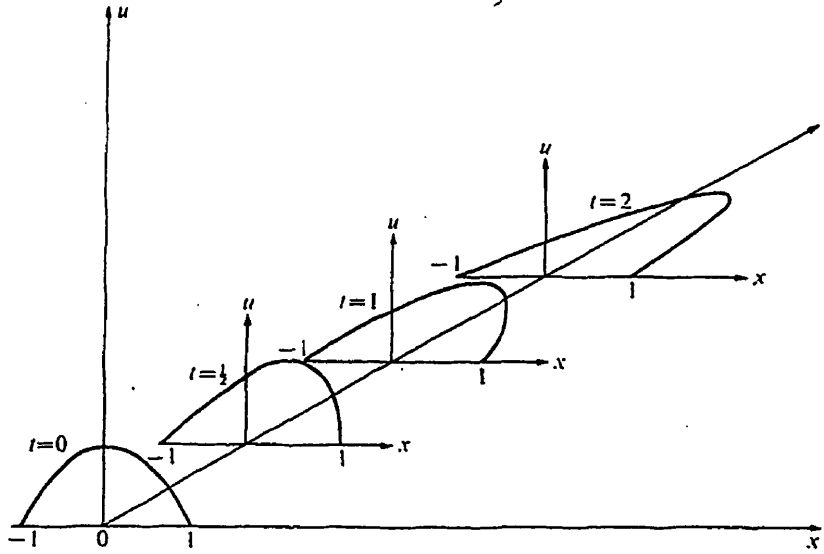


Figure 1.2: Development of a parabolic pulse governed by Eq. (1.12) (from Bhatnagar, 1979)

1895) is the simplest model of dispersive and nonlinear waves. Therefore, in our examination of the KdV equation we will look to see what determines the appropriate balance between dispersion and nonlinearity.

The KdV equation can be generalized to the following well recognizable form:

$$u_t + uu_x + Ku_{xxx} = 0, \quad K < 0 \quad (1.16)$$

Let us first consider the dispersion relation for Eq. (1.16). To do this, we first linearize Eq. (1.16), which leads to

$$u_t + Ku_{xxx} = 0 \quad (1.17)$$

from which we find the following dispersion relation

$$\omega = Kk^3 \quad (1.18)$$

So, by inspection we can see that for $0 \leq k < \infty$ we will have all real roots for ω and that $\omega''(k) = \frac{\partial^2 \omega}{\partial k^2}$ will indeed not be zero. Therefore, the wave is dispersive.

Now, let us consider a traveling wave solution of Eq. (1.16), such that

$$u(x, t) = u(x - ct) = u(\xi)$$

Substituting this into Eq. (1.16) yields

$$-cu_\xi + uu_\xi + Ku_{\xi\xi\xi} = 0 \quad (1.19)$$

which on integration leaves

$$-cu + \frac{1}{2}u^2 + Ku_{\xi\xi} = A \quad (1.20)$$

where A is a constant of integration. If we multiply Eq. (1.20) by u_ξ and integrate again, we get

$$-\frac{1}{2}cu^2 + \frac{1}{6}u^3 + \frac{1}{2}Ku_\xi^2 = Au + B \quad (1.21)$$

which can be rearranged to produce

$$3Ku_\xi^2 = -u^3 + 3cu^2 + 6Au + 6B \equiv f(u) \quad (1.22)$$

Now $f(u)$ is cubic and therefore has three roots. The roots of $f(u)$ will determine the type of solution we get for the original KdV equation. For our purposes, we will only be interested in non-constant, bounded solutions, which correspond to three

real roots for $f(u)$: α , β and γ . We shall also assume that the roots are real and have the following order: $\alpha \geq \beta \geq \gamma$.

It can be shown that three unique solutions for Eq. (1.16) arise depending on the values of α , β and γ . We do not present the formal derivations for each situation, but refer the reader to Bhatnagar (1979) for further details. If $\alpha \neq \beta \neq \gamma$ then the solution to the KdV equation is periodic waves, generally called Cnoidal waves. If $\alpha = \beta \neq \gamma$ then the solution is unbounded, and is therefore of little interest. The last possibility is that $\alpha \neq \beta = \gamma$. It is for this situation that the solitary wave is the solution to Eq. (1.16). Figure 1.3 illustrates how this combination of the roots would appear if Eq. (1.22) were plotted. We also notice that for this solution to be possible the function $f(u)$ must be positive between $\beta = \gamma$ and α . It is interesting that while solitary waves are considered synonymous with the KdV equation, the solitary wave is only one of the possible solutions to the KdV equation for particular initial conditions.

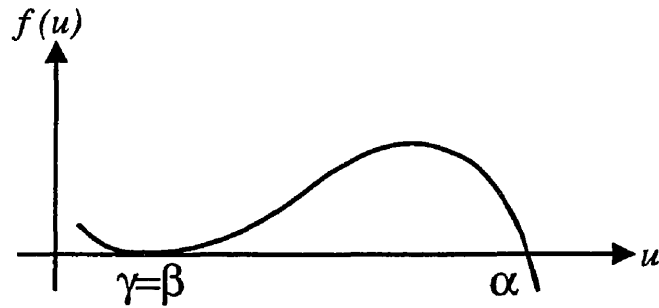


Figure 1.3: Appearance of roots of $f(u)$ for solitary wave solution for Eq. (1.16)

Therefore, we see that the balance of dispersion and nonlinearity is manifested in the combination of the roots of $f(u)$. Therefore, only specific values of K and c

will admit the solitary wave solution. Further, we can determine whether a solitary wave will exist by plotting Eq. (1.22) and confirming that the double root and the single root exist and that the function is positive in between.

If we were considering a generic PDE, would it be possible to generalize the above approach to determine if it also had a solitary wave solution? The answer is, in fact, yes and is the basis of the method presented in this dissertation.

For a single PDE for a function u with independent variables x and t , we begin by assuming that the solution will take the form of a traveling wave and substitute $u = f(x - ct) = f(\xi)$ into our PDE. This creates an ordinary differential equation (ODE) with independent variable ξ . Next, we take the ODE and attempt to put it in the form

$$f'^2 = f_c(f)$$

where $f_c(f)$ depends on the original form of the PDE. Based upon the procedure described above, we can determine if solitary waves exist for the original PDE by simply plotting $f_c(f)$. If the plot of $f_c(f)$ reveals a double root, a single root and the function is positive on the interval between the roots then it will have a solitary wave as one of its solutions. An application of this to the specific case of elastic tubes will be presented in greater detail in Chapter 2.

1.2 Background

Having given a general introduction to the basic concepts used in our approach, it may also be useful to provide a brief introduction to previous work done in this field. The problem of solitary waves in fluid-filled elastic tubes is derived from the

study of two fields that have developed independently. Therefore, the background for our work will be initially divided into two components: solitary waves and waves in fluid-filled tubes. From there we will discuss their convergence and the previous work specifically considering solitary waves in fluid-filled tubes.

1.2.1 Solitary Waves

The first observation of a solitary wave was made in 1834 by John Scott Russell and was first reported in 1837 at a meeting of the Society for the Advancement of Science (Russell, 1837). The best description of what he observed is from Russell himself:

“I was observing the motion of a boat which was rapidly drawn along a narrow channel by a pair of horses, when the boat suddenly stopped—not so the mass of water in the channel which it had put in motion; it accumulated around the prow of the vessel in a state of violent agitation, then suddenly leaving it behind, rolled forward with great velocity assuming the form of a large solitary elevation, a rounded, smooth and well-defined heap of water, which continued its course along the channel apparently without change of form or diminution of speed. I followed it on horseback, and overtook it still rolling at a rate of some eight or nine miles an hour, preserving its original form some thirty feet long and a foot to a foot and a half in height. Its height gradually diminished, and after a chase of one or two miles I lost it in the windings of the channel. Such, in the month of August, 1834, was my first chance interview with that singular and beautiful phenomenon.”

At the time, many were reluctant to accept Russell's observations as they appeared to contradict the prevailing shallow water theory, which, in part, claimed that a wave of finite amplitude could not propagate undeformed (e.g., see Ablowitz and Clarkson, 1999, for a more detailed discussion). Theoretical investigations of solitary waves were carried out at the time by Boussinesq and Rayleigh in an effort to resolve the apparent paradox (for a full discussion of these studies see Miles, 1980). While these studies provided valuable insight and support of Russell's observations, it was the work of Korteweg and de Vries (1895) that is considered the seminal work in the field. It is from this work that the famous KdV equations [cf. Eq. (1.16)] was derived. The existence of solitary waves was conclusively resolved because, as was shown above, the KdV equation has permanent wave solutions that include the solitary wave.

After the existence of solitary waves was firmly established, interest in the subject seems to have waned. It is considered by some (see Allen, 1998) that a renewed interest in solitary waves was spurred by the work of Adlam and Allen (1958). In their study Adlam and Allen (1958) examined the propagation of hydromagnetic waves in a collisionless plasma and happened across a solitary wave, though this was not their intention. While it is not at all obvious, in retrospect this work could be considered the launching point towards the study of solitary waves in fluid-filled elastic tubes for reasons that will be explained later.

The next significant work on solitary waves was a study by Zabusky and Kruskal (1965). The major contribution of the work by Zabusky and Kruskal (1965) was their determination that solitary waves traveling towards each other will collide and interact elastically, emerging from the collision with no alterations in speed or shape. It was also in this paper that the term *soliton* was first used. While Zabusky and

Kruskal (1965) considered no physical situation specifically, they were also interested in hydromagnetic waves.

The work of Zabusky and Kruskal (1965) stimulated further interest in solitary waves in plasmas. Of most interest to us is the development of what has been termed the reductive perturbation technique. The formal development of the reductive perturbation technique was undertaken in the late 1960s (Washimi and Taniuti, 1966; Taniuti and Wei, 1968). It was originally developed as a method to examine ion-acoustic waves in collisionless plasmas, but was inspired by work done on hydromagnetic waves. A parallel development of this technique was also presented at the time by Su and Gardner (1969). The study by Taniuti (1974) is considered the culmination of the original development of the reductive perturbation technique. This study also presented other possible applications for the technique.

The reductive perturbation technique will be referred to throughout this dissertation and so it seems appropriate to present a brief description of its application. The reductive perturbation technique requires that the waves under consideration be dispersive, weakly nonlinear waves that have long wavelengths. The long wavelength approximation implies that the wave number, k , is small ($\ll 1$). Consequently, the reductive perturbation technique is only applicable to small-but-finite amplitude waves. Based on that framework the reductive perturbation technique utilizes a coordinate stretching, resulting in a change of independent variables. The coordinate stretching enables the waves to be considered in the far field. The dependent variables are then re-written in terms of a perturbation expansion from which the KdV equation appears as the first order approximation.

From our perspective, it was the development of the reductive perturbation technique for studying ion-acoustic waves that stimulated the study of solitary waves in fluid-filled tubes.

1.2.2 Waves in Fluid-Filled Elastic Tubes

The propagation of waves in fluid-filled tubes has been an ongoing area of study for at least 200 years. The body of literature that exists on this topic today is immense and continues to grow rapidly. It would be impossible to provide a detailed account of all the studies in this area. As a result, we propose a short introduction to some of the more important historical studies and then to concentrate on the literature concerning solitary waves in fluid-filled elastic tubes. For a detailed background of this field, specifically related to blood flow in large arteries, the books by Pedley (1980) and Fung (1997) are recommended. Reviews by Skalak (1966) and Sawatzky and Moodie (1988) also provide a comprehensive account of the literature of the field.

The first published work concerning pressure waves in elastic tubes was by Young (1808). In this work, Young derived a formula for the velocity of propagation of a pressure pulse through an incompressible fluid contained in an elastic tube. He derived his equation by drawing an analogy with the propagation of sound in a compressible fluid. He also considered the application of his formula to blood flow in a subsequent paper (Young, 1809).

It is interesting that, while Young was the first to publish results on this topic, the first mathematical model was actually developed by Leonhard Euler in 1775. Euler had developed the basic equations governing blood flow in arteries by assuming an

unsteady flow of an incompressible fluid in a distensible tube. Euler was, however, unable to find a solution to his equations. In the end, his work was not published until 1862. An interesting evaluation of Euler's work can be found in Skalak (1966).

The equation derived by Young (1808) was re-derived several times by investigators such as Moens, Korteweg and Lamb. A summary of each of their contributions can be found in Skalak (1966). The most common form of the equation for the speed of propagation of waves in elastic tubes is credited to Korteweg (1878), but is known as the Moens-Korteweg equation. The Moens-Korteweg wave speed has been used to non-dimensionalize velocities in many studies.

The modern consideration of waves in fluid-filled tubes began with the work of Morgan and Kiely (1954) and Womersley (1955). In these studies, periodic waves were considered for linearized, viscous fluid equations and equations for a thin-walled isotropic membrane. This work provided much of the basis for the development of the field over the next decade, where extensions to these linear theories were examined in order to model the transmission of pulse waves more precisely (e.g. see Sawatzky and Moodie, 1988, for more detail).

In the 1970's and 1980's the investigation of waves in fluid-filled elastic tubes continued to progress rapidly. The literature during this time expanded significantly. Much of the work still utilized linear theory (for example see Pedley, 1980), but extended it for aspects such as prestresses, tube wall viscoelasticity, tube taper and even nonlinearity.

It has also been inevitable that the wide availability of massive computing power has resulted in the consideration of these problems from a purely numerical perspective such as in Bathe and Kamm (1999). Nevertheless, the analytical model has

been established as an indispensable tool in obtaining an accurate description of the propagation of waves in elastic tubes, with particular application to blood flow in arteries.

1.2.3 Solitary Waves Meet Fluid-Filled Tubes

The specific study of solitary waves in fluid-filled elastic tubes was initiated primarily by the development of the reductive perturbation technique (RPT) in plasma physics. As a result, over the last 15 years the study of solitary waves in fluid-filled elastic tubes has expanded. Additionally, the vast majority of studies examining solitary waves have used the reductive perturbation technique.

One of the original studies to examine solitary waves in fluid-filled elastic tubes was Hashizume (1985). Solitary waves were found using the RPT for a thin elastic tube containing an inviscid, incompressible fluid. The membrane equations used included some approximation, but a two-dimensional fluid model was used. In a subsequent study by Yomosa (1987), a further simplified tube model was considered. The deformations in the axial direction were neglected and the fluid properties were averaged over the tube radius, varying only in the axial direction. The significant contribution of this study was that the solitary wave solution was considered in light of experimental data and was found to approximate the pulse wave in larger arteries. A study conducted by Demiray (1996) also considered the shell and the fluid as one-dimensional, with limitations on the displacements, but considered a constitutive equation constructed for biological material (Demiray, 1972), whereas the earlier studies had not.

The practice of neglecting the axial displacement has been applied in a number

of other studies as well. This was often done based on the consideration of the long wave approximation used in the reductive perturbation technique, where small radial displacements of the tube are assumed to produce negligible axial displacements. Demiray (1998a) assumed that the tube was axially tethered and so neglected all axial displacements, while also considering both a one and two-dimensional fluid model. In another study Demiray (1999d) again neglects axial displacements but this time considers only the two-dimensional fluid model. All of these studies considered only inviscid and incompressible fluids.

A two-dimensional viscous fluid was considered by Demiray (1998b) where only the radial displacements were considered. The results showed the solution to be a solitary wave only for specific magnitudes of the viscosity. In a very recent article, Demiray (2001a), still neglecting axial displacements, considers an incompressible two layer fluid model. In doing so Demiray considers an outer flow region, which is two-dimensional and inviscid, and an inner fluid core, where the flow does not vary radially and viscosity is not negligible.

In order to better account for the axial displacements, Demiray (1997c) assumed that the axial displacements were small, but not negligible, and linearized the field equations in terms of the axial displacement. The stresses were also determined through a series expansion and the fluid was assumed one-dimensional. In Demiray and Dost (1998a) a solitary wave solution is found when both the axial and radial displacements of the tube are considered using the exact membrane equations. A two-dimensional inviscid fluid model is also considered.

Recently, there has been some work done on developing perturbation methods that retain higher order terms than the reductive perturbation technique. The most

common of these approaches utilizes the hyperbolic tangent method (Malfliet and Hereman, 1996) to include higher order terms. The resulting equations have been termed 'dressed solitary waves' by Malfliet and Wieers (1996).

The concept of dressed solitary waves has been used in studies by Malfliet and Ndayirinde (1998) and Sarioglu (1999) for one-dimensional equations for both the shell and fluid, and studies by Demiray (1999a,b) for a two-dimensional fluid model and a thick walled tube, respectively. A parallel approach, referred to as the modified reductive perturbation approach, has also been used by Demiray (2001b, 2000b). The solitary waves predicted using the modified RPT reduces to a dressed solitary wave for similar parameters.

The reductive perturbation technique has also been used to find solitary waves propagating in fluid-filled thick walled elastic tubes (see Demiray, 1997a; Demiray and Dost, 1998b). The existence of solitary waves in fluid-filled viscoelastic tubes (see Erbay et al., 1992; Demiray, 1997b,c) has been found to depend on the magnitude of certain parameters.

Chapter 2

Direct Approach for Solitary Waves in Fluid-Filled Elastic Tubes¹

2.1 Introduction

In considering models for waves in fluid-filled tubes, we see that many different solution techniques have emerged to deal with the wide range of the analytical models. If we canvas the vast literature in the field, we find the use of techniques such as the method of characteristics (Moodie and Haddow, 1977), the inverse scattering method, the Fourier approach, and various asymptotic methods (Jeffrey and Kawahara, 1982). With attention focused on solitary waves in particular, it is clear that the reductive perturbation technique is the most commonly used approach.

The reductive perturbation technique (RPT) was formally developed in the late 1960's (Washimi and Taniuti, 1966; Taniuti and Wei, 1968; Su and Gardner, 1969). In considering solitary waves, the RPT utilizes the long-wave approximation which asserts that the wavelength must be much greater than the tube radius. Put another way, only waves of small amplitude with small slopes may be considered. In addition, the RPT applies a coordinate stretching, resulting in a change of independent variables. Finally, the dependent variables are re-written in terms of a perturbation expansion.

¹This chapter is based on the article: Epstein, M. and Johnston, C. (1999) Improved solution for solitary waves in arteries. *Journal of Mathematical Biology*, **39**, 1–18.

The existence of solitary waves in fluid-filled elastic tubes has been investigated by means of the reductive perturbation technique by Hashizume (1985); Yomosa (1987); Erbay et al. (1992); Demiray (1996, 1999d), where an equation of the Korteweg-de Vries (KdV) type results for the first order approximation. There are, however, a number of potential causes for concern inherent in using the reductive perturbation technique.

The first concern that should be considered is that the solitary wave obtained using the RPT might be an artifact of the approximation procedure, rather than a feature of the exact solution. In other words, the existence of solitary waves as the first-order approximation may be perceived as a necessary but not sufficient condition for a solitary wave solution of the governing equations. In fact, that this question has only been considered recently (Sun and Shen, 1995).

The second consideration results from the dependence of the RPT on the long-wave approximation. The long-wave approximation requires that the wavelength be very large as compared to the tube radius. This in turn imposes a limitation on the amplitude of the wave that can be considered, so that the RPT is only valid for small amplitude waves. The long-wave approximation is also sometimes invoked as the rationale for neglecting the slope squared terms in the governing equations of the tube, as was done in Demiray (1996, 1998a).

A final obvious limitation of the RPT is that the obtained shape of the solitary wave and the the relationship between its amplitude and its speed of propagation are approximate, with no clear estimate of the errors involved. The fact that the KdV equation appears as the first order approximation places even greater significance on this issue. Certainly for very small amplitude waves this error may not be

significant, but the approximate nature of the solution further limits the range of wave amplitudes reasonably assessed by a solution attained using the RPT.

With this as a framework, this chapter shall be concerned with presenting a procedure that produces a solitary wave solution for the original field equations without recourse to a perturbation procedure. This direct procedure allows the wave speed, wave amplitude and the shape of the solitary wave to be determined to any desired accuracy. By operating directly on the differential equations we are able to extend the analysis beyond the long-wave approximation and to establish the range of validity of the reductive perturbation technique.

As a means of comparison, we have chosen to examine a problem originally considered by Demiray (1996). As a starting point all axial variations have been neglected for this case study. This effectively reduces the field equations to one-dimensional for the tube. We also utilize a one-dimensional inviscid fluid model, where the velocity has been averaged over the tube cross section.

Section 2.2 provides a detailed mathematical description of our proposed exact procedure. Two special cases of the field equations are considered in detail. In §2.3 the one-dimensional field equations for a tube and a one-dimensional fluid model are presented. Section 2.4 presents a numerical example for the field equations and §2.5 compares the results obtained using our direct method to the results arrived at using the reductive perturbation technique. In §2.6 the possibilities for extending this procedure and the limitations of the reductive perturbation technique are examined. Finally, §2.7 summarizes the main outcomes of this chapter.

2.2 Mathematical Preliminaries

For the limited purposes of this work, we adopt the following, admittedly imperfect, definition of a solitary wave:

Definition. A partial differential equation (PDE) for a function w of two independent variables, x and t , is said to admit solitary waves if a solution of the form

$$w = f(\xi) \tag{2.1}$$

with

$$\xi = x - ct \tag{2.2}$$

exists such that:

1. c is a constant (the speed of propagation);
2. f is bounded; and
3. $\lim_{\xi \rightarrow \infty} f$ exists.

For our particular application, we will replace condition (3) by the more stringent condition:

- 3'. f approaches its limits at infinity exponentially fast, from one side.

This last restriction implies that outside of a "small" interval of ξ , the function f does not oscillate and is practically indistinguishable from a constant function (usually zero). It follows from Eq. (2.1) and (2.2) that

$$\frac{\partial w}{\partial x} = f' \tag{2.3}$$

and

$$\frac{\partial w}{\partial t} = -cf' \quad (2.4)$$

where primes indicate ξ derivatives. Introducing these results into the original PDE, therefore, one obtains an ordinary differential equation (ODE) for f . If we assume, for example, that the original equation was a quasi-linear second-order PDE, with coefficients not explicitly dependent on x or t , the resulting ODE can be brought to the form

$$f'' = F_c(f, f') \quad (2.5)$$

where F_c is a function whose form depends on the original PDE and on the parameter c . The properties and long-term features of the solutions of this generic nonlinear equation are amenable to treatment by means of the theory of dynamical systems (see e.g. Guckenheimer and Holmes, 1986)². We will confine our attention to two particular cases corresponding to special forms of the right-hand side of Eq. (2.5).

Case 1. The first case we shall consider is given by the following

$$f'' = F_c(f) \quad (2.6)$$

Let us assume henceforth, for definiteness, that we are searching for a solitary wave of the general appearance shown in Figure 2.1. It is obvious, then, that F_c must satisfy the following conditions:

²Guckenheimer and Holmes (1986): "We must start by admitting that almost nothing beyond general statements can be made about most nonlinear systems. [Any] tool in the workshop of applied mathematics, including numerical integration, perturbation methods, and asymptotic analysis, can and should be brought to bear on a specific problem."

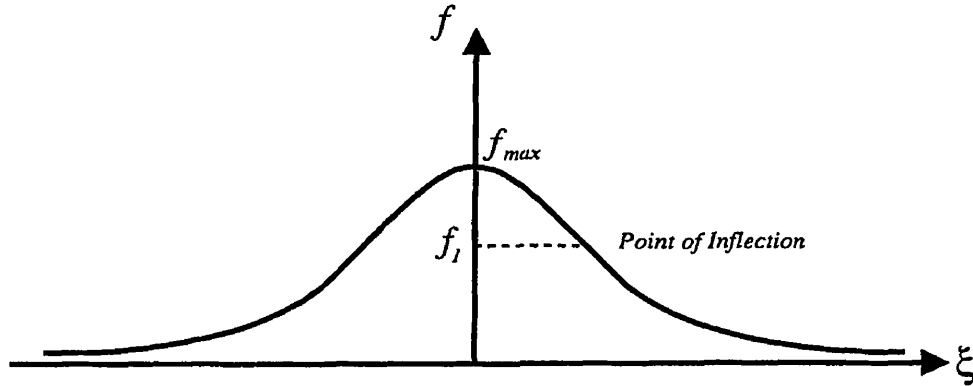


Figure 2.1: General appearance of solitary wave

- (i) it must have two roots, one at $f = 0$ (behaviour at infinity), and the other one at some (positive) finite value $f = f_1$ (point of inflection);
- (ii) it must be positive in the interval $(0, f_1)$, and negative in the interval (f_1, f_{max}) ; and
- (iii) the integral of $F_c(f)$ between 0 and f_{max} must vanish, as it follows by integrating Eq. (2.6) between those limits and enforcing the vanishing thereat of the slope of f .

Figure 2.2 shows the desired general appearance of $F_c(f)$. The actual shape, it must be remembered, is controlled by the parameter c , so that the value of f_{max} satisfying condition (iii), if it exists, depends on c . The behaviour of $F_c(f)$ beyond the interval $[0, f_{max}]$ is of no interest. A different way to arrive at the above conditions is by noting that the first-order ODE

$$\frac{1}{2}(f')^2 = \int_0^f F_c(\varphi) d\varphi + C \quad (2.7)$$

where C is a constant, is a first integral of Eq. (2.6), as can be verified directly

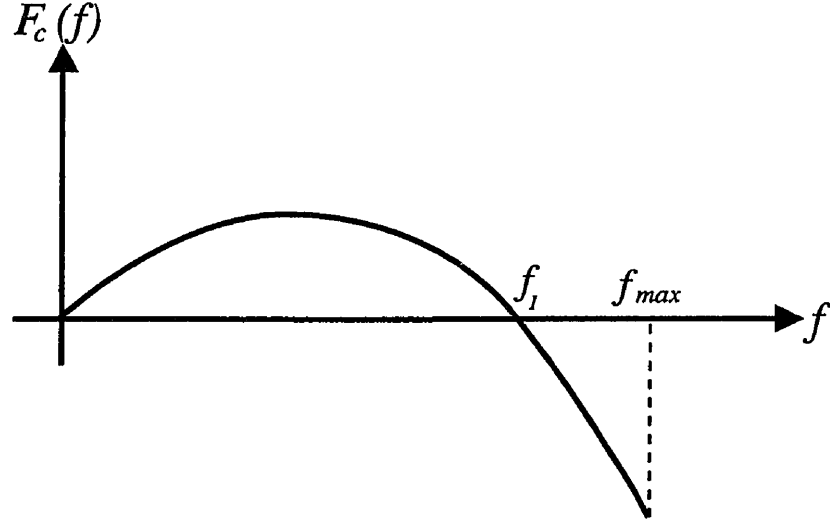


Figure 2.2: General appearance of F_c

by differentiation of Eq. (2.7) with respect to ξ . The analysis then requires that the right-hand side of Eq. (2.7) have a double root at $f = 0$ (which implies that $C = 0$ and $F_c(0) = 0$) and a single root at $f = f_{max}$, and be positive in the interval $(0, f_{max})$. One should bear in mind, however, that although every solution of Eq. (2.6) satisfies Eq. (2.7), the converse is not true. For example, when Eq. (2.7) is differentiated we find

$$f' f'' = F_c(f) f'$$

In order to recover Eq. (2.6) we must divide both sides by f' which is only valid if $f' \neq 0$. This means that Eq. (2.7) can admit the solution $f = const$ and therefore Eq. (2.7) has a solution which equation Eq. (2.6) does not. Therefore, for numerical

integration purposes it is best to operate directly on Eq. (2.6).

When integrating Eq. (2.6) numerically, one should observe that if the initial conditions satisfy: $f'(0) = 0$ and $0 < f(0) < f_{max}$, the behaviour will be smoothly periodic, while if the initial conditions satisfy: $f'(0) = 0$ and $f(0) > f_{max}$, the behaviour will drastically change and may become unbounded. Therefore, the solitary wave can also be identified, for a given c , as that solution corresponding to a value of $f(0)$ situated exactly at the transition between those two modes of behaviour. In a phase portrait of Eq. (2.6), therefore, the solitary wave will correspond to the separatrix between regions of closed and open orbits (see Arnold, 1978, p19).

More general cases of Eq. (2.5), where first derivatives are present, can also be considered.

Case 2. We will confine our attention to the particular form

$$f'' = G_c(f) + H_c(f)f'^2 \quad (2.8)$$

where G_c and H_c are smooth functions. It is remarkable that this case can be reduced to the previous one, as shown in the following proposition.

Proposition. *Let*

$$h(f) = \exp\left(-\int_0^f H_c(\varphi)d\varphi\right) \quad (2.9)$$

and

$$k(f) = 2 \int_0^f G_c(\varphi)h^2(\varphi)d\varphi \quad (2.10)$$

Then: (a) the expression

$$h^2(f)f'^2 - k(f) = D \quad (2.11)$$

where D is a constant, is a first integral of Eq. (2.8); and

(b) every (non-constant) solution of Eq. (2.8) is also a solution of

$$f'' = G_c(f) + H_c(f) \frac{k(f) + D}{h^2(f)} \quad (2.12)$$

and, vice-versa, among all the solutions of Eq. (2.12), that corresponding in Eq. (2.7) to $C = D/2$, is also a solution of Eq. (2.8).

Proof. Part (a) follows directly by differentiating Eq. (2.11) and making use of definitions Eq. (2.9) and (2.10). Part (b) is obtained by introducing Eq. (2.11) into Eq. (2.8) and, vice-versa, by enforcing Eq. (2.7) on the right-hand side of Eq. (2.12) and integrating by parts. For this last step it is convenient to write Eq. (2.9) as: $H_c = -h^{-1} dh/df$.

For a solution of the form shown in Figure 2.1, the conditions at infinity imply that $D = 0$ and $G_c(0) = 0$. □

2.3 Analysis of the equations of motion

We begin by writing the non-dimensionalized governing field equations for a thin membrane, allowing for radial displacements only, measured from a prestressed reference configuration, as derived by Demiray (1996):

$$\frac{S_1}{m} \frac{\partial^2 \bar{w}}{\partial \bar{x}^2} - \frac{S_2}{(1 + \bar{w})} + \frac{1}{2} \bar{p}(1 + \bar{w}) = \frac{\partial^2 \bar{w}}{\partial \bar{t}^2} \quad (2.13)$$

$$\frac{\partial \bar{v}_f}{\partial \bar{t}} + \bar{v}_f \frac{\partial \bar{v}_f}{\partial \bar{x}} + \frac{\partial \bar{p}}{\partial \bar{x}} = 0 \quad (2.14)$$

$$\frac{\partial \bar{w}}{\partial \bar{t}} + \frac{1}{2}(1 + \bar{w}) \frac{\partial \bar{v}_f}{\partial \bar{x}} + \bar{v}_f \frac{\partial \bar{w}}{\partial \bar{x}} = 0 \quad (2.15)$$

where

$S_1, S_2 =$ total non-dimensional longitudinal and hoop stresses;

$S_{1\infty}, S_{2\infty} =$ initial (prestress) non-dimensional longitudinal and hoop stresses;

$\bar{w} =$ radial displacement (measured from initial radius);

$\bar{x} =$ axial coordinate;

$\bar{p} =$ total pressure;

$\bar{p}_\infty = 2S_{2\infty} =$ initial fluid pressure;

$\bar{t} =$ time coordinate; and

$\bar{v}_f =$ fluid speed, which is assumed constant across the tube cross-section.

These quantities have been rendered non-dimensional as follows:

$\sigma_1 = \mu S_1 =$ true longitudinal stress;

$\sigma_2 = \mu S_2 =$ true hoop stress;

$w = R\bar{w} =$ true radial displacement;

$x = L_0\bar{x} =$ true longitudinal coordinate;

$p = \frac{h\mu}{2R} \bar{p} =$ total fluid pressure;

$t = T_0\bar{t} =$ true time;

$v_f = \frac{L_0}{T_0} \bar{v}_f$

with

$\mu =$ shear modulus of the isotropic and incompressible elastic tube material;

$L_0 = \left(\frac{Rh\rho}{2\rho_f}\right)^{1/2}$

$T_0 = \left(\frac{\rho}{\mu}\right)^{1/2} R$

$h =$ tube wall thickness;

$\rho =$ tube material density;

$\rho_f =$ fluid density;

$R =$ initial (prestressed) radius; and

$m = (\frac{L_0}{R})^2 = \frac{h\rho}{2R\rho_f} =$ thickness parameter.

Equation (2.13) is the equation of motion of the tube, and Eq. (2.14) and (2.15) represent, respectively, the continuity and balance of momentum for the (inviscid) fluid. Equation (2.13) is approximate only in the sense that the slope is assumed small everywhere, so that terms proportional to $(\frac{\partial \bar{w}}{\partial x})^2$ have been neglected.

At this point, we begin to apply the direct approach. Our first step towards the search for possible solitary waves for the field equations (2.13), (2.14) and (2.15), consists of effecting the main substitution implied in the definition and expressed in Eq. (2.1) and (2.2) for a traveling wave. As a result, and taking into account Eq. (2.3) and (2.4), we obtain the following system of ODE's:

$$(\frac{S_1}{m} - c^2)\bar{w}'' - \frac{S_2}{(1 + \bar{w})} + \frac{1}{2}\bar{p}(1 + \bar{w}) = 0 \quad (2.16)$$

$$(-c + \bar{v}_f)\bar{v}'_f + \bar{p}' = 0 \quad (2.17)$$

$$(-c + \bar{v}_f)\bar{w}' + \frac{1}{2}(1 + \bar{w})\bar{v}'_f = 0 \quad (2.18)$$

where, with some abuse of notation, we have retained the same symbols already used for the two-variable functions \bar{S}_1 , \bar{S}_2 , \bar{w} , \bar{v}_f , \bar{p} , to indicate the corresponding functions of the single variable ξ . Fortunately, Eq. (2.17) and (2.18) turn out to be exactly integrable, yielding the following links between \bar{p} , \bar{v} and \bar{w} :

$$\bar{p} = c\bar{v}_f - \frac{1}{2}\bar{v}_f^2 + C \quad (2.19)$$

and

$$\bar{v}_f = c - \frac{D}{(1 + \bar{w})^2} \quad (2.20)$$

where C and D are constants of integration. Imposing the initial conditions $\bar{w} = \bar{v}_f = 0$ and $\bar{p} = \bar{p}_\infty$, these integration constants are obtained as $C = \bar{p}_\infty$ and $D = c$, so that we may finally write the following explicit expression connecting the pressure with the radial displacement:

$$\bar{p} = \bar{p}_\infty + \frac{1}{2}c^2\left(1 - \frac{1}{(1 + \bar{w})^4}\right) \quad (2.21)$$

which, substituted into Eq. (2.16), results in the following final form for the single ODE governing the radial amplitude of the solitary wave:

$$\bar{w}'' = \frac{\frac{S_2}{(1+\bar{w})} - \frac{1}{2}(\bar{p}_\infty + \frac{1}{2}c^2(1 - \frac{1}{(1+\bar{w})^4}))}{\frac{S_1}{m} - c^2}(1 + \bar{w}) \quad (2.22)$$

which is of the form Eq. (2.6). The explicit forms of the functions S_1 , S_2 in terms of \bar{w} depend on the particular constitutive equation chosen for the tube material. For the sake of comparison, we shall use two of the constitutive equations employed by Demiray (1996), namely, the (I-H-T) strain energy density (Ishihara et al., 1951), and Demiray's own (D1) (Demiray, 1972). Both equations are expressed in terms of the first two invariants, I_1 and I_2 , of the Green deformation tensor:

$$I_1 = \Lambda_1^2 + \Lambda_2^2 + \frac{1}{\Lambda_1^2 \Lambda_2^2} \quad (2.23)$$

and

$$I_2 = \frac{1}{\Lambda_1^2} + \frac{1}{\Lambda_2^2} + \Lambda_1^2 \Lambda_2^2 \quad (2.24)$$

where, within the small-slope approximation, the principal hoop and longitudinal stretches Λ_1, Λ_2 are given in terms of the known initial (prestress) values $\lambda_z, \lambda_\theta$ by

$$\Lambda_1 = \lambda_z \quad (2.25)$$

and

$$\Lambda_2 = \lambda_\theta(1 + \bar{w}) \quad (2.26)$$

For a given non-dimensional strain energy density Σ , the stresses are found by

$$\begin{aligned} S_1 &= \Lambda_1 \frac{\partial \Sigma}{\partial \Lambda_1} \\ S_2 &= \Lambda_2 \frac{\partial \Sigma}{\partial \Lambda_2} \end{aligned} \quad (2.27)$$

The non-dimensionalized I-H-T strain energy function is given as

$$\Sigma_{I-H-T} = \frac{1}{2}[b(I_1 - 3) + (1 - b)(I_2 - 3) + \beta(I_1 - 3)^2] \quad (2.28)$$

where b and β are material constants. We obtain, by differentiation as shown in Eq. (2.27), the following expressions for the non-dimensional stresses:

$$S_1 = [b + 2\beta(I_1 - 3)](\Lambda_1^2 - \frac{1}{\Lambda_2^2 \Lambda_1^2}) + (1 - b)(\Lambda_2^2 \Lambda_1^2 - \frac{1}{\Lambda_1^2}) \quad (2.29)$$

and

$$S_2 = [b + 2\beta(I_1 - 3)](\Lambda_2^2 - \frac{1}{\Lambda_2^2 \Lambda_1^2}) + (1 - b)(\Lambda_2^2 \Lambda_1^2 - \frac{1}{\Lambda_2^2}) \quad (2.30)$$

It is important to verify that, for the Mooney-Rivlin material (obtained from the above expressions by setting $\beta = 0$), effecting all the substitutions implied in equations (2.23)-(2.29) into Eq. (2.22), one obtains:

$$\bar{w}'' = \frac{[\frac{b}{\lambda_\theta^2 \lambda_z^2} + \frac{1-b}{\lambda_\theta^2} - \frac{c^2}{4}][(1 + \bar{w})^4 - 1]}{\frac{(1+\bar{w})}{m} [b((1 + \bar{w})^2 \lambda_z^2 + \frac{1}{\lambda_\theta^2 \lambda_z^2}) + (1 - b)(\lambda_z^2 \lambda_\theta^2 (1 + \bar{w})^4 - \frac{(1+\bar{w})^2}{\lambda_z^2})] - c^2} \quad (2.31)$$

The numerator of the right-hand side of this equation is a polynomial in \bar{w} whose only real positive root is at zero. Therefore, according to condition (i) of Section 2.2, there will be no solitary waves for a tube wall made of the Mooney-Rivlin material. It is remarkable that this fact, as we have just proven, is intrinsic in the field equations themselves, namely, it is not merely a result of the approximation entailed in obtaining the Korteweg-deVries equation as a first-order perturbation of the field equations (Erbay et al., 1992; Demiray, 1996).

Turning now to the non-dimensionalized D1 strain energy function

$$\Sigma_{D1} = \frac{1}{2\alpha} \{ \exp[\alpha(I_1 - 3)] - 1 \} \quad (2.32)$$

for which the stresses are again found by Eq. (2.27) so that

$$S_1 = (\Lambda_1^2 - \frac{1}{\Lambda_1^2 \Lambda_2^2}) \exp[\alpha(I_1 - 3)] \quad (2.33)$$

and

$$S_2 = (\Lambda_2^2 - \frac{1}{\Lambda_1^2 \Lambda_2^2}) \exp[\alpha(I_1 - 3)] \quad (2.34)$$

For any prescribed constitutive equation, our task is to find, for given values of c and m , whether or not, in addition to the zero root, there exists a second root \bar{w}_1 for the right-hand side of Eq. (2.22), and a value \bar{w}_{max} satisfying condition (iii) of Section 2.2.

2.4 Sample calculations

In order to illustrate the numerical procedure used, we present a detailed account of one particular case corresponding to the D1-material. The following values are

chosen: $\alpha = 1.948$, $m = 0.4$, $\lambda_\theta = 1.2$, $\lambda_z = 1.5$, and $c = 8$, which lie within the ranges used by Demiray (1996) in his examples and are of the order of magnitude of actual biologically relevant parameters (see Yomosa, 1987, for experimental data in dogs). The Mathematica[®] package is used for all numerical computations. Figure 2.3 shows the right-hand side of Eq. (2.22) for the given values of the constants. The positive root is found at $\bar{w}_1 = 0.0691952$, and, by numerical integration, the value \bar{w}_{max} satisfying condition (iii) is found at 0.0933322. Figure 2.4a and b, obtained directly from the Mathematica[®] differential equation solver, show respectively the solutions for the initial conditions 0.0933321 and 0.0933322.

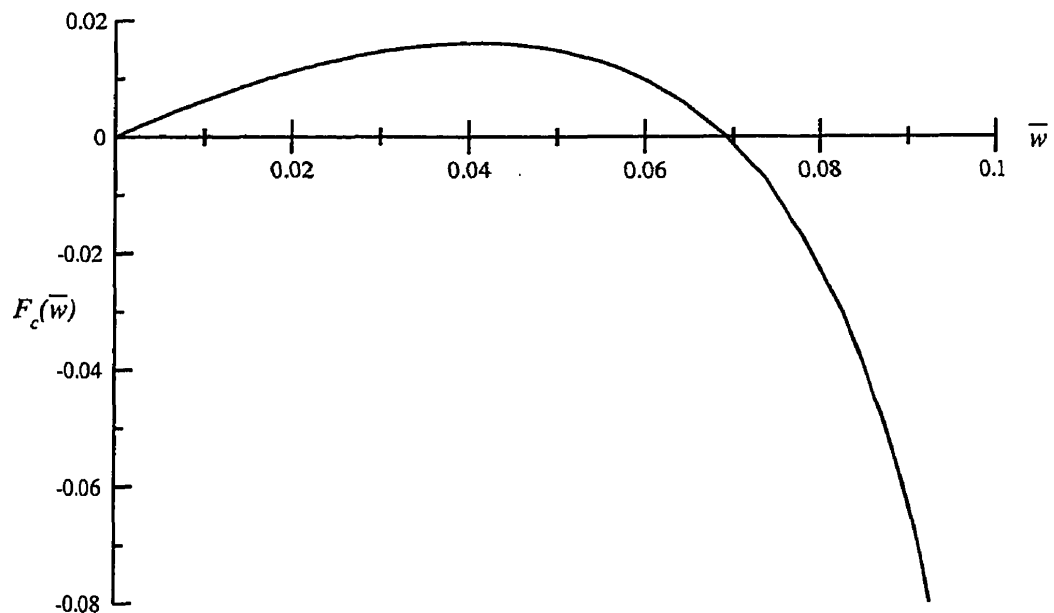


Figure 2.3: RHS of Eq. (2.22) in numerical example

The dramatic change in behaviour of the solution for a change in initial conditions

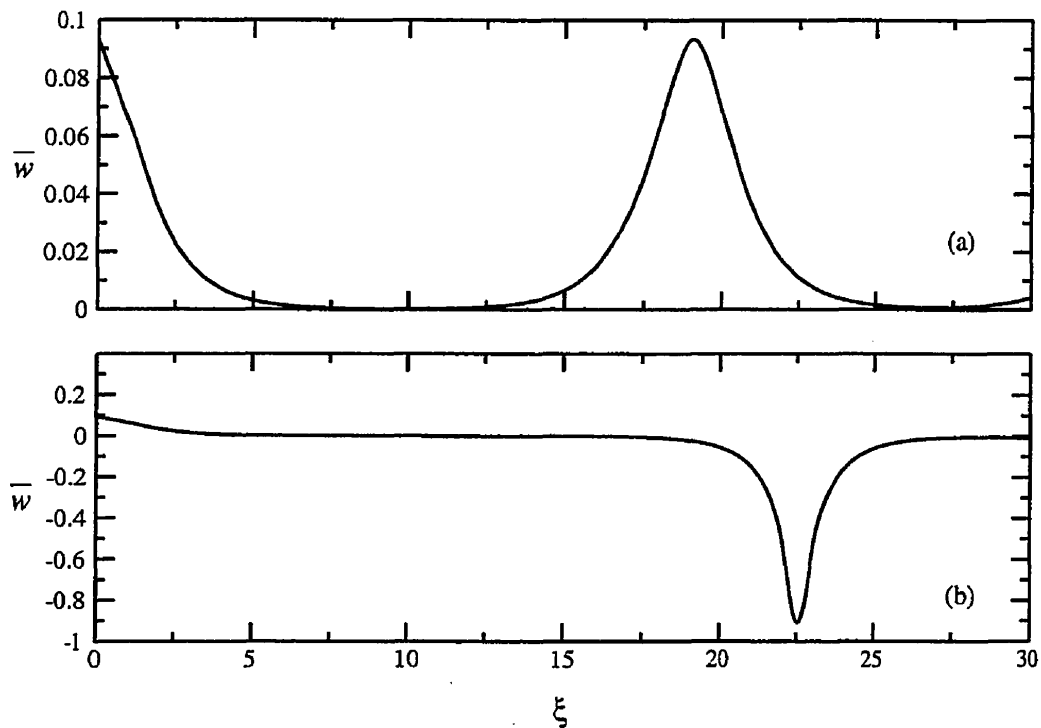


Figure 2.4: (a) Periodic behaviour of solution with $\bar{w}(0) = 0.0933321$, (b) Divergent behaviour of solution with $\bar{w}(0) = 0.0933322$

of little over one part per million, clearly illustrates the presence of a solitary wave solution, as anticipated by the satisfaction of conditions (i)-(iii). The shape of the solitary wave is accurately represented by the shape of any one period just before the transition, as per Figure 2.4a.

An alternative way of searching for the solitary wave, without resorting to finding the root of F_c , consists of specifying (rather than \bar{w}_{max}) a very small positive initial value $\bar{w}(0)$. The solution will then be periodic but, as the value of $\bar{w}(0)$ becomes

vanishingly small, the solution will approach the solitary wave. In our example, for the values of $\bar{w}(0) = 10^{-3}, 10^{-6}$, we obtained the amplitudes 0.093328, 0.093332, respectively.

The solitary wave just found is of moderate amplitude, so that it is to be expected that a comparison with Demiray (1996) application of the perturbation technique will produce satisfactory results. To effect such a comparison we recall that Demiray (cf. Erbay et al., 1992) introduces a coordinate stretching given by

$$\eta = \epsilon^{1/2}(\bar{x} - g\bar{t}), \tau = \epsilon^{3/2}g\bar{t} \quad (2.35)$$

where ϵ is “a small parameter measuring the weakness of dispersion and the non-linearity,” and the quantity g is defined in terms of the pressure and the slope $S'_2(0)$ of the hoop-stress constitutive equation at the initial state of prestress as

$$g^2 = S'_2(0) - \bar{p}_\infty \quad (2.36)$$

The first-order perturbation, containing the solitary wave as a solution to the Korteweg-de Vries equation, results in the following approximation:

$$\bar{w} \approx \frac{\epsilon a}{2g} \operatorname{sech}^2[(\gamma a)^{1/2} \zeta] \quad (2.37)$$

where a is an arbitrary constant representing the amplitude, and

$$\zeta = \eta - \nu\tau \quad (2.38)$$

The constants γ and ν are given by

$$\gamma = \frac{K}{6(1 - \frac{S_{100}}{mg^2})}, \nu = \frac{Ka}{3} \quad (2.39)$$

with K involving up to the second derivative, $S''_2(0)$, of the hoop-stress constitutive equation at the initial state through the expression:

$$K = \frac{S'_2(0) + S''_2(0) - 2\bar{p}_\infty}{4g^3} \quad (2.40)$$

By introducing Eq. (2.35), (2.38) and (2.39) into Eq. (2.37), we obtain that the actual (non-dimensional) speed of propagation is related to the amplitude \bar{w}_{max} by:

$$c \approx g \left(1 + \frac{2Kg}{3} \bar{w}_{max} \right) \quad (2.41)$$

an expression not explicitly determined when using the reductive perturbation technique, but implied in the derivation. Moreover, at the point of inflection of the perturbation solution one always has:

$$\bar{w}_1 = \frac{2}{3} \bar{w}_{max} \quad (2.42)$$

For the chosen values of the constants, we obtain $g = 6.59736$ and $K = 0.415564$, whereby Eq. (2.41) yields the value $c = 7.723$ for the approximate speed predicted by the reductive perturbation technique for a wave amplitude of 0.0933321. The discrepancy with the 'exact' value ($c = 8$) is of about 3.5%. Likewise, at the point of inflection the perturbation technique predicts the approximate value $\bar{w}_1 = 0.06222$, representing an error of 10% relative to the exact value. This error is less severe than it appears, when one realizes that the points of inflection themselves are located at $\xi = 0.912$ and 1.057, respectively, for the 'exact' and the approximate solutions. To emphasize this point, Figure 2.5 shows a composite picture of the two profiles. It is interesting to note that Eq. (2.41) predicts, in the limit of vanishingly small amplitudes, a propagation speed equal to g , which is thus to be interpreted as the

smallest possible speed of propagation for a solitary wave for the particular initial stretches. Accordingly, our numerical solution of the 'exact' field equations should yield the coincidence of the two roots at zero. And indeed this is the situation, as can be seen from Figure 2.6.

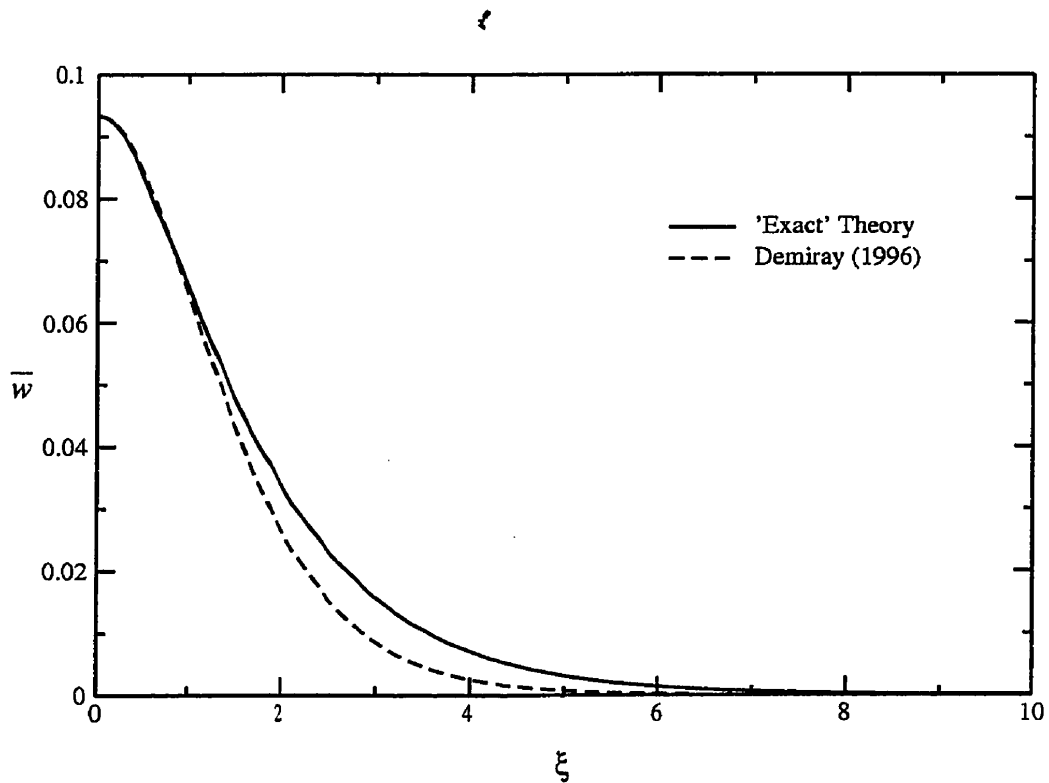


Figure 2.5: Comparison between the 'exact' and Demiray (1996) solution

2.5 Comparative results

Following the technique of the example just discussed, the speeds of propagation have been calculated for a range of amplitudes up to 25% of the initial radius of the tube,

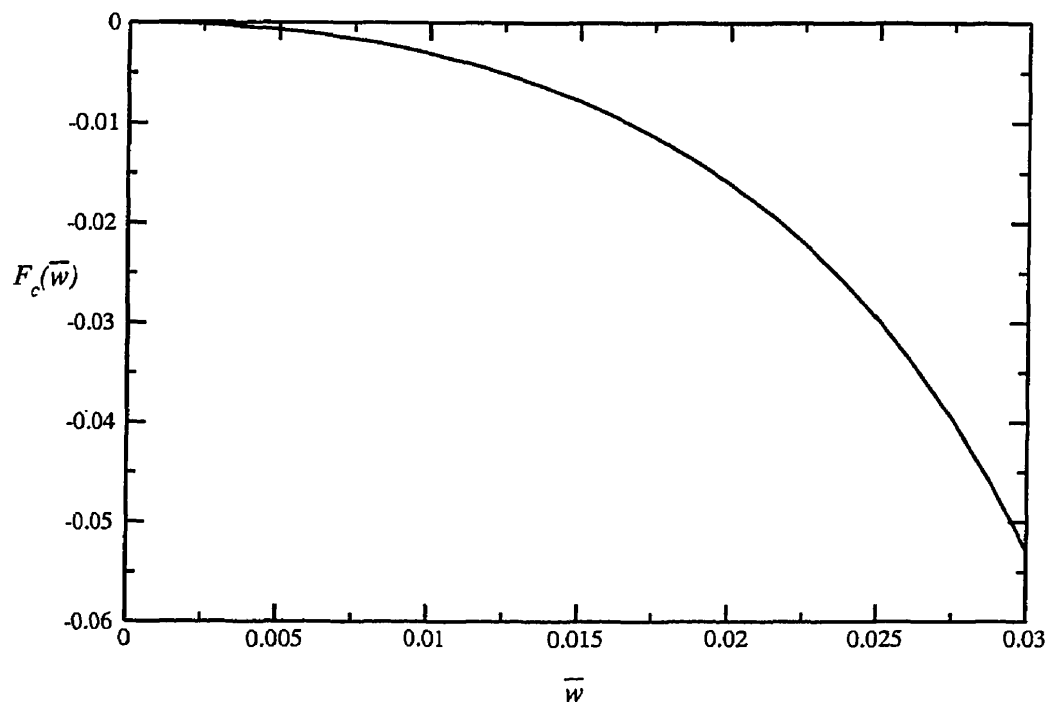


Figure 2.6: Behaviour of F_c for limiting propagation speed

made of a D1 material. As Table 2.1 shows, Demiray's (Demiray, 1996) perturbation technique yields generally excellent results, but the error in the estimated speed progressively increases, reaching a value of about 20% for an amplitude of 0.25. The table includes also a comparison of the magnitude of the radial displacement at the point of inflection, but (as already pointed out) this is not a true estimate of the discrepancy between the wave profiles on a global scale, as Figure 2.5 clearly shows.

Table 2.1: Comparison between 'exact' method and Demiray's approach

Amplitude	Speed of Propagation		Magnitude at Inflection	
	'exact'	Demiray ¹	'exact'	Demiray ¹
0.0	6.5974	6.5974	0.0	0.0
0.03094	7	6.9704	0.02151	0.02062
0.06419	7.5	7.3714	0.046287	0.04279
0.09333	8	7.7228	0.06920	0.06222
0.1192	8.5	8.0347	0.09046	0.07947
0.1426	9	8.3169	0.1103	0.09507
0.1639	9.5	8.5737	0.1288	0.1093
0.1833	10	8.8077	0.1462	0.1222
0.2012	10.5	9.0235	0.1625	0.1341
0.2177	11	9.2225	0.1780	0.1451
0.2331	11.5	9.4082	0.1926	0.1554
0.2474	12	9.5806	0.2064	0.1649

¹ Demiray (1996)

2.6 Extension of the theory

The preceding numerical technique, not being bound by asymptotic considerations, should be applicable to more complex modeling of the solid kinematics. In order to avoid the necessarily lengthy presentation of additional theoretical elements, the development is confined to the extension of the kinematic formulation of the membrane theory by adopting a version of the field equations before the terms containing squares of the tube-profile slope were neglected (on the basis of the long-wave approximation). Obviously, more sophisticated shell theories could be invoked, such as Budiansky (1968). That is left for a later chapter. The inclusion of some of the neglected slope-square terms should clearly demonstrate the versatility of the direct approach presented in this chapter. The reinstatement of the neglected terms results

in, among other effects, an additional term in Eq. (2.13), which naturally propagates also into Eq. (2.16) and (2.22), and in a more complicated relation between the initial and final longitudinal stretches. Accordingly, Eq. (2.22) should be replaced by

$$\bar{w}'' = \frac{\frac{S_2}{(1+\bar{w})} - \frac{1}{2}(\bar{p}_\infty + \frac{1}{2}c^2(1 - \frac{1}{(1+\bar{w})^4})) (1 + \bar{w}) - \frac{1}{m} \frac{\partial S_1}{\partial \bar{w}} (\bar{w}')^2}{\frac{S_1}{m} - c^2} \quad (2.43)$$

and Eq. (2.25) by

$$\Lambda_1 = \lambda_z [1 + \frac{(\bar{w}')^2}{m}]^{1/2} \quad (2.44)$$

It is important to note that Eq. (2.43) is no longer of the form Eq. (2.6), since it includes a (quadratic) term in the first derivative of \bar{w} and, in addition, it depends also on this derivative through the implementation of Eq. (2.44) in the constitutive equations. Even with the corrections just suggested, the equations for the tube are still not kinematically exact. This is the case for a number of reasons, including the fact that horizontal displacements (and the accompanying dynamic equation) have been altogether neglected, and that the elements of length and area have not been consistently updated everywhere. The numerical calculations are confined to the correction entailed in Eq. (2.43), which is severe enough to modify the equations in a substantial way. The derivative of the stress appearing in the new term will be calculated, firstly, as the constant value at the initial state, and, secondly, as the more correct variable present state. The corrections stemming from Eq. (2.44) will be ignored.

To apply the numerical procedure, we note that Eq. (2.43) is of the form Eq. (2.8). Since all the additional terms are even functions of \bar{w}' , the solitary wave profile

will still be symmetric, so that the initial condition $\bar{w}' = 0$ can still be enforced. A good starting point for guessing the amplitude of the solitary wave could be derived by using the alternative technique suggested in Section 2.4, namely, by specifying a small initial value and reading the amplitude of the resulting periodic solution. For our calculations, however, we have preferred to program Mathematica[®] to actually perform the integrations entailed in Eq. (2.9) and (2.10), and to then integrate the resulting right-hand side of Eq. (2.12) so as to find the value f_{max} satisfying condition (iii) of Section 2.2 with any desired accuracy. Comparative results for a few values of the speed of propagation are shown in Table 2.2. The material constants are the same as for Table 2.1. The results show that significant differences can be expected in a fully consistent kinematically nonlinear theory. We have purposely compared amplitudes for equal speeds, rather than vice versa, in order to emphasize this point, since the amplitude of solitary waves is extremely sensitive to small changes in the coefficients of the equations of motion. Moreover, even for the moderate radial displacement regime corresponding to a speed of $c = 8$, the correction term $\frac{1}{m} \left[\frac{\partial S_1}{\partial \bar{w}} \right]_0 (\bar{w}')^2$ attains a value of as much as 2% of the term $\frac{1}{2} p_\infty$, although the square of the slope is only of the order of 0.1%. We note, finally, that for amplitudes larger than 0.1107 (corresponding to a speed of 7.762), the ‘more nonlinear’ version of the theory fails to produce solitary waves that tend to zero at infinity. This example should serve as a warning signal against the use of kinematically approximate theories for the tube without a careful estimate of their true range of validity.

Table 2.2: Comparison of wave amplitudes with additional slope-square terms

Wave Speed	Wave Amplitude		
	no slope-squares	some slope-squares	more slope-squares
7	0.03094	0.03322	0.03365
7.5	0.06419	0.07209	0.07762
8	0.09333	0.1060	N/A
8.5	0.1192	0.1346	N/A
9	0.1426	0.15847	N/A

2.7 Conclusions

Based on theoretical considerations implicit in the very definition of a solitary wave, a numerical scheme has been presented which predicts with a high degree of accuracy the speed and shape of solitary waves of any given amplitude in an elastic tube. Using this method, it has become possible to establish the magnitude of the errors incurred through the use of reductive perturbation techniques. As expected, these errors are initially very small, but increase dramatically with the amplitude (and speed) of the wave, reaching, in a specific example, a value of 20% of the speed, for amplitudes of about 25% of the radius of the tube. As a by-product of the technique employed, it was shown that the absence of solitary waves, within the small-slope regime, in a tube made of a Mooney-Rivlin material, is a direct consequence of the governing field equations, rather than a feature of the linear degeneration of the first-perturbation approximation. Finally, it was demonstrated that the inclusion of more geometrically nonlinear terms in the field equations can influence the results to a significant degree.

Chapter 3

Example of Direct Approach in Plasma Physics¹

3.1 Introduction

The investigation of the solitary wave as a solution for certain nonlinear systems of equations has been driven, perhaps to a greater extent than in wave propagation in elastic tubes, by the field of plasma physics. A renewed interest in solitary waves began with the work of Adlam and Allen (1958), in which they examined the propagation of hydromagnetic waves in a collisionless plasma. The formal development of the reductive perturbation technique (see for example Washimi and Taniuti, 1966; Taniuti and Wei, 1968) was intended for examining ion-acoustic waves in collisionless plasmas. Many investigations examining ion-acoustic waves have utilized this technique (Ikezi, 1973; Das and Tagare, 1975; Verheest, 1988). The reductive perturbation technique was only later applied as a method to solve for solitary waves in fluid-filled elastic tubes.

Recognizing the limitations of the RPT, attempts were made to include higher order terms, but it was found that singular terms appeared. While techniques to work around this problem were suggested, the solutions presented additional hazards and consequently this approach was not widely used. Recently, there has been further work done on developing perturbation methods that would seek to retain higher order terms without the difficulties of the earlier attempts. The most common of these

¹This chapter is based on the article: Johnston, C.R. and Epstein, M. (2000) On the exact amplitude, speed and shape of ion-acoustic waves. *Physics of Plasmas*, 7, 906-910.

approaches utilizes the Hyperbolic Tangent method (Malfliet and Hereman, 1996) to include higher order terms and 'dressed solitary waves' (so termed by Malfliet and Wieers, 1996) result.

In their systematic study of this problem, Malfliet and Wieers (1996) advocated the use of a traveling wave solution up to a third-order perturbation and also suggest a modification to the RPT. As a result of their analysis they show that, for a particular example, the first order solution would underestimate the amplitude of the solitary wave by as much as 20%. Thus, Malfliet and Wieers (1996) clearly illustrate the dangers and limitations inherent in the use of *any* perturbation technique.

Not surprisingly, the concept of dressed solitary waves has also been applied to problems of solitary waves in fluid-filled elastic tubes. Dressed solitary waves have been examined in studies by Malfliet and Ndayirinde (1998); Sarioglu (1999) with one-dimensional equations for both the shell and fluid and studies by Demiray (1999a,b) for a two-dimensional fluid model and a thick walled tube, respectively. A parallel approach, referred to as the modified reductive perturbation approach, has also been applied to ion-acoustic waves (Demiray, 1999c, 2000a) and fluid-filled elastic tubes (Demiray, 2001b, 2000b). The solitary waves predicted using the modified RPT were virtually identical to those of a dressed solitary wave.

The relevance of including a chapter on ion-acoustic waves in cold-collisionless plasma in this dissertation is based upon three considerations. First, considering the historical association between ion-acoustic waves and solitary waves in fluid-filled elastic tubes in terms of the reductive perturbation technique, this chapter allows us to demonstrate the broader application of our direct approach and to show that the advantages of using this approach are not limited to one area.

Secondly, when considering ion-acoustic waves we are able to extend the analytic portion of our solution further than for fluid-filled tubes. For example, the exact amplitude of the ion-acoustic wave involves only the finding of a root of a simple algebraic equation. By illustrating this feature for ion-acoustic waves, we are able to illustrate more effectively how the computational effort involved in finding the exact solution is minimal.

Finally, with the recent activity aimed at retaining higher order terms in the perturbation approach this chapter permits us to compare our results to a dressed solitary wave found by Malfliet and Wieers (1996). In doing this, we are able to highlight that while the retention of higher order terms can improve the accuracy of the solution, the effort required is substantially greater than required to find the exact solution using our direct approach. Moreover, the technique we propose is not limited to the particular equations at hand, but can in principle, be applied to situations beyond the range of validity of the simplifying physical assumptions of the theory.

Section 3.2 introduces the governing equations for ion-acoustic waves in cold collisionless plasma. The direct approach is applied to these equations giving a relationship of the form $f'' = F_c(f)$. In §3.3 it is shown that the analytic considerations can be extended to the point where the maximum wave amplitude is determined by finding the root of a simple algebraic equation. In §3.4 a numerical example is presented for a moderate amplitude wave. In §3.5 the exact solution is compared to the dressed solitary wave found by Malfliet and Wieers (1996) and the relative benefits of our procedure are discussed. Finally, §3.6 presents a summary of the major results from this chapter.

3.2 The Governing Equations and their Reduction

We begin this analysis with the well-known dimensionless set of nonlinear equations describing a one dimensional, collisionless plasma given by Davidson (1972) as

$$\frac{\partial n_i}{\partial t} + \frac{\partial(n_i v_i)}{\partial x} = 0 \quad (3.1)$$

$$\frac{\partial v_i}{\partial t} + v_i \frac{\partial v_i}{\partial x} = -\frac{\partial \varphi}{\partial x} \quad (3.2)$$

$$\frac{\partial^2 \varphi}{\partial x^2} = \exp(\varphi) - n_i \quad (3.3)$$

where n_i is the ion density, v_i is the flow velocity of the ions and φ is the electrostatic potential. At equilibrium $n_i = 1$, $v_i = 0$ and $\varphi = 0$. Our interest is in examining the fluctuations of the ion density and so we introduce the substitution $n_i = 1 + n$, where n is now the fluctuation of the ion density from its equilibrium value.

Following the approach set out in §2.2, our first step in the search for solitary waves for the field equations Eq. (3.1), Eq. (3.2) and Eq. (3.3) is to perform the substitutions implied in assuming the traveling wave solution, so that $\xi = x - ct$. The approach of assuming the solution to be a function of $\xi = x - ct$ has been used as far back as Adlam and Allen (1958) in a setting of simplified field equations. Since then it has also been applied to cases of multi-component and relativistic plasmas (Bhattacharyya and Roychoudhury, 1988; Chatterjee and Roychoudhury, 1994; Popel et al., 1995) by using the pseudopotential approach. It is important to note that our method exploits this assumption ($\xi = x - ct$) as a starting point in obtaining an exact solution of the complete field equations.

By substituting $\frac{\partial v_i}{\partial x} = f'$ and $\frac{\partial v_i}{\partial t} = -cf'$ into Eq. (3.1), Eq. (3.2) and Eq. (3.3) we obtain the following set of ODE's

$$(v_i - c)n' + (1 + n)v_i' = 0 \quad (3.4)$$

$$\varphi'' - \exp(\varphi) + (1 + n) = 0 \quad (3.5)$$

$$-cv_i' + \left(\frac{1}{2}v_i^2\right)' + \varphi' = 0 \quad (3.6)$$

where, without risk of confusion, the original variable names are used to indicate corresponding functions of the single variable. Integrating Eq. (3.4) exactly yields the following link between v_i and n ,

$$v_i - c = \frac{A}{(1 + n)} \quad (3.7)$$

where A is a constant of integration. If we then impose the initial equilibrium conditions $v_i = \varphi = n = 0$ (from $n_i = 1$), the integration constant is found to be $A = -c$.

We now solve in terms of v_i to avoid the irrational expression (square root) which appears when solving for φ . Substituting Eq. (3.7) and the derivative of Eq. (3.6) into Eq. (3.5) results in the following single ODE governing the ion-acoustic solitary waves,

$$v_i'' = \frac{\exp(cv_i - \frac{1}{2}v_i^2) - (v_i/(c - v_i)) - 1 + (v_i')^2}{(c - v_i)} \quad (3.8)$$

which is of the form of Eq. (2.8). Following the description in §2.2, we can transform Eq. (3.8) into an equivalent equation of the form of Eq. (2.6), allowing us to apply conditions (i) - (iii) directly.

By inspection of Eq. (3.8), we determine $H_c(v_i)$ and $G_c(v_i)$ to be the following

$$H_c(v_i) = \frac{1}{c - v_i} \quad (3.9)$$

$$G_c(v_i) = \frac{1}{c - v_i} \left(\exp\left(cv_i - \frac{1}{2}v_i^2\right) - \frac{v_i}{c - v_i} - 1 \right) \quad (3.10)$$

Performing the integrations described in Eq. (2.9) and Eq. (2.10) we determine that

$$h(v_i) = \frac{c - v_i}{c} \quad (3.11)$$

$$k(v_i) = \frac{2}{c^2} (\exp(cv_i - \frac{1}{2}v_i^2) - 1 - cv_i) \quad (3.12)$$

We can now write Eq. (3.8) in the form of Eq. (2.12) by utilizing Eq. (3.11) and Eq. (3.12) from above. After re-writing Eq. (3.8) and performing some simplifications we are left with

$$\begin{aligned} v_i'' &= \frac{1}{(c - v_i)} \left(\exp(cv_i - \frac{1}{2}v_i^2) - \frac{c}{c - v_i} \right) \\ &+ \frac{2}{(c - v_i)^3} \left(\exp(cv_i - \frac{1}{2}v_i^2) - 1 - cv_i + \frac{c^2 D}{2} \right) \end{aligned} \quad (3.13)$$

By condition (i), establishing the behaviour at infinity, we must have $D = 0$, yielding

$$v_i'' = \frac{1}{(c - v_i)^3} ((c - v_i)^2 + 2) \exp(cv_i - \frac{1}{2}v_i^2) - c(c + v_i) - 2 \quad (3.14)$$

This ODE is equivalent to Eq. (3.8) but is in the form of Eq. (2.6), thus providing a reduced form of the governing equation for ion-acoustic solitary waves in a cold collisionless plasma.

3.3 Solitary Wave Solution

It is now necessary to verify whether and under what circumstances the RHS of Eq. (3.14) satisfies conditions (i)-(iii) (§2.2) for the existence of solitary waves. We notice that the root of Eq. (3.14) at $v_i = 0$ always exists, regardless of the value of the wave speed c . Our task now is to find, for any given value of c , whether or not, in addition to the zero root, there exists a positive root, v_{i1} , for the right-hand side of Eq. (3.14), and more importantly, prove the existence of a value $v_{i\max}$ satisfying condition (iii).

While Eq. (3.14) permits a complete numerical analysis of the solitary waves, in this problem we have been able to extend the closed-form analysis by integrating Eq. (3.14) to obtain a first integral exactly. Indeed, employing integration by parts we find the first integral,

$$\frac{1}{2}(v'_i)^2 = \frac{1}{(c - v_i)^2} \left(\exp \left(cv_i - \frac{1}{2}v_i^2 \right) - cv_i - 1 \right) + B \quad (3.15)$$

where B is the constant of integration (which is zero). Every solution of Eq. (3.8) will also satisfy Eq. (3.15). This allows us to find $v_{i\max}$ exactly by solving a simple *algebraic* equation, namely,

$$\exp \left(cv_i - \frac{1}{2}v_i^2 \right) - cv_i - 1 = 0 \quad (3.16)$$

which can be easily solved numerically to any degree of precision. To obtain the shape of the solitary wave, we need only to perform a numerical integration of Eq. (3.15) with $v_i(0) = v_{i\max}$. Finally, we must check that the solution satisfies the original Eq. (3.14).

3.4 Numerical Example

To demonstrate another application of our direct method, we present a detailed example of one particular case. We will choose a value of $c = 1.25$ for the example case presented here. This value of c corresponds to a case presented in Malfliet and Wieers (1996), permitting us to compare our approach to a perturbation approach which includes higher order terms.

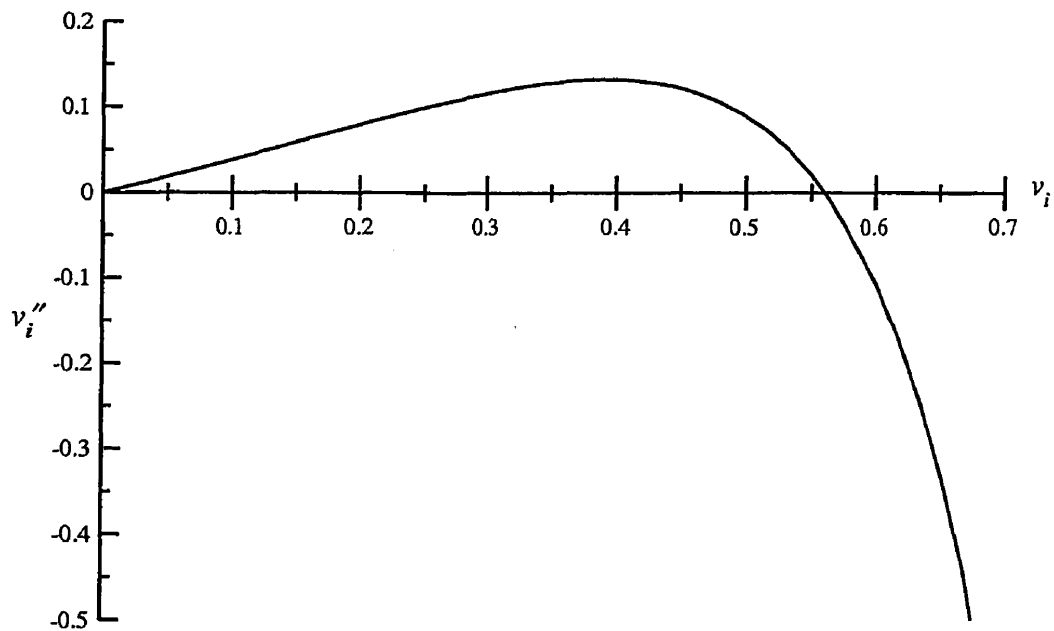


Figure 3.1: Evaluation of the RHS of Eq. (3.14) for a wave speed of $c = 1.25$.

Figure 3.1 shows the right-hand side of Eq. (3.14) evaluated for the value of c given above. We can determine that in addition to the root at zero, a second positive root does exist at $v_{i,1} = 0.56018$, which can be found to any specified degree

of precision. Figure 3.2 shows the right-hand side of Eq. (3.15), also evaluated with the value of c given above. The value of $v_{i\max} = 0.711603$, satisfying condition(iii), was determined by numerically solving Eq. (3.16). Again, this root can easily be found to any specified degree of accuracy.

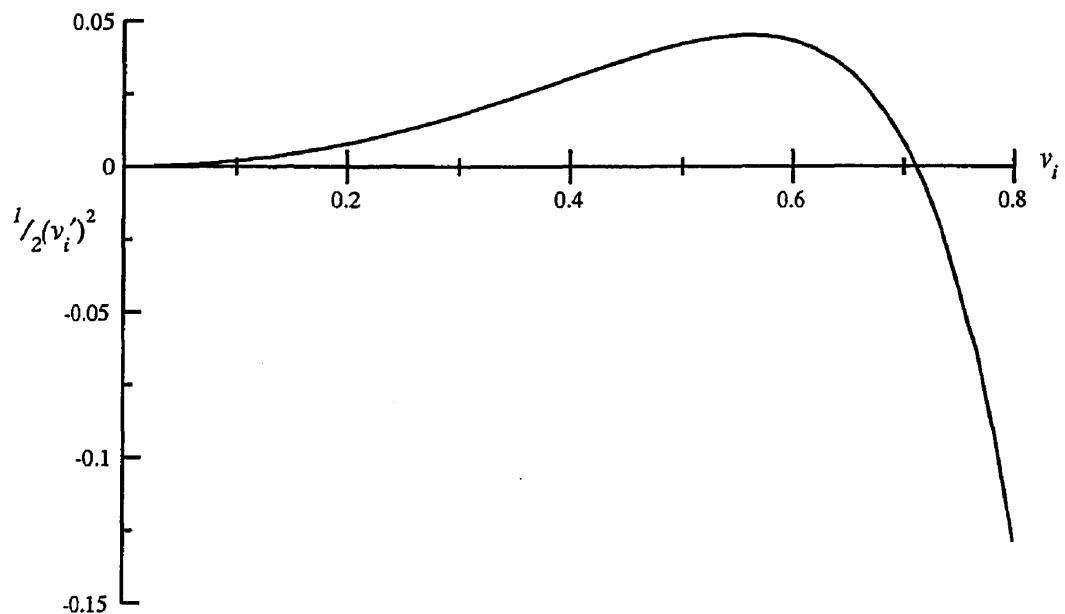


Figure 3.2: Evaluation of the RHS of Eq. (3.15) for a wave speed of $c = 1.25$.

By way of illustration, Figure 3.3a and Figure 3.3b, obtained directly from the Mathematica[®] differential equation solver, show the solutions of Eq. (3.14) for the initial conditions $v_i(0) = 0.711603$ and $v_i(0) = 0.711604$. The dramatic difference in solutions for a change in initial conditions of only one-one millionth, again illustrates the existence of a solitary wave solution. The shape of the solitary wave can be accurately represented by the shape of any one period, just before the transition, as

shown in Figure 3.3a.

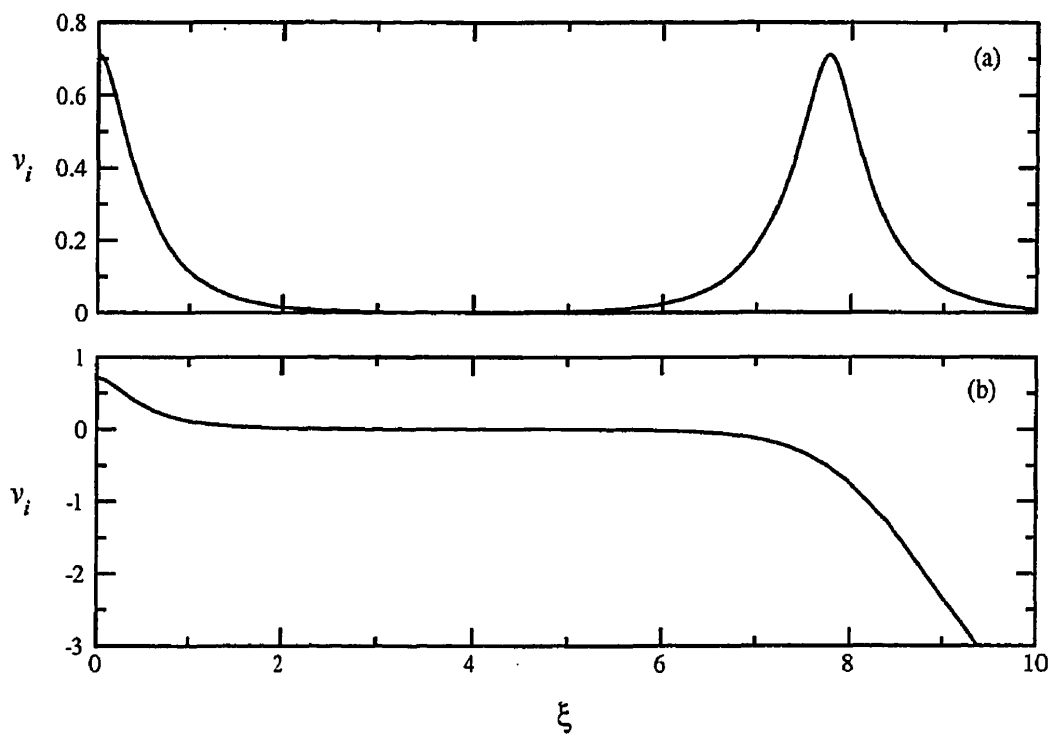


Figure 3.3: Solution of Eq. (3.14) for a wave speed of $c = 1.25$ showing (a) Periodic behaviour for $v_i(0) = 0.711603$ and (b) Divergent behaviour for $v_i(0) = 0.711604$.

We could also apply the alternate method of searching for the solitary wave given in §2.2, where a very small initial value for $v_i(0)$ is used as the initial conditions instead of $v_{i\max}$. In our example, for the values of $v_i(0) = 10^{-6}, 10^{-9}$, we obtain the amplitudes 0.711601 and 0.711602.

3.5 Discussion

The solitary wave found is of moderate amplitude, and a comparison with the results of Malfliet and Wieers (1996) perturbation reduction technique would be expected to produce satisfactory results. In order to make a comparison we recall that Malfliet and Wieers (1996) introduced a wave-number-like parameter, k , such that $v_i = k(x - ct)$. To determine a value of k , we use equation (14) from Malfliet and Wieers (1996) where

$$c = \frac{1}{(1 - 4k^2)^{\frac{1}{2}}} \quad (3.17)$$

and calculate that $k = 0.3$ for $c = 1.25$.

Substituting the above value of k into (31) of Malfliet and Wieers (1996) for $\xi = 0$ (initial shape at $t = 0$) yields $v_{i\ max} = 0.699925$ and a wave speed of $c = 1.24318$ (up to the k^6 approximation). For the ‘exact’ solution, we recall from above that $v_{i\ max} = 0.711603$ and $c = 1.25$. The error in the perturbation solution is then approximately 1.6% in $v_{i\ max}$ and 0.55% in c . To illustrate these differences, Figure 3.4 shows the comparison of the predicted solitary wave from the ‘exact’ solution and the dressed solitary wave of Malfliet and Wieers (1996). Although these differences do not appear significant, it should be pointed out that a third order perturbation was required to approach the ‘exact’ solution for a case of moderate amplitude. The perturbation approach would require an undetermined number of additional perturbations for waves of higher amplitude, yet it would still not be clear whether and in what sense the solution had converged. We should also note that the modified reductive perturbation technique used by Demiray (1999c) would produce the same wave as the dressed solitary wave shown in Figure 3.4.

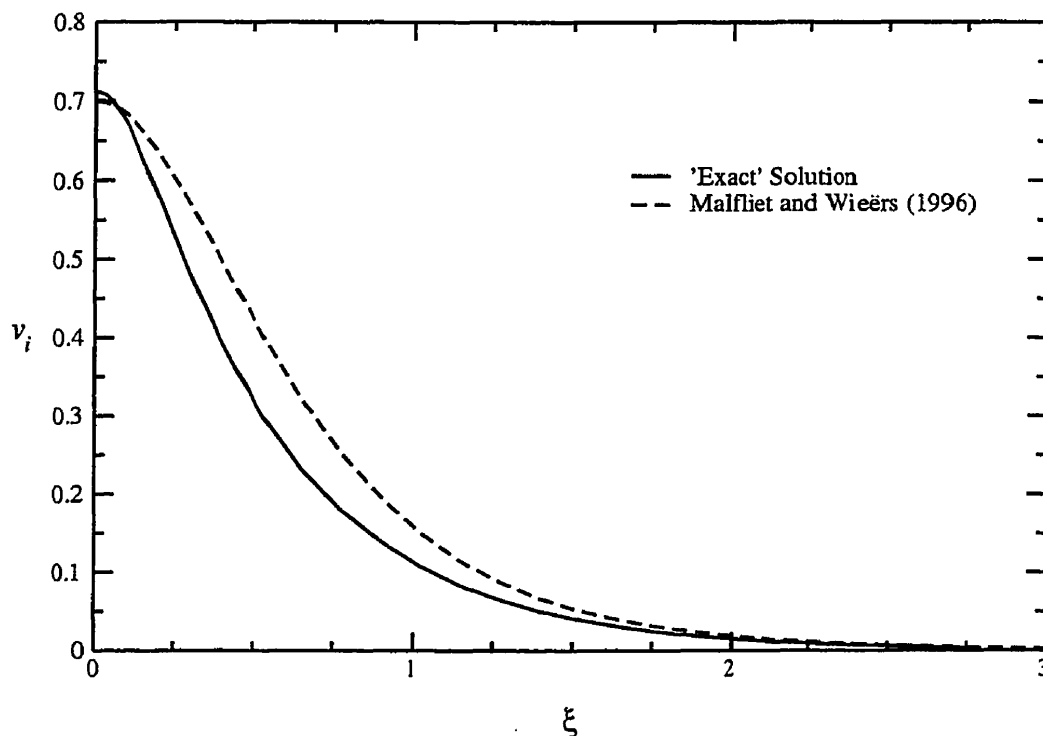


Figure 3.4: Comparison between the 'exact' solution (—) and the dressed solitary wave of Malfliet and Wieers (1996) (----) with $c = 1.25$ and $k = 0.30$.

It is interesting to note that Malfliet and Wieers (1996) observed that with successive (higher order) approximations, the predicted solitary wave became larger, taller and moved faster. In Figure 3.4 this trend continues from the highest order perturbation solution to the 'exact' solution, where the 'exact' solution is larger, taller and faster than the k^6 perturbation approximation.

While it may be argued that the perturbation approach could eventually approximate the 'exact' solution by including additional perturbations, there exist three

major advantages to the procedure developed here. Firstly, the approach used in this study is not limited to small amplitude waves, unlike the reductive perturbation approach. The relatively close agreement between the ‘exact’ solution and the perturbation solution was expected because the example considered was of moderate amplitude. If larger amplitudes (or faster waves) had been considered the discrepancy between the two solutions would have widened. Evidence of this is suggested by Malfliet and Wieers (1996). They point out that for waves with $k \leq 0.2$ (i.e. $c \rightarrow 0$) no significant difference is observed between successive approximations ($k^2 \rightarrow k^6$), yet for $k \geq 0.3$ (i.e. increasing c) they observe significant differences. Secondly, the proposed technique offers the advantage of yielding a highly accurate solution (one might say an exact solution) of the exact equations, with no intermediary equations. Thirdly, and perhaps most importantly, the ‘exact’ solution is obtained with less effort than the perturbation solution. This is especially true for large amplitude waves where an unspecified number of additional perturbations would be required.

3.6 Conclusions

Based on theoretical considerations implicit in the very definition of a solitary wave, in this chapter an analysis has been presented which predicts with high accuracy the amplitude and shape of ion-acoustic solitary waves for any given wave speed in a cold collisionless plasma.

Using this technique it is possible to determine the magnitude of errors incurred through use of the reductive perturbation techniques. As expected, the errors are relatively small for cases of moderate amplitude, but would be expected to increase

with the increase in amplitude (and speed) of the wave. While the retention of higher order terms will, to some degree, reduce these differences, the advantages of the proposed technique are that it is not limited to small amplitude waves, it yields a solution for the exact equations and the effort required to determine a solution does not vary with amplitude. Finally, the method proposed can be applicable to more general physical models.

Chapter 4

Two Dimensional Considerations for Solitary Waves in Fluid-Filled Elastic Tubes¹

4.1 Introduction

In the previous chapters (also in Epstein and Johnston, 1999; Johnston and Epstein, 2000), the reasons for abandoning the reductive perturbation technique were argued, particularly as it was shown that by operating directly on the original differential equations the speed and amplitude of the wave can be found exactly, and the shape of the wave found through a simple integration to any degree of accuracy. In this chapter, we will build on this and consider the common practice of invoking the long-wave approximation (Demiray, 1996; Demiray and Akgün, 1997; Demiray, 1998a; Malfliet and Ndayirinde, 1998) as the rationale for neglecting the axial displacements the solitary wave induces in the tube. This assumption unnecessarily rigidifies the elastic behaviour of the tube, but is adopted so as to reduce the number of dependent variables to one, thus rendering the problem tractable by certain numerical techniques.

The studies of Hashizume (1985); Demiray (1997d); Demiray and Dost (1998a); Antar and Demiray (1999) have included the axial displacement in the shell equations, but followed the common practice of finding a KdV type equation for the first-

¹This chapter is based on the article: Epstein, M. and Johnston, C. R. (2001) On the exact speed and amplitude of solitary waves in fluid-filled elastic tubes. Proc. R. Soc. Lond. A., 457, 1195–1213.

order approximation using the reductive perturbation technique. Unfortunately, the use of the reductive perturbation technique still limits the equations to small displacements.

The fortunate circumstance of having a method available that allows exact solutions for the displacements, with no limitation on their magnitude permits full consideration of the effect of the axial displacement on the predicted solitary wave. However, the consideration of large deformations and the associated inclusion of axial displacements leads to a coupled system of nonlinear differential equations, rather than just one equation.

Therefore, one of the main aims of this chapter is to show that by casting the problem in a variational formulation, and invoking Noether's theorem, enough conserved quantities can be derived to reduce the analysis of the two dependent variables (axial and radial displacement) to a situation similar to that with just one dependent variable. The availability of a variational formulation, essential to the treatment, emerges as a result of the exploitation of the usual modelling of the fluid-solid interaction.

Section 4.2 presents a derivation of the exact nonlinear membrane equations. These equations could have been obtained directly by particularizing exact field equations of general nonlinear shell theory (Budiansky, 1968). Nevertheless, the short independent derivation presented here, valid only for initially cylindrical membranes, is equivalent and renders this Chapter complete and self-contained while affording a direct interpretation of each of the terms in the equations. Section 4.3 presents the fluid equations and their treatment in the presence of solitary waves. The subtle point that the fluid equations are Eulerian while the solid equations are Lagrangian is discussed and resolved. Section 4.4 presents the variational formula-

tion and the explicit derivation of the conserved quantities. Section 4.5 discusses the basis for the numerical procedure. Section 4.6 presents numerical examples supporting the surprising conclusion that solitary waves exist but not necessarily where one would expect them on the basis of the long-wave approximation. In other words, the long-wave approximation appears to be qualitatively wrong, even when the amplitudes involved are very small. This point is further discussed in §4.7. Section 4.8 provides a recap of the main results presented in this Chapter and comments on their significance.

4.2 Derivation of the equations of motion

We adopt an infinite horizontal cylinder of radius R and axis x , shown in Figure 4.1, as a reference configuration for the membrane. For axisymmetric deformations, the displacement vector \mathbf{v} has only two components, u and w , along the axis and the radius, respectively. These components are functions of x alone. The axial and hoop elements of length, dx and $ds = Rd\theta$, become, respectively, upon deformation:

$$dx^* = \sqrt{(1 + u')^2 + w'^2} \, dx \quad (4.1)$$

$$ds^* = (R + w)d\theta = \left(1 + \frac{w}{R}\right)ds \quad (4.2)$$

where θ is the circumferential angular coordinate and where

$$()'' = \frac{\partial}{\partial x}() \quad (4.3)$$

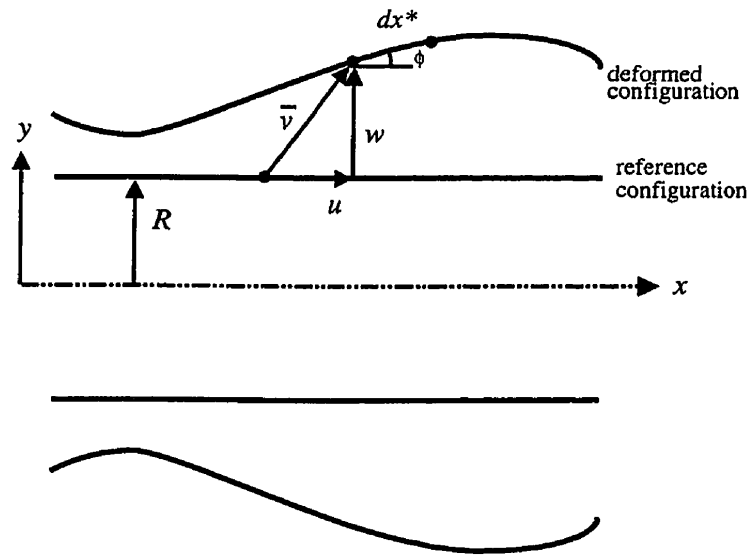


Figure 4.1: Reference and deformed configurations

The middle surface of the membrane, with reference area element $dA = dx ds$, is deformed to an element with area

$$dA^* = dx^* ds^* = \left(1 + \frac{w}{R}\right) \sqrt{(1 + u')^2 + w'^2} dA \quad (4.4)$$

The slope of the deformed meridian is given by

$$\tan \phi = \frac{w'}{1 + u'} \quad (4.5)$$

The preceding formulae are straightforward geometric facts and involve no limitations as to the magnitude of the displacements or slopes. In order to obtain exact equations of motion, we will utilize the 'physical' longitudinal and hoop components, σ_1 and σ_2 , of the three-dimensional Cauchy stress. Denoting by h^* the deformed thickness, by ρ the reference mass density, and by p the external normal pressure per unit

deformed area, shown in Figure 4.2, the longitudinal balance of momentum implies:

$$[n_1(1 + u')] - p(1 + \frac{w}{R})w' = \rho h \ddot{u} \quad (4.6)$$

where superimposed "dots" denote partial time-derivatives, and n_1 is the Kirchhoff longitudinal-stress resultant (per unit undeformed length):

$$n_1 = \frac{\sigma_1 h^* (1 + \frac{w}{R})}{\sqrt{(1 + u')^2 + w'^2}} \quad (4.7)$$

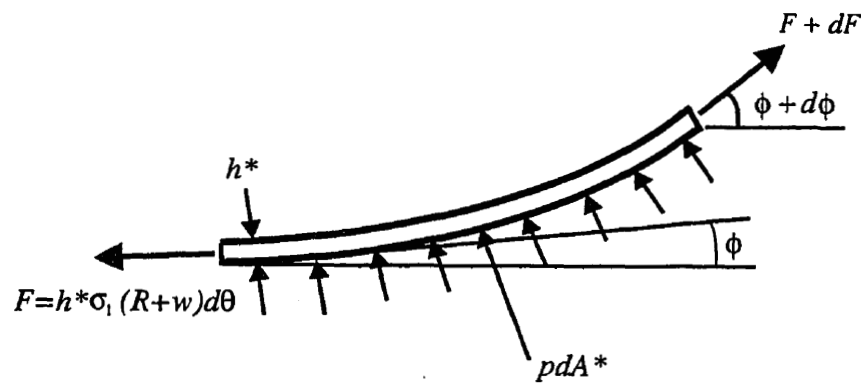


Figure 4.2: Forces acting upon element of deformed tube in longitudinal direction

Equation (4.6) has been obtained through imposition of Eq. (4.1), (4.2), (4.4), and (4.5) on the forces shown in Figure 4.2 and projection on x . Similarly, taking radial and hoop stress components shown in Figure 4.3, we obtain the radial equation of motion as:

$$[n_1 w'] - \frac{n_2 [(1 + u')^2 + w'^2]}{(R + w)} + p(1 + \frac{w}{R})(1 + u') = \rho h \ddot{w} \quad (4.8)$$

where

$$n_2 = \frac{\sigma_2 h^* (1 + \frac{w}{R})}{\sqrt{(1 + u')^2 + w'^2}} \quad (4.9)$$

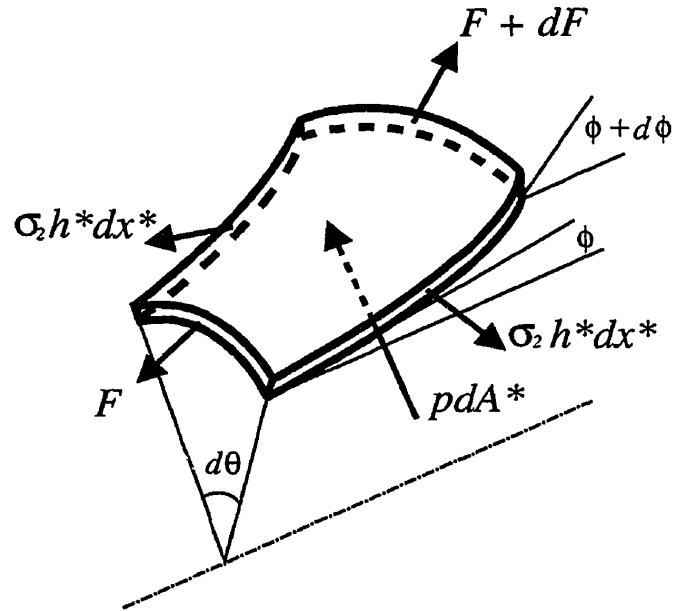


Figure 4.3: Hoop and longitudinal forces acting upon element of deformed tube

is the Kirchhoff hoop-stress resultant.

Equation (4.6) and (4.8) coincide, via the appropriate specialization to axisymmetric deformations of a cylinder, with the general nonlinear membrane equations of Budiansky (1968). In effecting the comparison, care has to be exercised when relating physical components (σ_i) with their doubly contravariant tensor counterparts (σ^{ij}). In our case:

$$\sigma_1 = \sigma^{11}((1 + u')^2 + w'^2) \quad (4.10)$$

$$\sigma_2 = \sigma^{22}(R + w)^2 \quad (4.11)$$

When the material is incompressible, Eq. (4.6) and (4.8) can be slightly simplified to the extent that the radicals involved in the definitions of Eq. (4.7) and (4.9)

disappear. Indeed, incompressibility means that

$$h^* dA^* = h dA \quad (4.12)$$

or using Eq. (4.1), (4.2) and (4.4):

$$h^* \left(1 + \frac{w}{R}\right) \sqrt{(1 + u')^2 + w'^2} = h \quad (4.13)$$

whence:

$$\begin{aligned} n_1 &= \frac{\sigma_1 h}{(1 + u')^2 + w'^2} \\ n_2 &= \frac{\sigma_2 h}{(1 + u')^2 + w'^2} \end{aligned} \quad (4.14)$$

The exact equations of motion for an incompressible membrane undergoing axisymmetric deformations are, therefore,

$$\left[\sigma_1 \frac{1 + u'}{(1 + u')^2 + w'^2} \right]' - \frac{p}{h} \left(1 + \frac{w}{R}\right) w' = \rho \ddot{u} \quad (4.15)$$

$$\left[\sigma_1 \frac{w'}{(1 + u')^2 + w'^2} \right]' - \frac{\sigma_2}{R + w} + \frac{p}{h} \left(1 + \frac{w}{R}\right) (1 + u') = \rho \ddot{w} \quad (4.16)$$

An important point to be made is that, since nothing beyond its cylindrical shape has been assumed for the reference configuration, these equations will have the same form for any cylindrical reference, regardless of whether it is stress-free or not. To check that this is the case, let U (a linear function) and W (a constant) denote displacements from one cylindrical reference to another, and let hatted quantities represent those measured with respect to the second reference. Then

$$\begin{aligned} d\hat{x} &= (1 + U') dx & \frac{\partial}{\partial \hat{x}} &= \frac{1}{1 + U'} \frac{\partial}{\partial x} & \hat{R} &= R + W & \hat{w} &= w - W \\ \hat{u} &= u - U & \hat{\rho} \hat{h} &= \frac{\rho h}{(1 + U')(1 + \frac{W}{R})} & \hat{u} &= \ddot{u} & \hat{w} &= \ddot{w} \\ \hat{\sigma}_1, \hat{\sigma}_2, \hat{h}^*, \hat{p}, \hat{\rho} &= \sigma_1, \sigma_2, h^*, p, \rho & \frac{\partial \hat{u}}{\partial \hat{x}} &= \frac{u' - U'}{1 + U'} & \frac{\partial \hat{w}}{\partial \hat{x}} &= \frac{w'}{1 + U'} \end{aligned} \quad (4.17)$$

These relations, when substituted back into Eq. (4.15) and (4.16) or Eq. (4.6) and (4.8), reproduce identical equations in terms of the hatted quantities.

4.3 Fluid-solid Interaction

Equations (4.15) and (4.16) are exact. To obtain a complete theory for the axisymmetric dynamics of fluid-filled elastic tubes, two elements are still missing: (i) a formula for the pressure p , representing the fluid-solid interaction, and (ii) a constitutive equation for the (incompressible) tube material.

As far as the fluid-solid interaction, we follow Chapter 2 by adopting a simple model, whereby the conservation of mass and momentum are enforced under the assumption that the velocity profile is constant throughout the tube cross section. At this point, however, we examine the fluid model within a broader context.

The axial coordinate x is a material coordinate for the tube. Let us denote by q a spatial coordinate in the axial direction, so that while each x represents a fixed material tube cross section, each q represents a fixed position in space along the axis. Any dynamical variable, Φ say, is expressible either in terms of x and t , or, equivalently, in terms of q and t . The connection between the two descriptions is obtained through the motion of the solid wall, i.e.,

$$q(x, t) = x + u(x, t) \quad (4.18)$$

We then have, with a typical abuse of notation,

$$\Phi' = \frac{\partial \Phi(x, t)}{\partial x} = \frac{\partial \Phi(q, t)}{\partial q} (1 + u') \quad (4.19)$$

$$\dot{\Phi} = \frac{\partial \Phi(x, t)}{\partial t} = \frac{\partial \Phi(q, t)}{\partial q} \dot{u} + \frac{\partial \Phi(q, t)}{\partial t} \quad (4.20)$$

Note that x is not a material coordinate for the fluid, so whenever Φ measures a fluid property, the passage from q to x is to be regarded as a mere change of variables. Denoting by v_f the fluid speed and ρ_f the (constant) fluid density, the continuity and linear momentum equations are obtained in a standard Eulerian way as:

$$\frac{\partial w(q, t)}{\partial t} + v_f \frac{\partial w}{\partial q} + \frac{1}{2}(R + w) \frac{\partial v_f}{\partial q} = 0 \quad (4.21)$$

$$\rho_f \left[\frac{\partial v_f(q, t)}{\partial t} + v_f \frac{\partial v_f}{\partial q} \right] + \frac{\partial p}{\partial q} = 0 \quad (4.22)$$

By means of the transformation formulas (4.19) and (4.20), we cast equations (4.21) and (4.22) in the form

$$\dot{w} + \dot{w}u' - w'\dot{u} + v_f w' + \frac{1}{2}(R + w)v_f' = 0 \quad (4.23)$$

$$\rho_f(\dot{v}_f + \dot{v}_f u' - v_f' \dot{u} + v_f v_f') + p' = 0 \quad (4.24)$$

We repeat that these are not Lagrangian equations, but simply Eulerian equations pulled back to another coordinate system. Within the context of the constant velocity profile, these equations are exact, in the sense that they impose no limitation to the magnitudes of the displacements.

As far as the constitutive equation of the tube is concerned, we will only assume a hyperelastic isotropic behaviour, governed by a stored energy density Σ per unit volume of a natural state, given by:

$$\Sigma = \Sigma(\Lambda_1, \Lambda_2) \quad (4.25)$$

where Λ_1 and Λ_2 are the principal stretches measured from the natural state. If, for instance, the reference configuration happens to be in a natural state, the principal

stretches are given by

$$\begin{aligned}\Lambda_1 &= \sqrt{(1 + u')^2 + w'^2} \\ \Lambda_2 &= 1 + \frac{w}{R}\end{aligned}\tag{4.26}$$

For any other (cylindrical) reference configuration, the formulas for the principal stretches are obtained from Eq. (4.17) as:

$$\begin{aligned}\Lambda_1 &= (1 + U')\sqrt{(1 + \hat{u}')^2 + \hat{w}'^2} \\ \Lambda_2 &= \frac{1 + \frac{\hat{w}}{R}}{1 - \frac{\hat{W}}{R}} = \left(1 + \frac{W}{R}\right)\left(1 + \frac{\hat{w}}{R}\right)\end{aligned}\tag{4.27}$$

where ‘hatted’ quantities are measured from the prestressed reference configuration and U' is the constant longitudinal prestretch with respect to the natural configuration. We recall from Eq. (2.27) the Cauchy stresses are obtained as

$$\begin{aligned}\sigma_1 &= \Lambda_1 \frac{\partial \Sigma}{\partial \Lambda_1} \\ \sigma_2 &= \Lambda_2 \frac{\partial \Sigma}{\partial \Lambda_2}\end{aligned}\tag{4.28}$$

4.4 Solitary Waves and Variational Formulation

In a typical problem, the tube is assumed to be prestressed uniformly while the fluid moves at a constant speed $v_{f\infty}$. It is upon this background state that the solitary pulse travels. Therefore, to look for the traveling wave we seek a solution of the form

$$\begin{aligned}\hat{u} &= \hat{u}(\hat{x}, t) = \hat{u}(\hat{x} - \hat{c}t) \\ \hat{w} &= \hat{w}(\hat{x}, t) = \hat{w}(\hat{x} - \hat{c}t)\end{aligned}\tag{4.29}$$

where \hat{c} is the wave speed and where, as before, hatted quantities refer to the prestressed background configuration. For the natural state, therefore, according to Eq.

(4.17) we must have, after some simple transformations,

$$\begin{aligned} u &= u(x - ct) + U'ct = u(\xi) + U'ct \\ w &= w(x - ct) = w(\xi) \end{aligned} \quad (4.30)$$

where u and w are the shape functions to be found and c is the solitary wave speed per unit length (x) of the natural state.

Retaining the primes for ξ -derivatives, and substituting Eq. (4.30) into Eq. (4.15) and (4.16), yields the reduced system of nonlinear ODEs

$$\left[\sigma_1 \frac{1 + u'}{(1 + u')^2 + w'^2} \right]' - \frac{p}{h} \left(1 + \frac{w}{R} \right) w' = \rho c^2 u'' \quad (4.31)$$

$$\left[\sigma_1 \frac{w'}{(1 + u')^2 + w'^2} \right]' - \frac{\sigma_2}{R + w} + \frac{p}{h} \left(1 + \frac{w}{R} \right) (1 + u') = \rho c^2 w'' \quad (4.32)$$

Similarly, Eq. (4.23) and Eq. (4.24) yield

$$(v_f - (1 + U')c)w' + \frac{1}{2}(R + w)v_f' = 0 \quad (4.33)$$

$$\rho_f(v_f - (1 + U')c)v_f' + p' = 0 \quad (4.34)$$

Remarkably, although Eq. (4.23) and Eq. (4.24) contain terms involving derivatives of the axial displacement u , these terms cancel out upon enforcing the conditions embodied in Eq. (4.30). Recalling §2.3, we know that these two equations can be integrated *exactly* to obtain an explicit connection between pressure and radial displacement. A straightforward integration yields:

$$p = p_\infty + \frac{1}{2}\rho_f((1 + U')c - v_{f\infty})^2 \left[1 - \left(\frac{R + w_\infty}{R + w} \right)^4 \right] \quad (4.35)$$

where p_∞ , v_∞ and w_∞ are known conditions at infinity. This rather sophisticated pressure-displacement coupling will be the basis for our considerations. In fact, since an observer moving with the solitary wave will perceive a state of steady flow in a fixed tube, Eq. (4.35) could have been obtained directly by elementary means, a fact that will be used in a later chapter.

Whatever configuration is used as reference, therefore, once the values of W and U' are specified, the values of Λ_1 and Λ_2 in the prestressed configuration can be calculated, and hence the corresponding values of the stress components. Moreover, given the background fluid velocity $v_{f\infty}$, the value of the pressure at infinity can be calculated from Eq. (4.32), using $w'_\infty = w''_\infty = 0$, as

$$p_\infty = \frac{\sigma_{2\infty} R h}{(R + w_\infty)^2 (1 + u'_\infty)} \quad (4.36)$$

We now attempt to provide a variational formulation for the whole problem. In other words, we seek a Lagrangian density $L = L(u, u', w, w')$ whose associated Euler-Lagrange equations are Eq. (4.31) and (4.32), with p given by Eq. (4.35). It should not be surprising that the elastic part of these equations may be cast in a variational form governed by the stored energy function. What seems less likely is that the complicated terms involving the pressure, as given by Eq. (4.35), may also be obtainable in this way. Indeed, if we regard Eq. (4.31) and (4.32) as a dynamical system with two degrees of freedom (imagining for a moment that the primes denote time derivatives), it is apparent that the pressure terms are not conservative, since

they involve derivatives. Nevertheless, it can be verified that the function

$$L = \frac{1}{2}\rho c^2(u'^2 + w'^2) - \Sigma(\Lambda_1, \Lambda_2) + \frac{1+u'}{2hR}(R+w)^2 \left[p_\infty + \frac{1}{2}\rho_f(v_{f\infty} - (1+U')c)^2 \left(1 + \left(\frac{R+w_\infty}{R+w} \right)^4 \right) \right] \quad (4.37)$$

when used in the variational statement

$$\delta \int L d\xi = 0 \quad (4.38)$$

yields the desired result. Indeed, it can be verified by direct calculation that the Euler-Lagrange equations of Eq. (4.38), viz,

$$\frac{\partial L}{\partial u} - \frac{d}{d\xi} \left(\frac{\partial L}{\partial u'} \right) = 0 \quad (4.39)$$

$$\frac{\partial L}{\partial w} - \frac{d}{d\xi} \left(\frac{\partial L}{\partial w'} \right) = 0 \quad (4.40)$$

reproduce exactly Eq. (4.31) and (4.32), with the pressure given by Eq. (4.35). In the dynamical system analogy, we observe that the pressure contribution to Eq. (4.37) will affect both the “potential” and the “kinetic” energy of the system.

4.5 Noether's Theorem, first integrals and numeric solvability

If Eq. (4.31) and (4.32) are regarded as a general coupled nonlinear system of second-order ODEs, the problem of finding a solution with the typical shape of a solitary wave would be frighteningly difficult. This is because, for any assumed value of the speed of propagation c , we would have to find, by trial and error, the finely tuned

values of the ‘initial’ conditions (at say $\xi = 0$) which lie exactly at the transition (the separatrix) between the oscillatory and divergent behaviours. When only one displacement component is considered, this task is reasonably simple, but luckily we do not have to resort to such brute force approaches. We hold the advantage of having a way to *calculate* the amplitude which admits a solitary wave for a particular wave speed either numerically or analytically a-priori, as has already been demonstrated for a single dependent variable in Chapter 2 and Chapter 3. In the case of two coupled displacement variables, these a-priori calculations become absolutely necessary.

The key to such procedures resides in finding first integrals (‘conserved quantities’). When a variational principle is involved, a celebrated theorem of Noether (see, for example Lovelock and Rund, 1975) establishes, roughly, that for every symmetry of the Lagrangian there is an associated conserved quantity. Symmetries, in the most general setting, are given by one-parameter groups of transformations leaving the Lagrangian unaffected. Noether’s theorem then gives explicit conserved quantities in terms of quantities associated with the corresponding group. In our case, moreover, two symmetries of the Lagrangian are obvious: the absence of an explicit dependence on u (conservation of axial ‘momentum’), and the absence of an explicit dependence on ξ (conservation of ‘energy’). The associated conserved quantities do not have the physical meaning of momentum and energy, but have the same formal meaning and mathematical usefulness. The conservation law associated with u is obvious from Eq. (4.39):

$$\frac{\partial L}{\partial u'} = C_1 \quad (4.41)$$

while the conserved quantity associated with the explicit absence of ξ is, according

to Noether's theorem:

$$L - \frac{\partial L}{\partial u'} u' - \frac{\partial L}{\partial w'} w' = C_2 \quad (4.42)$$

where C_1 and C_2 are constant on the solutions of the system. Equation (4.42) is also known as Jacobi's integral. These conservation laws would have been very hard to recognize by direct inspection of Eq. (4.31) and (4.32), but emerge quite naturally from the variational formulation.

Combining Eq. (4.37) with (4.41) we obtain:

$$\begin{aligned} & \rho c^2 u' - \sigma_1 \frac{1 + u'}{(1 + u')^2 + w'^2} + \\ & \frac{(R + w)^2}{2hR} \left[p_\infty + \frac{1}{2} \rho_f (v_{f\infty} - (1 + U')c)^2 \left(1 + \left[\frac{R + w_\infty}{R + w} \right]^4 \right) \right] = C_1 \end{aligned} \quad (4.43)$$

By enforcing the conditions at infinity (including $w'_\infty = 0$) we obtain:

$$C_1 = \rho c^2 u'_\infty - \frac{\sigma_{1\infty}}{1 + u'_\infty} + \frac{(R + w_\infty)^2}{2hR} (p_\infty + \rho_f (v_{f\infty} - (1 + U')c)^2) \quad (4.44)$$

Note the presence of c as a parameter. Using Eq. (4.42) for the second conserved quantity, and taking account of Eq. (4.37) and (4.41), we obtain:

$$\begin{aligned} & \frac{1}{2} \rho c^2 (u'^2 + w'^2) - \Sigma(\Lambda_1, \Lambda_2) + \\ & \frac{1 + u'}{2hR} (R + w)^2 \left[p_\infty + \frac{1}{2} \rho_f (v_{f\infty} - (1 + U')c)^2 \left(1 + \left[\frac{R + w_\infty}{R + w} \right]^4 \right) \right] - \\ & C_1 u' - \left(\rho c^2 w' - \sigma_1 \frac{w'}{(1 + u')^2 + w'^2} \right) w' = C_2 \end{aligned} \quad (4.45)$$

Again, using the conditions at infinity yields the value of C_2 as:

$$\begin{aligned} C_2 = & -\frac{1}{2} \rho c^2 u_\infty'^2 - \Sigma_\infty + \sigma_{1\infty} \frac{u'_\infty}{1 + u'_\infty} + \\ & \frac{(R + w_\infty)^2}{2hR} [p_\infty + \rho_f (v_{f\infty} - (1 + U')c)^2] \end{aligned} \quad (4.46)$$

It is worth noting that the dependence on w' is everywhere through its square.

Let us represent Eq. (4.43) and (4.45) as:

$$\mathcal{F}_c(u', w, w'^2) = 0 \quad (4.47)$$

$$\mathcal{G}_c(u', w, w'^2) = 0 \quad (4.48)$$

where \mathcal{F}_c and \mathcal{G}_c are the functions embodied in Eq. (4.43) and (4.45), with the constants given by Eq. (4.44) and (4.46), and where the dependence on the speed c is specified as a parameter. In the vicinity of points where a suitable Jacobian determinant does not vanish, the implicit function theorem allows us to eliminate u' from Eq. (4.47) and (4.48) and to write the result as a function of the form

$$w'^2 = f_c(w) \quad (4.49)$$

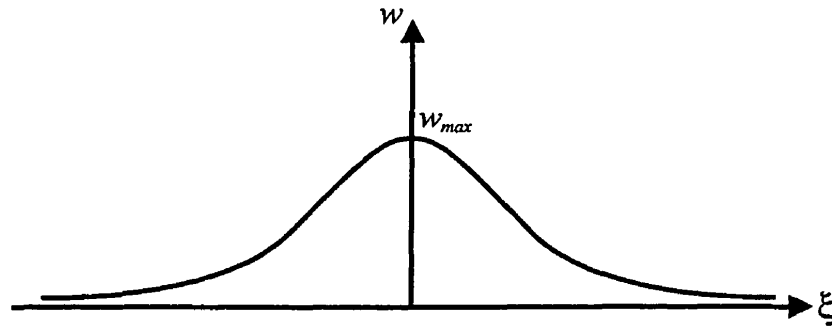


Figure 4.4: General shape of the solitary wave

Let us now confine our attention to a solitary wave having the general appearance shown in Figure 4.4, that is, satisfying the following condition: it has one ‘bump’

and then it tends exponentially, without any oscillations, to a common value, w_∞ on either side of the origin. In other words, outside of the ‘small’ interval where the pulse exists, the function is practically indistinguishable from a constant. This case is analogous to the situation examined in Chapter 3, where the first integral was determined exactly. Equation (4.49) therefore immediately implies that the function f_c must have a double root at $w = w_\infty$ and have another (simple) root at $w = w_{max}$ ($> w_\infty$), namely, at the value of the amplitude of the wave. The general appearance of f_c is shown in Figure 4.5. The behavior outside the interval (w_∞, w_{max}) is irrelevant. Note that since Eq. (4.49) prescribes that f_c at w_∞ must be non-negative, it follows that the curvature of f_c at $w = w_\infty$ must be positive. We recall then that all that has to be done in order to find the amplitude of the solitary wave for any specified speed c is: (i) verify that the function f_c and its first derivative vanish at $w = w_\infty$, and that the curvature thereat is positive; and (ii) find the next root ($w = w_{max}$). If either (i) or (ii) are not feasible, then there is no solitary wave. From the practical point of view, then, we simply plot the function to get an idea about whether and where the root lies and then find the root to any desired degree of accuracy by, say, the method of halving the interval, or any other such simple procedure.

Because the shape of the wave is of interest, we could proceed to integrate Eq. (4.49) with the initial condition $w = w_{max}$. But, as has been discussed previously, this procedure would run into the difficulty that the solution $w = constant = w_{max}$ has been introduced in the process of producing the first integrals. One way to eliminate this problem consists of differentiating Eq. (4.49) and dividing by w' resulting in the

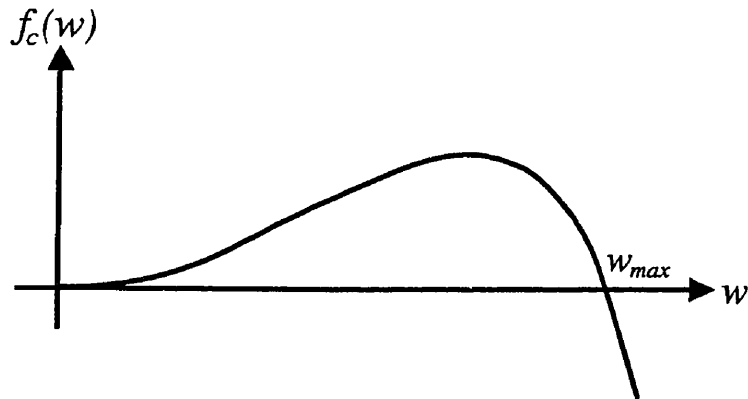


Figure 4.5: General appearance of Eq. (4.49)

second order equation

$$w'' = \frac{1}{2} \frac{df_c}{dw} \quad (4.50)$$

with the, now known, initial conditions $w(0) = w_{max}$, $w'(0) = 0$. Either this equation or, better still, the original system of coupled differential equations ((4.31) and (4.32)), can now be integrated by any of the common forward integration procedures for initial value problems in ordinary differential equations.

The crucial point has been the obtaining of the initial conditions by a direct procedure. For our direct approach, specifying initial conditions $w(0) < w_{max}$, $w'(0) = 0$ results in the behaviour of the solution becomes oscillatory where if $w(0) > w_{max}$, $w'(0) = 0$ the behaviour is divergent. It is a good idea, as has been shown, to verify that once a solution has been produced, a slight change of initial condition produces the desired effect.

To complete this section, we verify that the condition of w_∞ being a double root is

satisfied automatically, regardless of the constitutive equation for the wall material. We start by noting that, by construction of the constants of integration, w_∞ must be a root. Moreover, the derivative of f_c with respect to its argument (w) is given by the corresponding implicit expression as:

$$\frac{df_c}{dw} = \frac{\mathcal{F}_{u'}\mathcal{G}_w - \mathcal{G}_{w'}\mathcal{F}_w}{\mathcal{F}_{u'}\mathcal{G}_{w'^2} - \mathcal{F}_{w'^2}\mathcal{G}_{u'}} \quad (4.51)$$

where the subscripts in the right-hand side denote partial differentiation with respect to the indicated variable. From Eq. (4.43) and (4.45) we obtain:

$$\mathcal{F}_{u'}]_\infty = \rho c^2 - \left. \frac{\partial \sigma_1}{\partial u'} \right]_\infty \frac{1}{1 + u'_\infty} + \frac{\sigma_{1\infty}}{(1 + u'_\infty)^2} \neq 0 \quad (4.52)$$

$$\mathcal{G}_{w'}]_\infty = 0 \quad (4.53)$$

$$\mathcal{G}_w]_\infty = 0 \quad (4.54)$$

$$\mathcal{G}_{w'^2}]_\infty = -\frac{1}{2}\rho c^2 + \frac{1}{2} \frac{\sigma_{1\infty}}{(1 + u'_\infty)^2} \neq 0 \quad (4.55)$$

Equation (4.53) and Eq. (4.54) follow from a careful substitution of the values of C_1 and p_∞ . Equation (4.51) \rightarrow (4.55) imply that the root at w_∞ is indeed a double root.

4.6 Numerical Example

In order to demonstrate the usefulness of our direct method with two displacement components, we present a numerical example. We will make a qualitative comparison of the results with the one-dimensional example presented in Chapter 2. For this

example, we adopted the natural state as the reference configuration. The equations for the strain will then be given by Eq. (4.26).

We begin by non-dimensionalizing Eq. (4.31) and (4.32), (4.35) and the first integrals, Eq. (4.43), (4.44), (4.45) and (4.46). We will adopt a non-dimensionalization similar to Chapter 2, where

$$\begin{aligned}\sigma_1 &= \mu S_1, & \sigma_2 &= \mu S_2, \\ w &= R\bar{w}, & u &= L_0\bar{u}, & x &= L_0\bar{x}, \\ p &= \frac{h\mu}{2R} \bar{p}, \\ t &= T_0\bar{t}, \\ v_f &= \frac{L_0}{T_0} \bar{v}_f,\end{aligned}$$

and where μ is a “shear modulus” of the isotropic and incompressible elastic tube material,

$$L_0 = \left(\frac{Rh\rho}{2\rho_f}\right)^{1/2}, \quad T_0 = \left(\frac{\rho}{\mu}\right)^{1/2} R,$$

h tube wall thickness before deformation, ρ is the tube material density, ρ_f is the fluid density, R is the unstressed radius, and

$$m = \left(\frac{L_0}{R}\right)^2 = \frac{h\rho}{2R\rho_f} \quad \text{is the thickness parameter.}$$

Rewriting Eq. (4.31), (4.32), (4.35), (4.43), (4.44), (4.45) and (4.46) in terms of non-dimensional variables yields

$$\left[S_1 \frac{1 + \bar{u}'}{(1 + \bar{u}')^2 + \bar{w}'^2/m} \right]' - \frac{1}{2} \bar{p} (1 + \bar{w}) \bar{w}' = mc^2 \bar{u}'' \quad (4.56)$$

$$\left[S_1 \frac{\bar{w}'/m}{(1 + \bar{u}')^2 + \bar{w}'^2/m} \right]' - \frac{S_2}{1 + \bar{w}} + \frac{1}{2} \bar{p} (1 + \bar{w}) (1 + \bar{u}') = c^2 \bar{w}'' \quad (4.57)$$

$$\bar{p} = \bar{p}_\infty + \frac{1}{2}(\bar{v}_{f\infty} - (1 + U')c)^2 \left[1 - \left(\frac{1 + \bar{w}_\infty}{1 + \bar{w}} \right)^4 \right] \quad (4.58)$$

$$mc^2\bar{u}' - S_1 \frac{1 + \bar{u}'}{(1 + \bar{u}')^2 + \bar{w}'^2/m} + \frac{(1 + \bar{w})^2}{4} \left[\bar{p}_\infty + \frac{1}{2}(\bar{v}_{f\infty} - (1 + U')c)^2 \left(1 + \left[\frac{1 + \bar{w}_\infty}{1 + \bar{w}} \right]^4 \right) \right] = \bar{C}_1 \quad (4.59)$$

$$\bar{C}_1 = mc^2\bar{u}'_\infty - \frac{S_{1\infty}}{1 + \bar{u}'_\infty} + \frac{(1 + \bar{w}_\infty)^2}{4} (\bar{p}_\infty + (\bar{v}_{f\infty} - (1 + U')c)^2) \quad (4.60)$$

$$\begin{aligned} & \frac{1}{2}mc^2(\bar{u}'^2 + \bar{w}'^2/m) - \bar{\Sigma}(\Lambda_1, \Lambda_2) + \\ & \frac{1 + \bar{u}'}{4}(1 + \bar{w})^2 \left[\bar{p}_\infty + \frac{1}{2}(\bar{v}_{f\infty} - (1 + U')c)^2 \left(1 + \left[\frac{1 + \bar{w}_\infty}{1 + \bar{w}} \right]^4 \right) \right] - \\ & \bar{C}_1\bar{u}' - \left(mc^2\bar{w}' - S_1 \frac{\bar{w}'}{(1 + \bar{u}')^2 + \bar{w}'^2/m} \right) \frac{\bar{w}'}{m} = \bar{C}_2 \end{aligned} \quad (4.61)$$

$$\begin{aligned} \bar{C}_2 = & -\frac{1}{2}mc^2\bar{u}'_\infty{}^2 - \bar{\Sigma}_\infty + S_{1\infty} \frac{\bar{u}'_\infty}{1 + \bar{u}'_\infty} + \\ & \frac{(1 + \bar{w}_\infty)^2}{4} [\bar{p}_\infty + (\bar{v}_{f\infty} - (1 + U')c)^2] \end{aligned} \quad (4.62)$$

The only information missing is an expression for the strain energy density, Σ . We will again adopt the D1 constitutive equation used in Demiray (1996), which, in dimensional form, is given as

$$\Sigma_{D1} = \frac{\mu}{2\alpha} \{ \exp[\alpha(I_1 - 3)] - 1 \} \quad (4.63)$$

where I_1 is

$$I_1 = \Lambda_1^2 + \Lambda_2^2 + \frac{1}{\Lambda_1^2\Lambda_2^2} \quad (4.64)$$

Using Eq. (4.28) we find the non-dimensional stresses to be

$$\begin{aligned} S_1 &= \left(\Lambda_1^2 - \frac{1}{\Lambda_1^2 \Lambda_2^2} \right) \exp[\alpha(I_1 - 3)] \\ S_2 &= \left(\Lambda_2^2 - \frac{1}{\Lambda_1^2 \Lambda_2^2} \right) \exp[\alpha(I_1 - 3)] \end{aligned} \quad (4.65)$$

Substituting Eq. (4.63) and (4.65) into Eq. (4.59) and (4.61) leaves two first order ODEs in terms of \bar{u}' , \bar{w} and \bar{w}'^2 which are the embodiment of Eq. (4.48) and (4.47). We can therefore find a function of the form of Eq. (4.49) and determine the existence of solitary waves through the method described in §2.3.

We begin by selecting a representative wave speed of $c = 3.175$ (which corresponds to $\hat{c} = 7$ in the prestressed reference configuration). Initial prestrains of the tube are $\Lambda_1 = 1.5$ in the axial direction and $\Lambda_2 = 1.2$ in the hoop direction, which correspond to $W = \bar{w}_\infty = 0.2$ and $U' = \bar{u}'_\infty = 0.5$. The constant α is 1.948 and m , in the natural reference configuration, is 0.864 (corresponds to $\hat{m} = 0.4$). The last constant in the equations to be considered is $\bar{v}_{f\infty}$, which in this example will be $c/2$ or 1.5875.

We note that since $\bar{v}_{f\infty}$ appears always in the combination $[\bar{v}_{f\infty} - (1 + U')c]^2$, it follows that if a solitary wave exists for some fluid speed $\bar{v}_{f\infty}$, the same solitary wave will propagate at the same speed c for a fluid speed of $2(1 + U')c - \bar{v}_{f\infty}$. For given prestress conditions, solitary waves will exist only for certain combinations of c and $\bar{v}_{f\infty}$, conforming a 'domain of existence' in the $c, \bar{v}_{f\infty}$ -plane which will be symmetric with respect to the line $\bar{v}_{f\infty} = (1 + U')c$. For the prestress conditions of our example, this domain of existence does not cut the $v_{f\infty}$ axis, namely, solitary waves do not propagate when the fluid velocity is below a certain threshold (depending on the wave speed). Nevertheless, in past studies based on the long-wave approximation (see Erbay et al., 1992; Demiray, 1996) $\bar{v}_{f\infty}$ has been assumed to be zero, as was

also done for our example in Chapter 2.

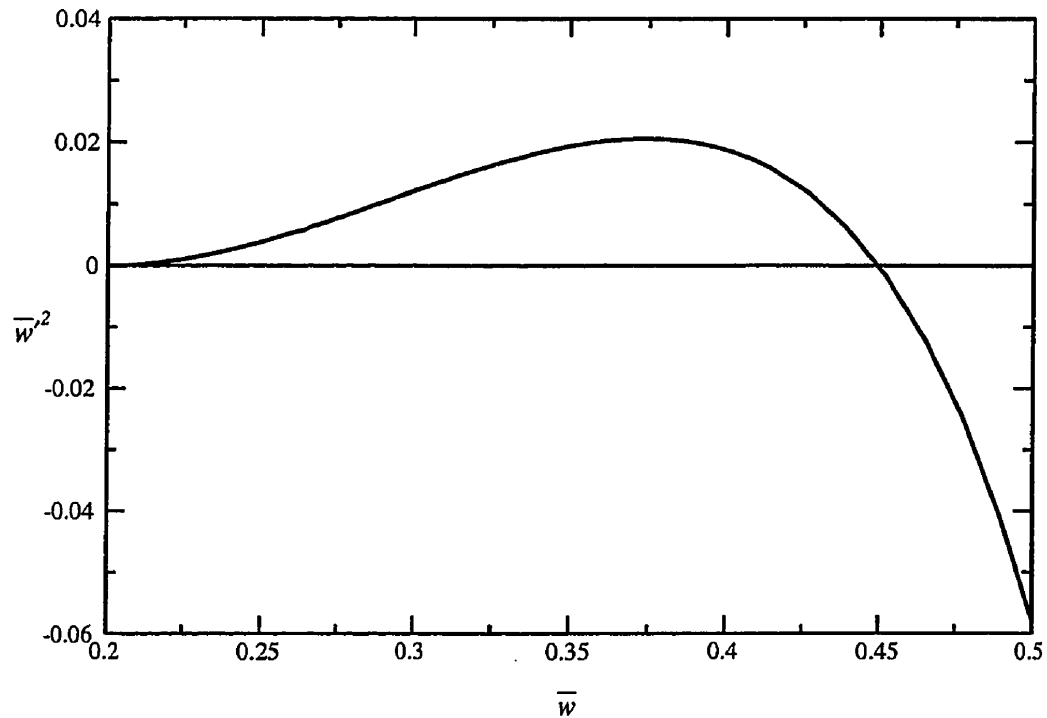


Figure 4.6: Actual shape of Eq. (4.49) for $c = 3.175$

With all the pieces in place, we can now attempt to determine a function of the form of Eq. (4.49) for this example. Upon inspection of equations (4.59) and (4.61) we can see that an equation of the form of Eq. (4.49) would be impossible to find analytically when using the D1 constitutive equation. As a consequence, the relationship between w^2 and w was calculated numerically by algebraic means. Figure 4.6 shows the relationship between \bar{w}^2 and \bar{w} as was determined for $c = 3.175$. We can see that this function does indeed have the predicted shape, shown in Figure

4.5. This function confirms the existence of a double root at $\bar{w}_\infty = 0.2$ and a single root at $\bar{w}_{max} = 0.449539$. In order to solve the original differential equations, we also need \bar{u}' at \bar{w}_{max} . By substituting \bar{w}_{max} and $\bar{w}' = 0$ into Eq. (4.48) and (4.47) we can solve for \bar{u}' . Doing this we find $\bar{u}' = 0.300717$ at \bar{w}_{max} .

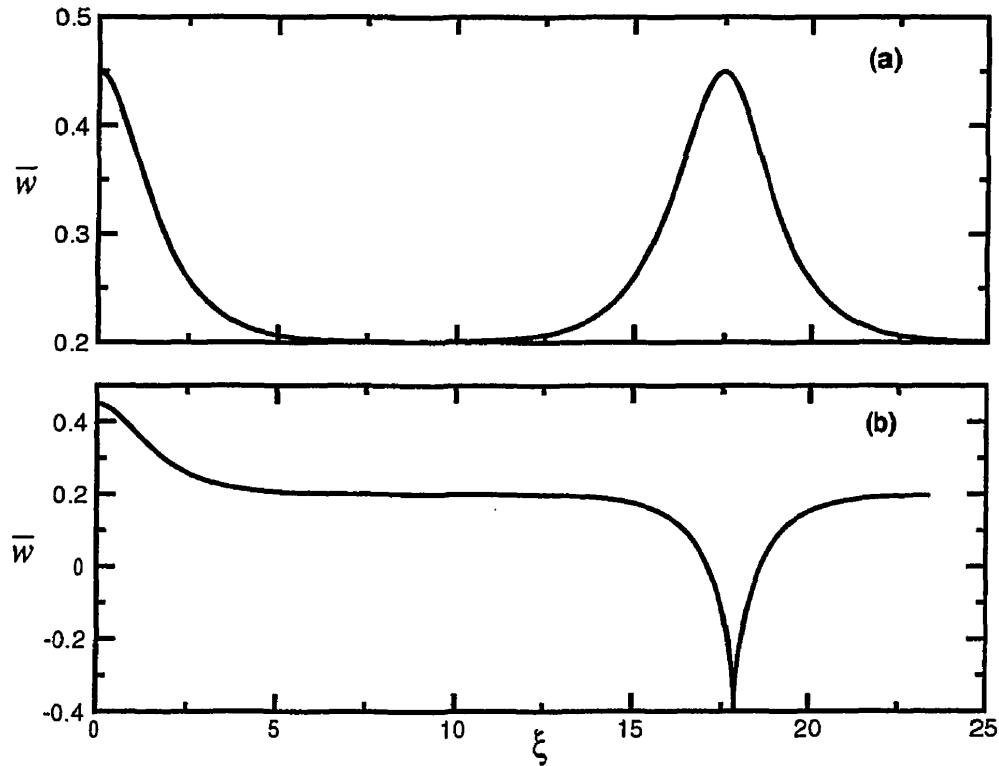


Figure 4.7: Comparison of solutions for initial conditions (a) $w_{max} = 0.4495390$ and (b) $w_{max} = 0.4495391$

It is important to note that the wave amplitude, \bar{w}_{max} , and the corresponding value of \bar{u}' were found, for a given speed, by purely algebraic means. To obtain the *shape* of the wave all we need is to solve the system of ordinary differential

equations (4.56) and (4.57) using these values as initial conditions. As a further definite verification that the initial conditions are correct, one observes the drastically different behaviours of the solution for very slight changes in the initial conditions. Indeed, if $\bar{w}(0) < \bar{w}_{max}$, the solution should be periodic, a feature that is lost as soon as $\bar{w}(0) > \bar{w}_{max}$. Figure 4.7a illustrates the solution obtained with Mathematica[®] when $\bar{w}_{max} = 0.4495390$ is used and Figure 4.7b illustrates the effect of increasing the initial condition to $\bar{w}_{max} = 0.4495391$. As the value of \bar{w}_{max} is increasingly refined, the period between successive pulses will increase until the solution reaches a limit of a single pulse. We can approximate this limit by the first pulse in the periodic solution. Figure 4.8 illustrates the shape of the solitary wave for a wave speed of $c = 3.175$. The final shape of the wave includes the effects of both \bar{w} and \bar{u} , with each material point, ξ having a position given by $\bar{w}(\xi)$ and $\xi + \bar{u}(\xi)$.

While there have been some observations concerning the legitimacy of neglecting the axial deformation (see Kuiken, 1984), there have been few attempts to determine the implications of this approximation analytically. Three recent papers (Demiray, 1997d; Demiray and Dost, 1998a; Antar and Demiray, 1999) are important in that they include axial displacements in the formulation of the equations of motion. Of particular interest for the purpose of comparison would be the first two (Demiray, 1997d; Demiray and Dost, 1998a), where the viscosity effects are neglected and where the reductive perturbation technique is used, as in most previous studies (Erbay et al., 1992; Demiray, 1996). The comparison with their own previous studies neglecting axial deformation, however, are not explicitly carried out in either of the studies of Demiray (1997d); Demiray and Dost (1998a). Our own results, based on the integration of the exact equations, seem to indicate qualitative differences with

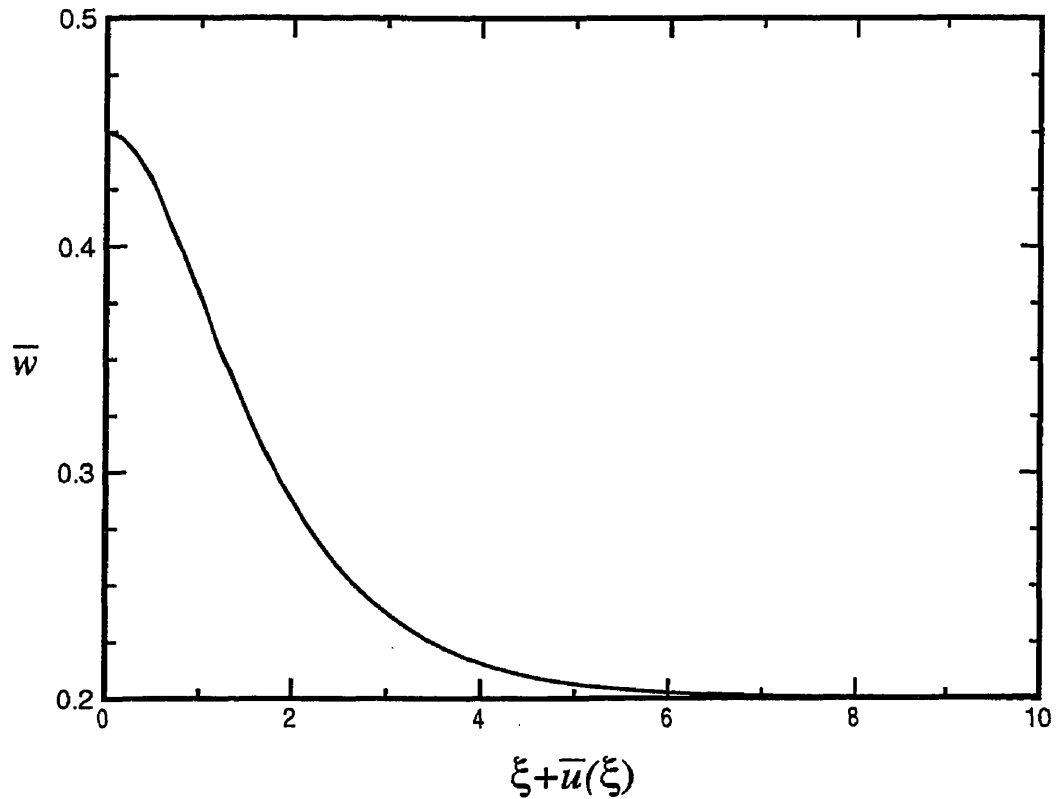


Figure 4.8: Calculated shape of the solitary wave for $c = 3.175$

those obtained using the reductive perturbation technique. In particular, the usual assumption $\bar{v}_{f\infty} = 0$ cannot be enforced in the solution of the exact equations.

As far as a comparison with our results obtained neglecting the axial displacement, the most notable difference is seen in the maximum amplitude of the solitary wave for equivalent wave speeds. The amplitude of the wave shown in Figure 4.8 is significantly larger (approximately 8 times) than that predicted in Table 2.1 (for $\hat{c} = 7$). This discrepancy suggests that the methodology of neglecting u (i.e. the long-

wavelength approximation) has a substantial impact on the physics of the problem. We can further examine this assertion by considering a less complex, but analogous closed form theoretical example.

4.7 Discussion

So as to understand qualitatively the underlying mathematical structure that may help to explain the drastic difference between solutions obtained by means of the long-wave approximation and those obtained from the exact equations, we consider now a highly simplified example that can be solved in closed form. Let the equations of motion for some system, after implementation of Eq. (4.30) be of the form

$$\rho\gamma^2 u'' = -(\gamma - \nu)^2 w' \quad (4.66)$$

$$\rho\gamma^2 w'' = -3w^2 + (\gamma - \nu)^2(2w + u') \quad (4.67)$$

It is easy to verify that this system derives from the Lagrangian density

$$L = \frac{1}{2}\rho\gamma^2(u'^2 + w'^2) + (\gamma - \nu)^2(wu' + w^2) - w^3 \quad (4.68)$$

In our intended analogy, γ and ν are parameters related to the wave speed and to the background fluid speed, respectively. In the long-wave approximation, Eq. (4.66) would be altogether neglected, while Eq. (4.67) becomes:

$$\rho\gamma^2 w'' = -3w^2 + 2(\gamma - \nu)^2 w \quad (4.69)$$

which has the first integral:

$$\frac{1}{2}\rho\gamma^2 w'^2 = -w^2(w - (\gamma - \nu)^2) + C \quad (4.70)$$

With $w_\infty = w'_\infty = 0$, the constant of integration C vanishes. The right-hand side has a double root at $w = 0$ and a single root at $w = (\gamma - \nu)^2$, and is positive in between, revealing that a solitary pulse-like wave corresponding to any speed γ will propagate with an amplitude:

$$w_{max} = (\gamma - \nu)^2 \quad (4.71)$$

Consider now, however, the original coupled system constituted by Eq. (4.66) and (4.67). Equation (4.66) has the first integral:

$$\rho\gamma^2 u' = -(\gamma - \nu)^2 w + D \quad (4.72)$$

where, from the conditions $u_\infty = w_\infty = 0$, the integration constant D vanishes. Substituting this result back into Eq. (4.67) yields:

$$\rho\gamma^2 w'' = -3w^2 + 2(\gamma - \nu)^2 w \left(1 - \frac{(\gamma - \nu)^2}{2\rho\gamma^2}\right) \quad (4.73)$$

which has the first integral

$$\frac{1}{2}\rho\gamma^2 w'^2 = -w^2 \left(w - (\gamma - \nu)^2 \left(1 - \frac{(\gamma - \nu)^2}{2\rho\gamma^2}\right)\right) \quad (4.74)$$

Thus we obtain the amplitude

$$w_{max} = (\gamma - \nu)^2 \left(1 - \frac{(\gamma - \nu)^2}{2\rho\gamma^2}\right) \quad (4.75)$$

which must be positive for the plot of the right-hand side of Eq. (4.74) to have the needed positivity between 0 and w_{max} . It follows that a solitary pulse-like wave will exist provided that

$$\gamma(1 - \sqrt{2\rho}) < \nu < \gamma(1 + \sqrt{2\rho}) \quad (4.76)$$

Assuming, for example, $\rho = 1/8$, it turns out that ν must lie in the interval $(\gamma/2, 3\gamma/2)$. In particular, $\nu = 0$ lies outside of this domain of existence (see Figure 4.9), so that, in this example at least, the fluid must have a non-vanishing background speed for the solitary wave to exist.

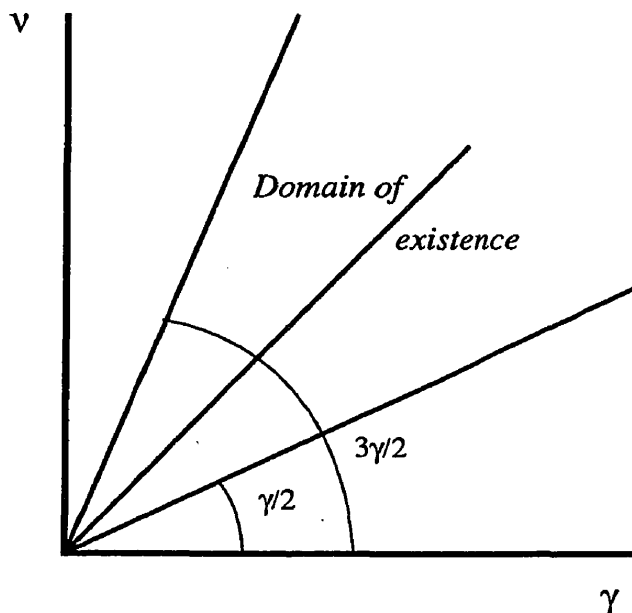


Figure 4.9: Domain of existence ($\rho = 1/8$) for simple model

This illustration, albeit an oversimplification of the model, shows the potential dangers involved in neglecting terms in a nonlinear setting. We turn now to the question of whether the long-wave approximation is justifiable in the case of an elastic membrane under small axisymmetric deformations. Prompted, perhaps, by the superficial analogy between these deformations and those of the classical linear beam theory, one may be tempted to conclude that the deformed meridian may

be obtained approximately by neglecting axial deformations. Nevertheless, in the case of a shell the radial deformation w is entirely accountable for the hoop strain (w/R) . The Poisson effect, therefore, will in general provide for the appearance of a longitudinal strain *of the same order of magnitude* as the hoop strain. Even assuming that the slope w' is negligible (long-wave approximation), the longitudinal strain is measured by u' . It follows that the neglected displacement derivative, u' , is of the same order of magnitude as the main (non-dimensionalized) displacement (w/R) which the theory is supposed to predict! In other words, what is wrong with the long-wave approximation is not the neglecting of the slope w' , but the disregard of that part of the longitudinal strain due to the derivative u' . Figure 4.10 shows \hat{u}' as a function of \hat{w} in the prestressed reference configuration for the numerical example of §4.6. Their ratio can be calculated to be about -0.63 , hardly a negligible amount! It is this type of reasoning that led us to the consideration of the coupled system described above.

4.8 Conclusions

In this chapter we have derived the kinematically exact governing equations for the tube wall accounting for both axial and radial displacements. The inclusion of both components of displacement produces a system of two nonlinear differential equations that must now be considered. This is accomplished through the use of the variational formulation of the governing equations. By invoking Noether's Theorem, we are able to exploit two obvious symmetries of the governing equations and find the corresponding first integrals. The first integrals are found to be functions of u' ,

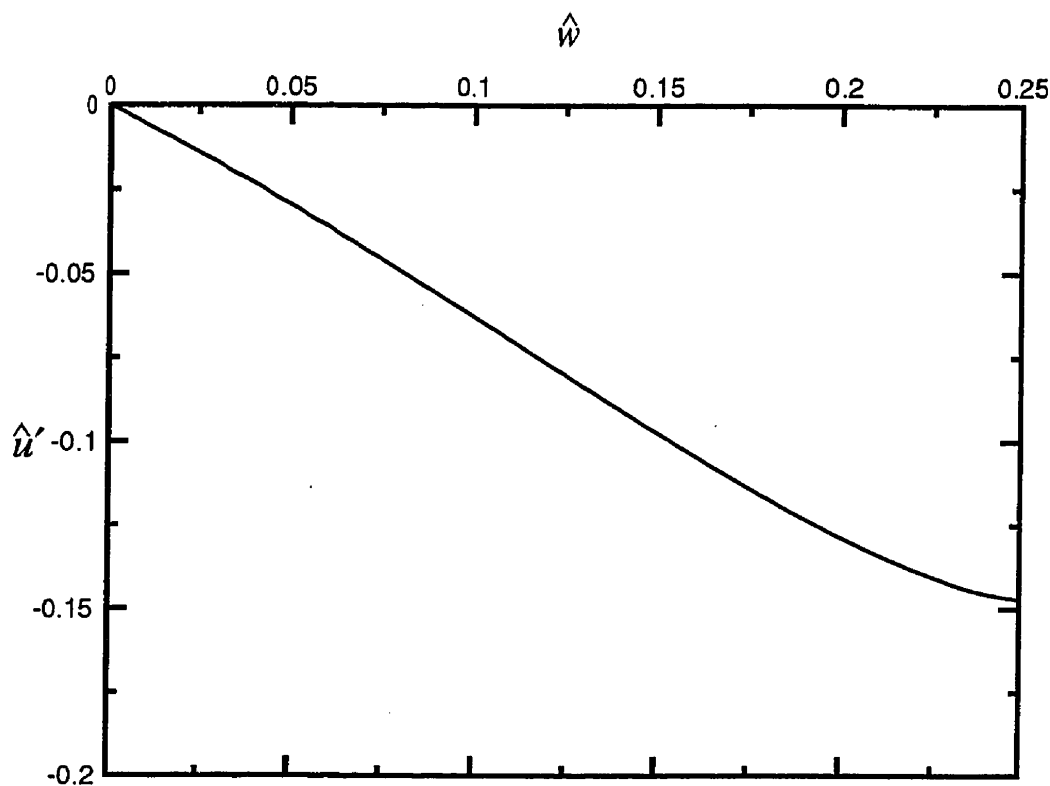


Figure 4.10: \hat{w} and \hat{u}' in the prestressed reference configuration of for $c = 3.175$

w and w'^2 alone. From this, a function of only w and w'^2 can be determined and the direct approach applied to the problem. Solitary wave solutions were determined for a wave speed of $c = 3.175$.

Several interesting consequences of including the axial displacement were found. Firstly, the wave amplitude determined in this chapter was found to be approximately 8 times greater than the amplitude found for the equivalent wave speed when only radial displacements are considered (Chapter 2). Additionally, it was found that the condition $v_{f\infty} = 0$ could not be enforced for the exact equations. This is exactly

opposite to the situation for the approximate equations when axial displacement is neglected.

In order to further examine the effects of including the axial displacement a simple theoretical example was examined. The benefit of this example was that it permitted a closed form solution to be determined. Based on this and an examination of the relationship between the axial and radial displacements in the prestress reference configuration, we concluded that the axial displacement is of the same order of magnitude as the radial displacement. This one point clearly illustrates the dangers in neglecting axial displacements and is perhaps the main contribution of this chapter.

In spite of its obvious extra complexity, the variational formulation with its attendant conserved quantities, permitted us to obtain a solution to the exact equations with hardly any extra computational effort. This is so because the existence of the first integrals allows for the prediction of the amplitude of the wave and the corresponding value of \bar{u}' by solving algebraic equations alone.

Chapter 5

Approximation of Axial Displacement

5.1 Introduction

The results of Chapter 4 clearly indicate the potential risk involved in assuming that the long wave approximation extends to allow the axial displacements to be neglected, as was done in Demiray (1996); Malfiet and Ndayirinde (1998) and many other studies. Clearly the axial displacement plays as significant a role as the radial displacement. While studies by Hashizume (1985), Demiray (1997d), Demiray and Dost (1998a), Antar and Demiray (1999) have investigated the effects of retaining the axial displacement, the solutions were determined through approximate techniques (RPT) and were not compared to existing results. In fact, Malfiet and Ndayirinde (1998) suggest in their study that neglecting u' has no significant effect on the solution. Clearly, that is not correct.

One of the motivations for neglecting u' in the governing equations is to render a problem of one dependent variable, which is less effort to solve than a problem of two dependent variables. In light of the approach presented in Chapter 4, which permits the determination of the exact solution of the two-dimensional equations with minimal effort, would a single variable problem be equally as compelling? In the end, there is still a certain appeal to formulating the problem in terms of only a single dependent variable.

How do we then do this when examination of the two-dimensional results clearly

shows that simply disregarding u' is not reasonable? A second possible option is to find a reasonable approximation for u' in terms of w . For this we can exploit the proposition that \bar{w} and \bar{u}' are not only of the same order of magnitude, but their relationship can be closely approximated by a linear function. This seems to be a reasonable assumption based upon the results shown in Figure 4.10.

In Chapter 4, the first integrals for the exact membrane equations were determined by applying Noether's theorem (Lovelock and Rund, 1975). Using the first integrals, the exact speed and amplitude of the solitary waves were determined through algebraic means. In this chapter, we also wish to utilize the first integrals, specifically the first integral of Eq. (4.15). In this chapter we will exchange Eq. (4.15) for its first integral, while retaining Eq. (4.16) exactly. Using this system of equations we can derive a single differential equation in terms of w , but one that also considers the contributions of u' .

In §5.2 we will derive the first integral of Eq. (4.15) in a manner similar to the derivation of the governing equations of the shell. We do this to present this approach in a self contained manner that does not rely on the use of variational principles. The formal description of this approximate approach is outlined in §5.2. The usefulness of this approach is illustrated in §5.4 by the presentation of two numerical examples. Finally, §5.5 presents a summary of the main points presented in this chapter.

5.2 Derivation of First Integral

We begin by considering a tube with the shape as shown in Figure 5.1, representing a section of a tube deformed by a solitary wave. Summing the forces in the axial

direction we find

$$2\pi(R+w)h^*\sigma_1 \cos \phi - \sigma_{1\infty}2\pi Rh + \int_{-\infty}^x p \sin \phi dA^* = \int_{-\infty}^x a_x dm \quad (5.1)$$

where σ_1 and $\sigma_{1\infty}$ represent the 'physical' longitudinal components of the three-dimensional Cauchy stress, as before, and a_x is the axial acceleration an element of tube dx long with mass dm . Substituting Eq. (4.4), $dA = dx ds$ and $ds = 2\pi R$ into Eq. (5.1) results in

$$2\pi(R+w)h^*\sigma_1 \cos \phi - \sigma_{1\infty}2\pi Rh + \int_{-\infty}^x p \sin \phi \left(1 + \frac{w}{R}\right) \sqrt{(1+u')^2 + w'^2} 2\pi R dx = \int_{-\infty}^x a_x dm \quad (5.2)$$

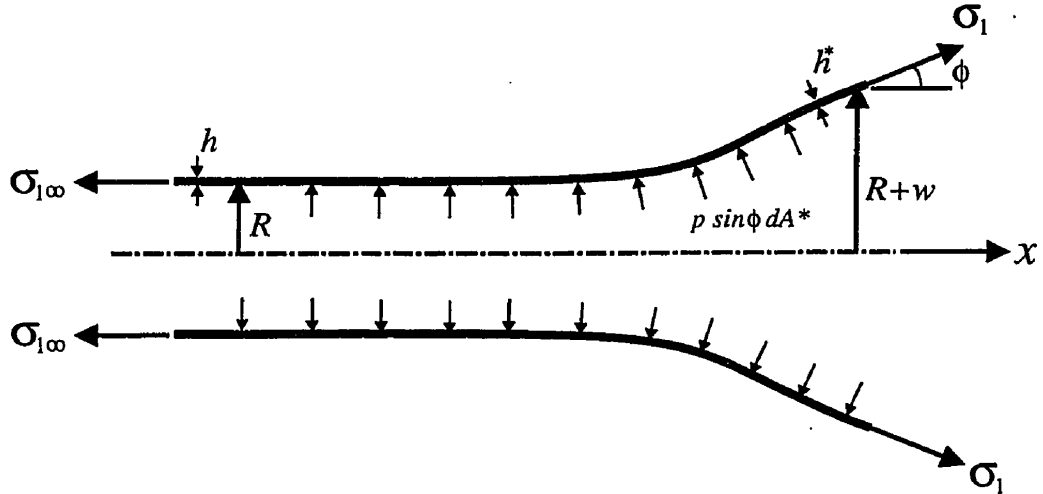


Figure 5.1: Section of tube deformed by solitary wave

From Eq. (4.5) we can find both $\sin \phi$ and $\cos \phi$. Substituting these into Eq.

(5.2) yields

$$\begin{aligned} \sigma_1 \left(\frac{1+u'}{\sqrt{(1+u')^2+w'^2}} \right) 2\pi(R+w)h^* - \sigma_{1\infty}2\pi Rh \\ + \int_{-\infty}^x p \left(\frac{w'}{\sqrt{(1+u')^2+w'^2}} \right) \left(1 + \frac{w}{R}\right) \sqrt{(1+u')^2+w'^2} 2\pi R dx = \int_{-\infty}^x a_x dm \end{aligned} \quad (5.3)$$

Again, we assume that the material is incompressible and so Eq. (5.3) can be simplified. Substituting Eq. (4.13) into Eq. (5.3) we find

$$\begin{aligned} \sigma_1 \left(\frac{1+u'}{(1+u')^2+w'^2} \right) 2\pi Rh - \sigma_{1\infty}2\pi Rh \\ + \int_{-\infty}^x pw' \left(1 + \frac{w}{R}\right) 2\pi R dx = \int_{-\infty}^x a_x dm \end{aligned} \quad (5.4)$$

If we consider the right hand side (RHS) of Eq. (5.4), we can write the mass of an element of the tube as $dm = \rho 2\pi Rh dx$ and that the acceleration of an element of mass in the axial direction $a_x = \ddot{u}$. If we substitute this into Eq. (5.4) we are left with

$$\begin{aligned} \sigma_1 \left(\frac{1+u'}{(1+u')^2+w'^2} \right) 2\pi Rh - \sigma_{1\infty}2\pi Rh \\ + \int_{-\infty}^x pw' \left(1 + \frac{w}{R}\right) 2\pi R dx = \int_{-\infty}^x \ddot{u} \rho 2\pi Rh dx \end{aligned} \quad (5.5)$$

It appears that without additional information concerning the variation of the dependent variables on x we cannot completely evaluate the integrals of Eq. (5.5). At this point, recalling that we have assumed a prestressed reference configuration, we invoke the traveling wave solution given by Eq. (4.29).

Retaining the primes for ξ -derivatives, and substituting Eq. (4.29) into Eq. (5.5)

yields the following

$$\begin{aligned} \sigma_1 \left(\frac{1 + u'}{(1 + u')^2 + w'^2} \right) 2\pi R h - \sigma_{1\infty} 2\pi R h \\ + \int_{-\infty}^{\xi} p w' \left(1 + \frac{w}{R} \right) 2\pi R d\xi = \int_{-\infty}^{\xi} c^2 u'' \rho 2\pi R h d\xi \end{aligned} \quad (5.6)$$

Recognizing that $dw = w'd\xi$ and $du' = u''d\xi$ and substituting this into Eq. (5.6), with the appropriate change of limits of integration, produces

$$\begin{aligned} \sigma_1 \left(\frac{1 + u'}{(1 + u')^2 + w'^2} \right) 2\pi R h - \sigma_{1\infty} 2\pi R h \\ + \int_0^w p \left(1 + \frac{w}{R} \right) 2\pi R dw = \int_0^{u'} c^2 \rho 2\pi R h du' \end{aligned} \quad (5.7)$$

The last piece of this puzzle comes in assuming a form for the expression for the pressure p , representing the solid-fluid interaction. We have already presented the basic equations for our one-dimensional, inviscid fluid model in terms of the traveling wave and have arrived at Eq. (4.35), which for the prestressed reference configuration will be

$$p = p_{\infty} + \frac{1}{2} \rho_f (c - v_{f\infty})^2 \left[1 - \left(\frac{R}{R + w} \right)^4 \right] \quad (5.8)$$

The free stream velocity is the fluid speed measured in the prestressed reference configuration. If we now substitute Eq. (5.8) into Eq. (5.7), perform the integrations and divide both sides by $2\pi R h$, we find the final result to be

$$\begin{aligned} c^2 \rho u' - \sigma_1 \left(\frac{1 + u'}{(1 + u')^2 + w'^2} \right) + \frac{(R + w)^2}{2Rh} \left(p_{\infty} + \frac{1}{2} \rho_f (c - v_{f\infty})^2 \left(1 + \left(\frac{R}{R + w} \right)^4 \right) \right) \\ + \sigma_{1\infty} - \frac{R}{2h} (p_{\infty} + \rho_f (c - v_{f\infty})^2) = 0 \end{aligned} \quad (5.9)$$

This equation represents the balance of forces acting on the tube, in the axial direction, for any deformation imposed by the solitary wave.

If we compare Eq. (5.9) to Eq. (4.43), including Eq. (4.44), we find that they are identical. While we could have skipped the above derivation by simply taking Eq. (4.43) directly from Chapter 4, the presentation of this alternate derivation of the first integral provides an alternate and independent approach, which is our aim in this chapter.

5.3 Approximation of u'

Having derived the first integral of Eq. (4.31), we can now choose to consider Eq. (5.9) in its place, while still retaining the radial equation of motion, Eq. (4.32), exactly. The advantage of making this substitution is that Eq. (5.9) provides the means to determine a direct relationship between u' and w , which can be used in Eq. (4.32) to eliminate the dependence on u' and leave a function of w only.

If we assume that all terms involving w'^2 in Eq. (5.9) can be neglected, (i.e. the waves are relatively long), we are left with

$$c^2 \rho u' - \sigma_1 \left(\frac{1}{1+u'} \right) + \frac{(R+w)^2}{2Rh} \left(p_\infty + \frac{1}{2} \rho_f (c - v_{f\infty})^2 \left(1 + \left(\frac{R}{R+w} \right)^4 \right) \right) + \sigma_{1\infty} - \frac{R}{2h} (p_\infty + \rho_f (c - v_{f\infty})^2) = 0 \quad (5.10)$$

which now involves only terms of u' and w .

If we refer to Figure 4.10, it would appear reasonable to assume that, in the prestressed reference configuration, the relationship between \bar{u}' and \bar{w} could be approximated well by a linear function. It would then follow that Eq. (5.10) could also

be approximated by a linear function. This is a consequence of the fact that any solution of Eq. (4.43) and Eq. (4.45) would have to satisfy both equations separately.

Let us then say that Eq. (5.10) could be replaced by a function of the form $u' = K_c w$, where the constant K_c is unique for each wave speed. The procedure for determining the constant K_c involves performing a simple linear regression on Eq. (5.10). Once the value of K_c is determined, $u' = K_c w$ can be substituted into Eq. (4.32), leaving

$$\left[\sigma_1 \frac{w'}{(1 + K_c w)^2 + w'^2} \right]' - \frac{\sigma_2}{R + w} + \frac{p}{h} \left(1 + \frac{w}{R}\right) (1 + K_c w) = c^2 \rho w'' \quad (5.11)$$

We would, of course, also need to substitute $u' = K_c w$ into Eq. (4.27), which would appear in Eq. (5.11) through σ . A problem of this form could then be easily tractable using the direct approach presented in Chapter 2.

We have, however, chosen to retain the w'^2 terms in Eq. (5.11). This is, in general, not necessary if the waves are small (long wavelength), but becomes significant when the waves take on larger amplitudes, as we have shown previously. It will be shown in the numerical example that the necessity of ignoring w'^2 in determining the linear approximation of u' does not introduce any significant error into the final solution.

5.4 Example of Approximate Solution

We now proceed to examine two sample cases numerically. In doing so, we begin by non-dimensionalizing our equations. We continue to use the non-dimensional parameters given in §4.6. We now consider Eq. (4.57) in place of Eq. (4.32) and the non-dimensionalized form of Eq. (5.10), where we recall that \bar{w}'^2 has been neglected,

so that

$$\begin{aligned}
mc^2\bar{u}' - \tilde{S}_1 \frac{1}{(1 + \bar{u}')} + \frac{(1 + \bar{w})^2}{4} \left[\bar{p}_\infty + \frac{1}{2}(\bar{v}_{f\infty} - c)^2 \left(1 + \left[\frac{1}{1 + \bar{w}} \right]^4 \right) \right] \\
+ \tilde{S}_{1\infty} - \frac{1}{4}(\bar{p}_\infty + (c - \bar{v}_{f\infty})^2) = 0
\end{aligned} \tag{5.12}$$

and \tilde{S} is an approximation of the true stress with $\bar{w}'^2 = 0$. In order to make a comparison to the results of Chapter 4, we will continue to use the D1 constitutive equation given by Eq. (4.63).

For this example, we will consider two wave speeds, $c = 6.05$, a small amplitude wave, and $c = 7$, a moderate wave amplitude. These values correspond to $c = 2.744$ and $c = 3.175$ in the natural reference configuration. The background fluid velocity, $\bar{v}_{f\infty}$, will be set to $c/3$ in each case (corresponding to $c/2$ in the natural reference configuration). We also choose the initial prestretches to be $\Lambda_1 = 1.5$ and $\Lambda_2 = 1.2$, which corresponds to $U' = 0.5$ and $W = 0.2$.

We now look to find a linear approximation to Eq. (5.12) for our two example wave speeds. Figure 5.2 and Figure 5.3 show the plots of Eq. (5.12) and the linear functions over appropriate intervals for $c = 6.05$ and $c = 7$, respectively. The best fit linear approximation for $c = 6.05$ is $\bar{u}' = -0.533376 \bar{w}$ and for $c = 7$ is $\bar{u}' = -0.637578 \bar{w}$.

We can now make a complete substitution of \bar{u}' in Eq. (4.57) as well as Eq. (4.27). This will leave us with a single second-order ODE, given by

$$\left[S_1 \frac{\bar{w}'/m}{(1 + K_c \bar{w})^2 + \bar{w}'^2/m} \right]' - \frac{S_2}{1 + \bar{w}} + \frac{1}{2} \bar{p}(1 + \bar{w})(1 + K_c \bar{w}) = c^2 \bar{w}'' \tag{5.13}$$

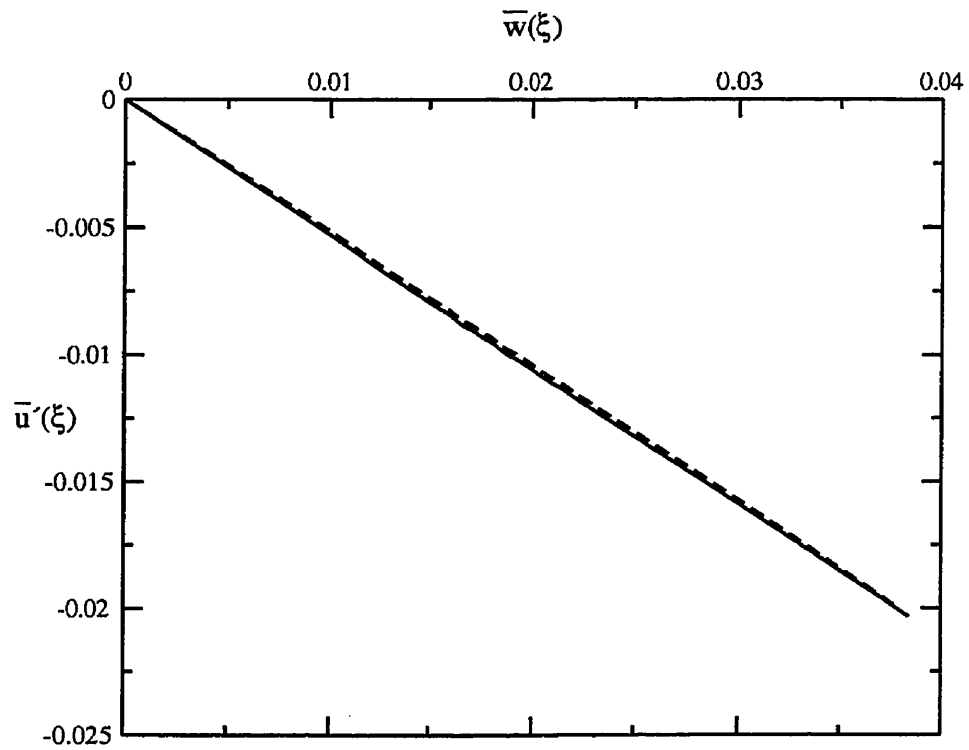


Figure 5.2: Plot of Eq. (5.12) (---) and the linear approximation (—) for $c = 6.05$

where the principal stretches are now

$$\Lambda_1 = (1 + U') \sqrt{(1 + \bar{u}')^2 + \frac{1}{m} \bar{w}'^2}$$

$$\Lambda_2 = (1 + W)(1 + \bar{w})$$

We can now solve this problem exactly using our direct approach. The approach for solving a problem of this form prescribes that we attempt to write Eq. (5.13) in the form given by Eq. (2.5), or

$$\bar{w}'' = F_c(\bar{w}, \bar{w}'^2)$$

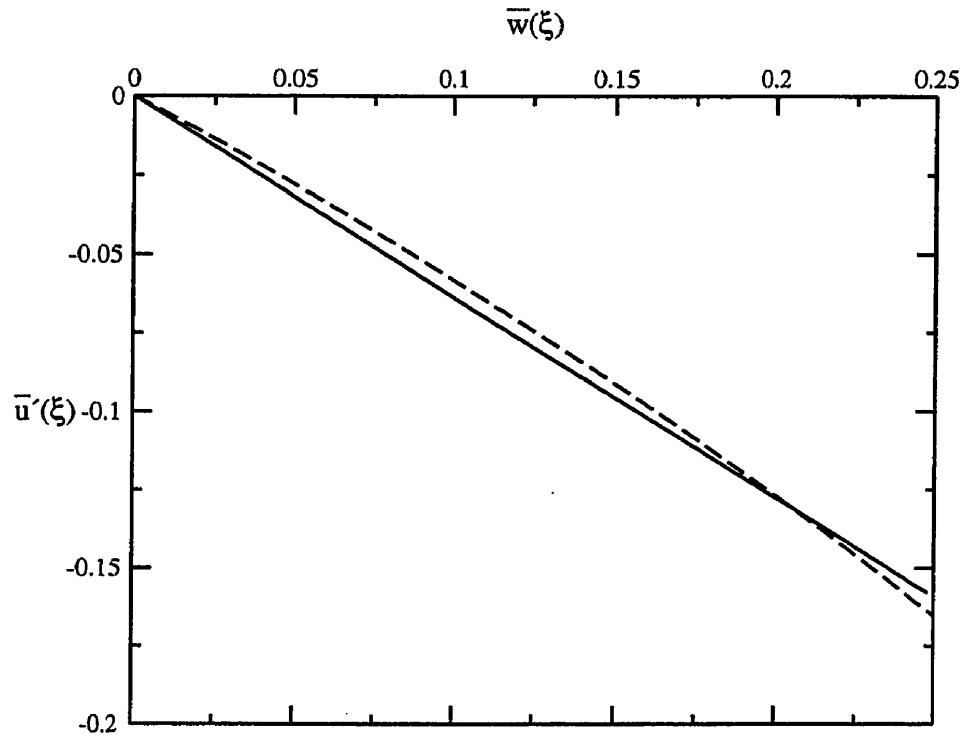


Figure 5.3: Plot of Eq. (5.12) (---) and the linear approximation (—) for $c = 7$

where \bar{w} and \bar{w}'^2 must be able to be separated into the form of Eq. (2.8). Rewriting Eq. (5.13) in this form would allow us to reduce it to the form of Eq. (2.6) and to determine the wave amplitude, \bar{w}_{max} , for which a solitary wave exists. Unfortunately, if the terms involving S_1 and S_2 are expanded, we find that we cannot separate the terms containing \bar{w} and \bar{w}'^2 into the form of Eq. (2.8). Consequently, we cannot match either Case 1 or Case 2 from §2.2.

The alternate approach presented in §2.4 is to consider a very small initial value of the wave amplitude as the initial conditions in the numerical integration. The solution will then proceed asymptotically to the maximum wave amplitude, \bar{w}_{max} , for

the specified wave speed. If we do this for Eq. (5.13), we find that the maximum wave amplitude for $c = 6.05$ is 0.040928 and for $c = 7$ is 0.203071, representing an error of approximately 3% from the exact values of 0.042190 and 0.207917 respectively. Using the maximum wave amplitude determined here, we are able to determine the shape of the solitary waves. Figure 5.4 illustrates the waves predicted using this approximate approach as compared to the waves determined using the exact approach in Chapter 4. We can clearly see that the predicted shape of the waves with the approximation for u' match closely with the shape of the exact waves.

If we were also to neglect w'^2 in Eq. (5.13) we would be able to simplify Eq. (5.13) to a function of the form $w'' = F_c(w)$, namely

$$w'' = \frac{\frac{\bar{S}_2}{1+\bar{w}} - \frac{1}{2}(\bar{p}_\infty + \frac{1}{2}(\bar{v}_{f\infty} - c)^2(1 - (\frac{1}{1+\bar{w}})^4))(1 + \bar{w})(1 + K_c\bar{w})}{\frac{\bar{S}_1/m}{(1+K_c\bar{w})^2} - c} \quad (5.14)$$

Using this relationship we could easily find the maximum amplitude for the solitary waves. Having done this, the maximum wave amplitude determined with $w'^2 = 0$ was 0.0471267 for $c = 6.05$ and 0.230291 for $c = 7$. This represents a 11% error from the exact wave amplitudes, for both wave speeds.

It should be noted that the appropriate interval for the linear fit is given by the maximum wave amplitude. In some cases this may need to be determined by an iterative procedure where an initial estimate of the maximum wave amplitude is used to determine the linear function. If the wave amplitude calculated using this linear function is significantly different from the initial guess, the linear function would be recalculated using the new wave amplitude. Iterations are continued until the calculated wave amplitude converges with the bounding amplitude of the linear fit.

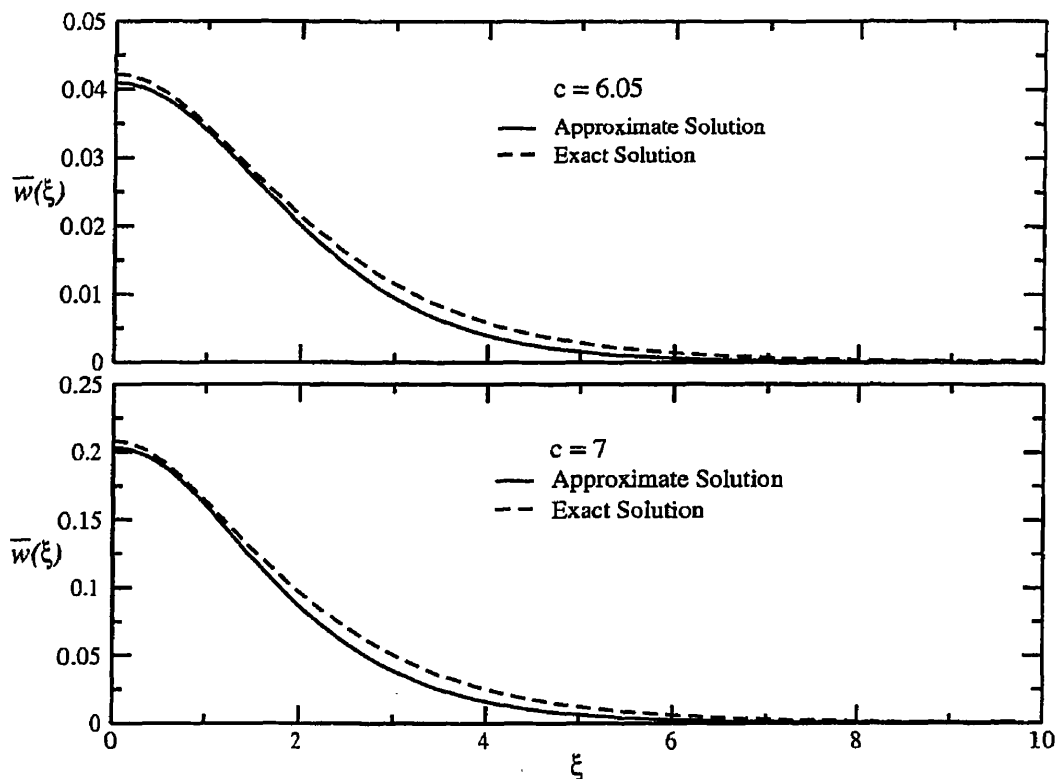


Figure 5.4: Solitary wave profiles for the approximation $\bar{u}' = K_c \bar{w}$ and the exact solution for $c = 6.05$ and $c = 7$

It is interesting to notice that a solution to Eq. (5.13) is also only possible if the value of $\bar{v}_{f\infty}$ is non-zero; exactly as it is for the exact equations. The significance of this is seen in Figure 5.5, which illustrates graphically the domain of existence for the solitary waves in the $c, \bar{v}_{f\infty}$ -plane. It was noted in Chapter 4 that the domain of existence will be symmetric with respect to the line $\bar{v}_{f\infty} = c$. We have not shown this symmetry in Figure 5.5. If we had proceeded by disregarding \bar{u}' completely (and consequently Eq. (4.31)), a solution would only be possible if the value of $\bar{v}_{f\infty}$ was

exactly zero. This certainly underscores the effect even small parameters can have on the solution of nonlinear problems.

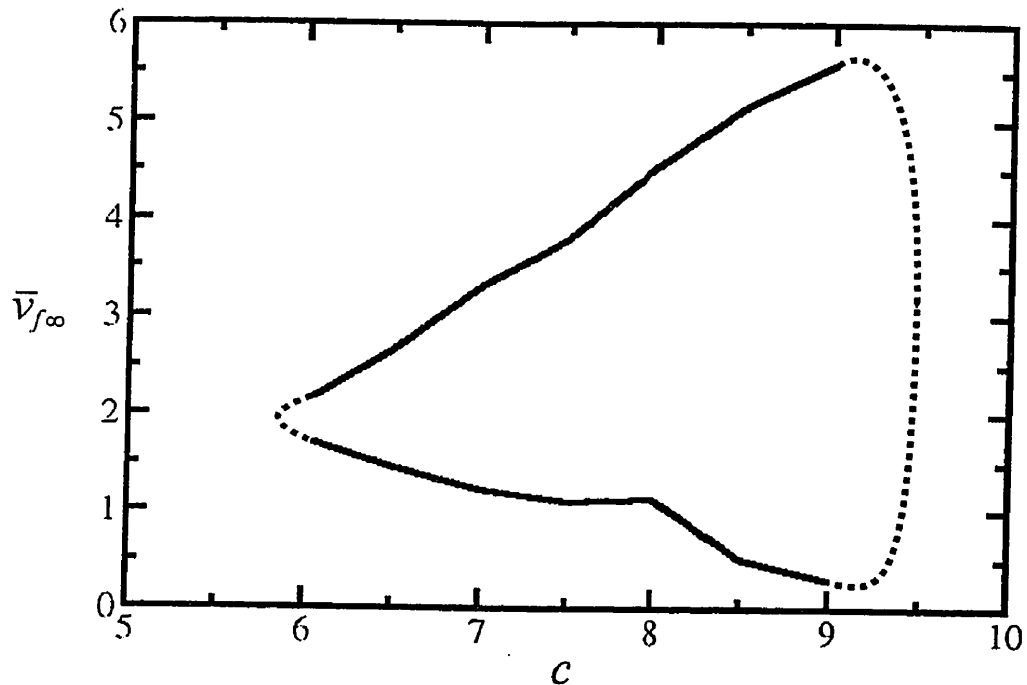


Figure 5.5: The Domain of Existence of the solitary wave solutions of Eq. (5.13)

It is interesting that a simple linear approximation for u' produces good results when compared to the exact solution. Indeed, this was not the first approach examined. The original development of this approach involved a Taylor series approximation of Eq. (5.12) about $\bar{w} = \bar{u}' = 0$. This approximation produced very poor results. The error of this approach was that by taking the series expansion about $\bar{w} = \bar{u}' = 0$, only a very small neighborhood of Eq. (5.12) was approximated when it is clearly the behaviour of u' over the entire range of wave amplitudes that must be

considered. Quadratic and cubic approximations were also examined, but the linear approximation still provided the best results.

5.5 Conclusions

In this chapter, an approach was developed where approximating the contribution of the axial displacement as a linear function of the radial displacement reduced the system of exact governing differential equations to a single equation of a single dependent variable. By using the derivation of the governing shell equations presented in §4.2 coupled with the derivation of the first integral of Eq. (4.15), presented in this chapter, an excellent approximation of the exact solution is obtained.

The results with the linear function approximating the contribution of u' differed by only 3% when compared to the exact solution. From this it is clear that the common practice of neglecting the axial displacement, either in conjunction with the long wave approximation or by arguing axial tethering, produces significant differences in the predicted amplitude and shape of the solitary waves sought.

It is also shown that if the slope squared terms are neglected from Eq. (5.13) that the maximum wave amplitudes are over predicted by approximately 10%. An increase in the error when slope-squared terms are neglected is consistent with the results of Chapter 2. This, however, is not as physically misrepresentative as neglecting the axial deformations.

If the axial displacements are to be neglected as part of the long wave approximation or based on other assumptions, then it needs to be done with the foreknowledge of its inherent limitations.

Chapter 6

Consideration of the Fluid Model¹

6.1 Introduction

The final area of the solitary wave model to be considered is the fluid model. To this point, we have only considered a one-dimensional fluid model where the velocity is assumed to be averaged over the radius of the tube. This has not been an uncommon assumption for many previous studies (Yomosa, 1987; Demiray, 1996, 1997d; Sarioglu, 1999) examining solitary waves in fluid-filled elastic tubes. At the same time, there have been other studies that have made a specific attempt to include both axial and radial velocities in their models (Hashizume, 1985; Demiray, 1998a; Demiray and Dost, 1998a).

As we have seen, the fluid model is responsible for the pressure exerted on the tube wall. It would not be unreasonable to assume that the pressure predicted at the wall, and consequently the shape of the solitary wave, could differ from a one to two-dimensional fluid model. With a number of studies having considered both fluid models, the comparison must already have been made. In fact, that is not the case. The difficulties lie in two main areas.

Firstly, while studies exist that have considered both one- and two-dimensional fluid models, only the study of Demiray (1998a) has attempted to make any comparison of the respective results. In Demiray's study, the effect of the fluid model on

¹The author wishes to thank Prof. R. Hugo for advice regarding the material contained in this Chapter.

the predicted solitary wave was examined, but was done using the reductive perturbation technique. This presents the second problem. Even if the existing data were compared, the reductive perturbation technique was used to determine the solitary wave profile. As we have seen already in this dissertation, the use of the reductive perturbation technique presents its own set of limitations.

As a result, we propose to examine what, if any, differences in the tube wall pressure exist by comparing the pressure predicted by our existing one-dimensional fluid model and a two-dimensional fluid model. For this purpose, we present a modified discrete-vortex method that will allow the pressure along the tube wall to be simulated as a two-dimensional flow.

The most common use of vortex methods has been in the modeling of two-dimensional shear layers. The first study of this type was undertaken by Rosenhead (1932) who calculated by hand the development of a spatially periodic, two dimensional shear layer using two, four, eight and twelve point vortices.

Several studies have also been conducted using vortex methods to model jet diffusion. One of the first studies of this type was performed by Acton (1980), where large eddy formation in axisymmetric jets exiting a tube was modeled through the superposition of a series of axisymmetric vortex rings. Similar studies have also been conducted by Chung and Troutt (1988) and Shimizu (1995). All of these studies, not surprisingly, focused their computational effort on the jet. However, the fluid flow in the tube was needed for the model and Acton, at least, attempted to model the flow in the tube but was unsuccessful. This part of the work was not discussed explicitly, but Acton (1980) did remark that the boundary conditions for the jet-tube surface could not be satisfied. Neither of the studies by Chung and Troutt (1988)

or Shimizu (1995) deviated from the procedure used by Acton (1980). The study by Acton (1980) provides part of the inspiration for the simulations undertaken in this chapter as her use of axisymmetric vortex rings is well suited to our axisymmetric model.

The other area of influence for this work is the panel method, originally presented by Hess and Smith (1966). The panel method is used, primarily, for modeling the flow around two-dimensional thin airfoils. The basics of the panel method involves the placement of distributed vortex panels of unknown strength along the surface of a body. By imposing boundary-flow conditions on the body surface, the unknown vortex circulations can be determined, which in turn allows the calculation of the velocity around the body. The modified discrete-vortex method proposed here could be considered a hybrid of the discrete-vortex method and the panel method.

Section 6.2 provides a formal derivation of the modified discrete-vortex model, including a detailed description of the boundary conditions. In §6.3, the parameters required by the vortex model are determined with special consideration paid to the solitary wave application. In §6.4, the results of the simulations using the modified discrete-vortex model are presented and discussed. Finally, §6.5 re-caps the main contribution of this chapter.

6.2 Modified Discrete Axisymmetric-Vortex Model

Let us begin a formal consideration of the modified discrete-vortex model by considering a single axisymmetric ring vortex.

We continue to employ a cylindrical coordinate system, where the direction of the

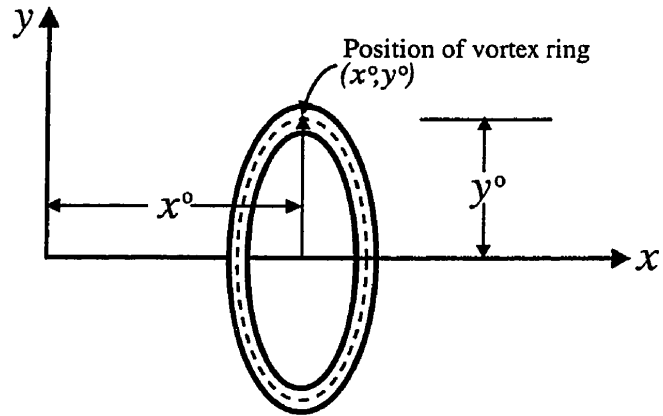


Figure 6.1: Orientation of a typical vortex ring element

vortex ring axis is x and the radius is y , as shown in Figure 6.1. For an axisymmetric vortex ring of strength κ , with its center at (x^o, y^o) , as shown in Figure 6.1, the Stokes stream function at (x, y) is given by Lamb (1945) as

$$\Psi(x, y) = -\frac{\kappa}{2\pi}(\ell_1 + \ell_2)(K(\lambda) - E(\lambda)) \quad (6.1)$$

where,

$$\ell_1 = ((x - x^o)^2 + (y - y^o)^2)^{\frac{1}{2}} \quad (6.2)$$

$$\ell_2 = ((x - x^o)^2 + (y + y^o)^2)^{\frac{1}{2}}$$

and

$$\lambda = \frac{\ell_2 - \ell_1}{\ell_2 + \ell_1} \quad (6.3)$$

The variables $K(\lambda)$ and $E(\lambda)$ are the complete elliptic integrals of the first and

second kind, respectively. They are given by

$$K(\lambda) = \int_0^1 \frac{dt}{\sqrt{(1-t^2)(1-\lambda^2 t^2)}} \quad (6.4)$$

$$E(\lambda) = \int_0^1 \frac{\sqrt{1-\lambda^2 t^2}}{\sqrt{1-t^2}} dt \quad (6.5)$$

The resulting stream function will have the appearance shown in Figure 6.2.

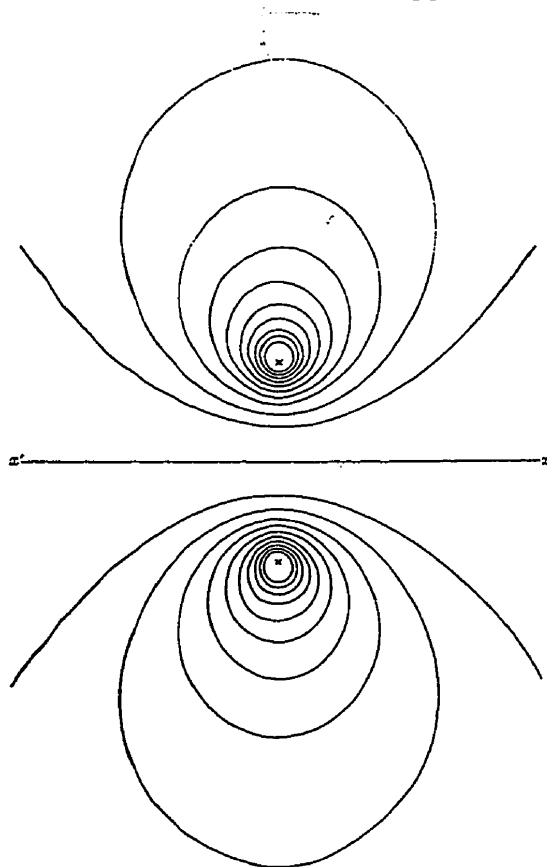


Figure 6.2: Stokes stream function for an axisymmetric vortex ring (Lamb, 1945)

We can find the axial and radial velocities from Eq. (6.1) through

$$u^o(x, y) = -\frac{1}{y} \frac{\partial \Psi}{\partial y}, \quad v^o(x, y) = \frac{1}{y} \frac{\partial \Psi}{\partial x} \quad (6.6)$$

If we calculate the derivatives of Eq. (6.1) in Eq. (6.6), we find that

$$\begin{aligned} u^o(x, y) = & \frac{\kappa}{2\pi y} \left(\left(\frac{y - y^o}{\ell_1} + \frac{y + y^o}{\ell_2} \right) (K(\lambda) - E(\lambda)) \right. \\ & \left. + \left(\frac{\partial K(\lambda)}{\partial \lambda} - \frac{\partial E(\lambda)}{\partial \lambda} \right) \left[\left(\frac{y + y^o}{\ell_2} - \frac{y - y^o}{\ell_1} \right) - (\ell_2 - \ell_1) \frac{\frac{y - y^o}{\ell_1} + \frac{y + y^o}{\ell_2}}{\ell_1 + \ell_2} \right] \right) \end{aligned} \quad (6.7)$$

and

$$\begin{aligned} v^o(x, y) = & -\frac{\kappa}{2\pi y} \left(\left(\frac{1}{\ell_1} + \frac{1}{\ell_2} \right) (x - x^o) (K(\lambda) - E(\lambda)) \right. \\ & \left. + \left(\frac{\partial K(\lambda)}{\partial \lambda} - \frac{\partial E(\lambda)}{\partial \lambda} \right) \left[\left(\frac{1}{\ell_2} - \frac{1}{\ell_1} \right) (x - x^o) - \frac{(\ell_2 - \ell_1) \left(\frac{1}{\ell_1} + \frac{1}{\ell_2} \right) (x - x^o)}{\ell_1 + \ell_2} \right] \right) \end{aligned} \quad (6.8)$$

These equations permit us to calculate the velocity at any position (x, y) due to the influence of a single axisymmetric vortex ring. The two limitations on Eq. (6.7) and Eq. (6.8) are at $y = 0$ and (x^o, y^o) , where the velocity becomes singular.

To this point, nothing has been assumed regarding the core size of the vortex ring. If we consider Acton (1980) we see that two core sizes were specified. As discussed in Saffman (1992), a core size must be specified to permit the calculation of the self-induced velocity of the vortex ring. For the free-jet simulation this is very important. In this study, however, the vortices are fixed to the tube boundary and we consequently never consider a self-induced velocity. The second value of the core is specified to eliminate model instabilities arising from two vortices coming in very

close contact while convecting in the jet. Again, because the vortex rings are fixed to the tube boundary, we need not worry about this problem. For our purposes then, assigning a core size is of little practical benefit.

The influence of several vortex rings can be determined by superimposing the individual contributions from each vortex at a specified point.

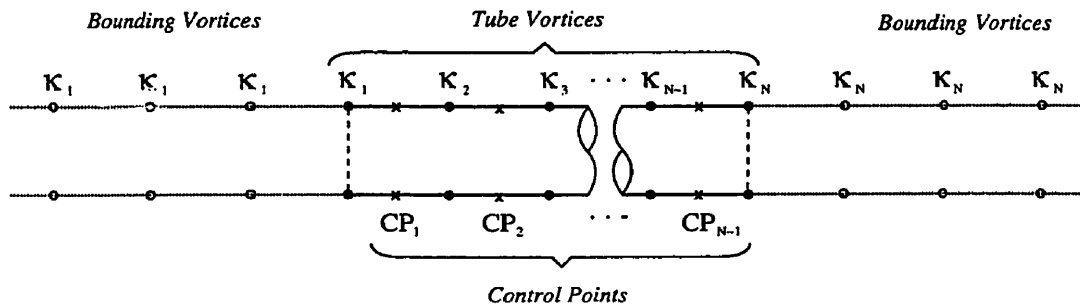


Figure 6.3: Illustration of placement of ring vortices, bounding vortices and control points for a simple tube

Let N be the total number of equally spaced axisymmetric vortex rings placed on the tube boundary, each defining a node, where $\kappa_1, \kappa_2, \dots, \kappa_N$ are the source strengths of the vortex rings. Figure 6.3 illustrates the positioning of the axisymmetric vortex rings on the tube boundary for a simple, uniform tube. Using superposition, we can write the velocity induced by all N vortices at any arbitrary point (x, y) as

$$u_i(x, y) = \sum_{i=1}^N u_i^o(x, y), \quad v_i(x, y) = \sum_{i=1}^N v_i^o(x, y) \quad (6.9)$$

where u_i^o and v_i^o represent the velocity contributions from the i^{th} vortex ring positioned at (x_i^o, y_i^o) .

We observe that both Eq. (6.7) and Eq. (6.8) have κ as a common term and as such, κ could be written explicitly in the summations of Eq. (6.9). If we do this we find that

$$u_i(x, y) = \sum_{i=1}^N \kappa_i \tilde{u}_i^o(x, y), \quad v_i(x, y) = \sum_{i=1}^N \kappa_i \tilde{v}_i^o(x, y) \quad (6.10)$$

where κ_i is the vortex strength of the i^{th} vortex ring and \tilde{u}_i^o and \tilde{v}_i^o are the axial and radial velocities per κ_i .

We now need to define boundary conditions at the inflow and outflow boundaries of the tube. We shall specify a zero-change boundary condition, such that no step-changes in circulation or velocity are permitted at the boundaries. Following an approach described in Leonard (1980), we will satisfy the inflow/outflow boundary condition by placing a series of bounding vortices at the inflow and outflow boundaries. The bounding vortices are assigned a vortex strength of κ_1 and radial position of y_1 at the inflow boundary and a vortex strength of κ_N and radial position of y_N at the outflow boundary. The bounding vortices are placed with the same axial spacing as the tube vortex rings. The placement and strength of the bounding vortices are also illustrated in Figure 6.3. The net effect of assigning bounding vortices is to numerically generate an infinitely long tube. The velocity at any point in the flow must now consider the contributions from the tube vortices and the bounding vortices.

Let us consider M bounding vortices placed at each boundary of the tube. If we consider the k^{th} bounding vortex at the inflow boundary and the l^{th} bounding vortex

at the outflow boundary, we find that

$$\begin{aligned} u_k(x, y) &= \kappa_1 \sum_{k=1}^M \tilde{u}_k^o(x, y) & v_k(x, y) &= \kappa_1 \sum_{k=1}^M \tilde{v}_k^o(x, y) \\ u_l(x, y) &= \kappa_N \sum_{l=1}^M \tilde{u}_l^o(x, y) & v_l(x, y) &= \kappa_N \sum_{l=1}^M \tilde{v}_l^o(x, y) \end{aligned} \quad (6.11)$$

where u_k , v_k , u_l and v_l are the velocity components at (x, y) due to the bounding vortices at positions (x_k^o, y_k^o) and (x_l^o, y_l^o) .

Writing the total axial and radial velocities, including contributions from both tube and bounding vortices, we find that

$$\begin{aligned} u_T(x, y) &= \kappa_1 \sum_{k=1}^M \tilde{u}_k^o(x, y) + \sum_{i=1}^N \kappa_i \tilde{u}_i^o(x, y) + \kappa_N \sum_{l=1}^M \tilde{u}_l^o(x, y) \\ v_T(x, y) &= \kappa_1 \sum_{k=1}^M \tilde{v}_k^o(x, y) + \sum_{i=1}^N \kappa_i \tilde{v}_i^o(x, y) + \kappa_N \sum_{l=1}^M \tilde{v}_l^o(x, y) \end{aligned} \quad (6.12)$$

Writing the terms for $i = 1$ and $i = N$ explicitly leaves

$$\begin{aligned} u_T(x, y) &= \kappa_1 \sum_{k=1}^M \tilde{u}_k^o(x, y) + \kappa_1 \tilde{u}_1^o(x, y) + \sum_{i=2}^{N-1} \kappa_i \tilde{u}_i^o(x, y) \\ &\quad + \kappa_N \tilde{u}_N^o(x, y) + \kappa_N \sum_{l=1}^M \tilde{u}_l^o(x, y) \end{aligned} \quad (6.13)$$

$$\begin{aligned} v_T(x, y) &= \kappa_1 \sum_{k=1}^M \tilde{v}_k^o(x, y) + \kappa_1 \tilde{v}_1^o(x, y) + \sum_{i=2}^{N-1} \kappa_i \tilde{v}_i^o(x, y) \\ &\quad + \kappa_N \tilde{v}_N^o(x, y) + \kappa_N \sum_{l=1}^M \tilde{v}_l^o(x, y) \end{aligned} \quad (6.14)$$

Grouping terms with like values of κ , we find

$$\begin{aligned} u_T(x, y) &= \kappa_1 \left(\sum_{k=1}^M \tilde{u}_k^o(x, y) + \tilde{u}_1^o(x, y) \right) + \sum_{i=2}^{N-1} \kappa_i \tilde{u}_i^o(x, y) \\ &\quad + \kappa_N \left(\tilde{u}_N^o(x, y) + \sum_{l=1}^M \tilde{u}_l^o(x, y) \right) \end{aligned} \quad (6.15)$$

$$\begin{aligned}
v_T(x, y) = \kappa_1 \left(\sum_{k=1}^M \tilde{v}_k^o(x, y) + \tilde{v}_1^o(x, y) \right) + \sum_{i=2}^{N-1} \kappa_i \tilde{v}_i^o(x, y) \\
+ \kappa_N \left(\tilde{v}_N^o(x, y) + \sum_{i=1}^M \tilde{v}_i^o(x, y) \right)
\end{aligned} \tag{6.16}$$

From Eq. (6.15) and Eq. (6.16) we can clearly see that the entire effect of the bounding vortices can be combined with the influence of the tube vortex rings at $i = 1$ and $i = N$. No other terms are affected. The velocity at any point in the flow (x, y) is then given by Eq. (6.15) and Eq. (6.16).

Now, let us define $N - 1$ control points, where the j^{th} control point is defined as the mid-point between the i and $(i + 1)$ tube vortices and let its inclination to the x axis be θ_j , as shown in Figure 6.4. No control points are assigned to the image vortices because they are defined outside the computational domain of the tube. We now let

$$\begin{aligned}
\sin \theta_j &= \frac{y_{i+1} - y_i}{l_j} \\
\cos \theta_j &= \frac{x_{i+1} - x_i}{l_j}
\end{aligned} \tag{6.17}$$

where $l_j = \sqrt{(x_{i+1} - x_i)^2 + (y_{i+1} - y_i)^2}$. The position of the j^{th} control point is given as x_j, y_j , such that

$$\begin{aligned}
x_j &= \frac{x_i + x_{i+1}}{2} \\
y_j &= \frac{y_i + y_{i+1}}{2}
\end{aligned} \tag{6.18}$$

At each control point we shall impose a no-flow boundary condition, such that the normal velocity at each control point must be zero. The no-flow boundary condition can be written as

$$v_T(x_j, y_j) \cos \theta_j - u_T(x_j, y_j) \sin \theta_j = 0 \tag{6.19}$$

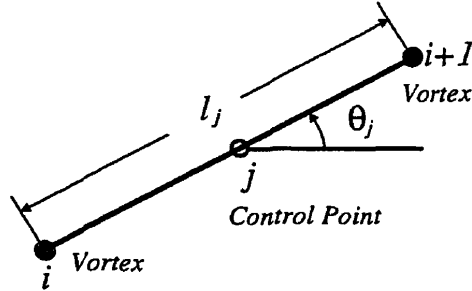


Figure 6.4: Orientation of arbitrary tube segment

To account for the boundary conditions at every control point over the entire tube, we sum j from 1 to $N - 1$, such that

$$\sum_{j=1}^{N-1} \left(v_T(x_j, y_j) \cos \theta_j - u_T(x_j, y_j) \sin \theta_j \right) = 0 \quad (6.20)$$

While no control points are defined for the bounding vortices they, of course, contribute to the no-flow boundary condition so that the values of $u_T(x_j, y_j)$ and $v_T(x_j, y_j)$ are given by Eq. (6.15) and Eq. (6.16).

The final boundary condition requires us to specify a velocity at some point in the flow. For the purposes of this work, a free stream velocity U_{fs} will be defined at the known location given by (x_{fs}, y_{fs}) . Additionally, the free stream velocity will always be defined in a uniform section of tube and is, therefore, a function of u alone (i.e. horizontal). This is not required, but greatly simplifies the calculations for this boundary condition. The free stream condition is given by

$$u_T(x_{fs}, y_{fs}) = U_{fs} \quad (6.21)$$

and where $u_T(x_{fs}, y_{fs})$ is given by Eq. (6.15).

Now, for a given tube configuration, (x_i^o, y_i^o) , (x_{fs}, y_{fs}) and U_{fs} will be known. The values of (x_j, y_j) , θ_j , (x_k^o, y_k^o) and (x_l^o, y_l^o) can then also be calculated. This leaves N simultaneous algebraic equations, given by Eq. (6.20), and (6.21), in terms of only the unknown vortex strengths, $\kappa_1, \kappa_2, \dots, \kappa_N$. The vortex strengths are then easily determined using any procedure for solving simultaneous equations. Once the values of $\kappa_1, \kappa_2, \dots, \kappa_N$ have been determined, the velocity at any point in the tube can be calculated.

6.3 Application of Modified Discrete-Vortex Model

The aim of this study is to use the the modified discrete vortex model to predict the pressure exerted on a tube wall using a two-dimensional inviscid fluid model and to compare that to the pressure predicted using the one-dimensional fluid model proposed in §4.4. We are specifically interested in examining the magnitude of the pressure difference between the two models to quantify the potential error of the solitary wave solution from using the one-dimensional fluid model. In order to proceed with our simulations, we must first specify a number of model parameters.

6.3.1 Tube Geometry

It is important that we consider tube geometries encompassing a wide range of solitary wave solutions. By examining small and large amplitude waves we can gain a broader assessment of the appropriateness of the current fluid model. Consequently, we investigated the tube wall pressure for four unique tube geometries corresponding to the solitary wave solutions for the wave speeds of $c = 3.175, 3.402, 3.629$ and 3.856 ,

measured in the natural reference configuration. The solitary wave solutions were determined using our direct method and the equations derived in Chapter 4. Figure 6.5 shows the geometry of the tube for each wave speed. The displacements are all measured with respect $y = 0$ in the undeformed reference configuration. The radial and axial distances are non-dimensionalized using the expressions given in §4.6. Therefore, all the axial distances quoted in this chapter are per L_o and all radial distances are per R . For $m = 0.864$, the value of m used earlier in the natural reference configuration, we can write $L_o = 0.93R$. The non-dimensionalized axial distances can be put in more physical terms by realizing that a unit axial distance is 93% of R .

Our application of the discrete-vortex model assumes that the flow in the tube is steady. In order to cast the flow for a traveling wave as a steady flow, we introduce an observer traveling with the wave. The moving observer has no effect on the reference configuration we have adopted. With the observer moving at the wave speed, the axial velocity will appear to be the speed of the fluid less the speed of the wave. Considering the definition of the free stream velocity for our vortex model, we can write it in terms of the solitary wave model as $U_{fs} = \bar{v}_{f\infty} - c(1 + U')$, where $\bar{v}_{f\infty}$ is the fluid speed in the undeformed tube and $c(1 + U')$ is the speed of the wave measured in the natural reference configuration.

We recall from §4.6 that $U' = 0.5$ and $\bar{v}_{f\infty} = c/2$. Therefore, for a wave of speed $c = 3.175$, the traveling observer would observe a free stream velocity of $U_{fs} = 3.175$. Therefore, the free stream velocity for the each tube geometry is simply the corresponding wave speed.

It is also interesting to notice that the term $\bar{v}_{f\infty} - c(1 + U')$ also appears in Eq.

(4.35), the pressure resulting for the one-dimensional model. This should not be a great surprise, in that the pressure will only be concerned with the relative speed of the fluid with respect to the boundary.

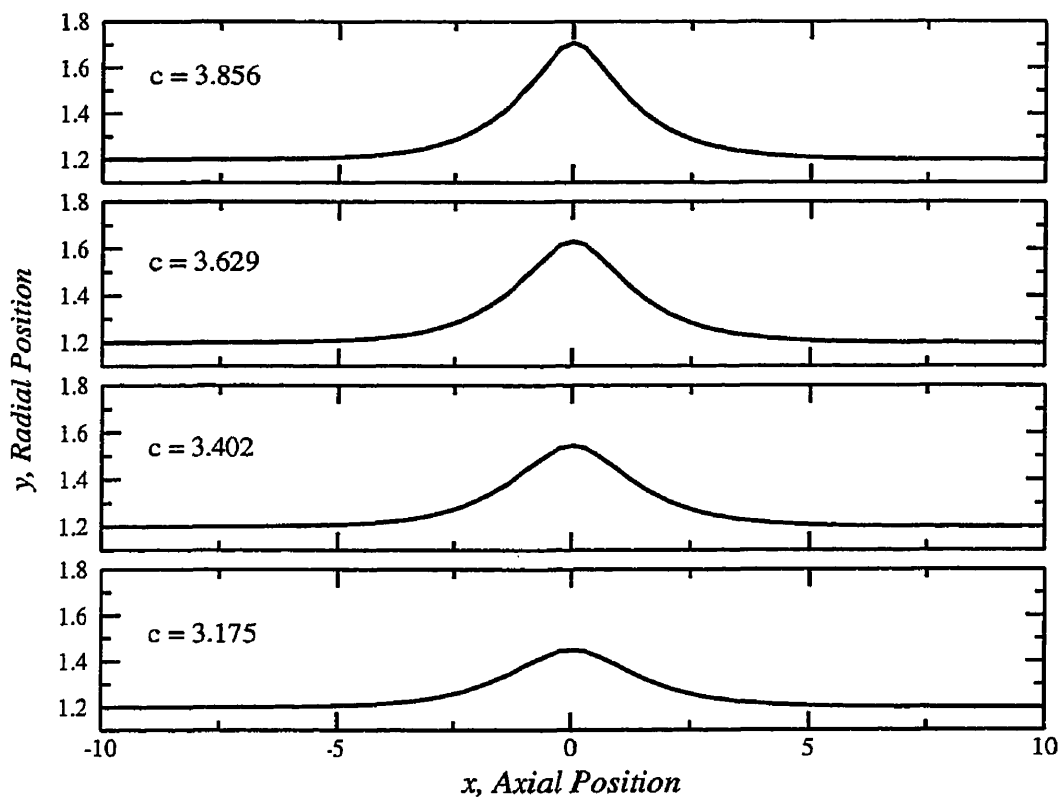


Figure 6.5: Tube geometries corresponding to the solitary wave solution for speeds $c = 3.175, 3.402, 3.629$ and 3.856

6.3.2 Vortex Spacing & Tube Length

In the formal derivation of the discrete vortex method above, we began by defining the total number of vortex rings. In practice, however, the number of vortex rings

is not set *a priori*, but rather is determined as a consequence of setting the spacing between each vortex ring, Δ_κ , and the overall length of tube, L_t . Let us first concern ourselves with examining the effect of the vortex spacing.

The vortex spacing plays a significant role in the effectiveness of the discrete vortex method. Upon further examination of Acton (1980) it is clear that the difficulty in modeling the tube flow was a direct result of the choice, or limitation, of the vortex spacing. The vortex spacing proposed by Acton (1980) (and by Chung and Troutt, 1988; Shimizu, 1995) was, in terms of the current non-dimensionalization, approximately 0.100. Therefore, to avoid difficulty with the tube wall boundary conditions we will need to employ a vortex spacing smaller than the one proposed by Acton. After some initial consideration, we considered the follow three vortex spacings: $\Delta_\kappa = 0.010, 0.004$ and 0.0025 .

The vortex spacing was evaluated by modeling the flow in a tube of radius $y = 1$ and length $-5 \leq x \leq 5$. The free stream velocity was set to $U_{fs} = 1$ at $x = 0$ and $y = 0.5$. The velocity profiles at several axial locations were calculated and evaluated against the exact solution for uniform, inviscid tube flow, namely the 'top hat' velocity profile. Not unexpectedly, the deviation from the exact solution occurred near the tube wall for each vortex spacing. Figure 6.6 shows the near wall velocities at $x = 0$ for each vortex spacing.

From Figure 6.6 we see that the best approximation of the 'top hat' velocity profile is achieved using $\Delta_\kappa = 0.0025$. Using this vortex spacing the predicted velocity profile deviates from the exact solution at $y = 0.995$. While, using vortex spacing does not allow us to exactly match the top hat velocity profile, it will allow us to calculate an excellent approximation of the tube wall pressure.

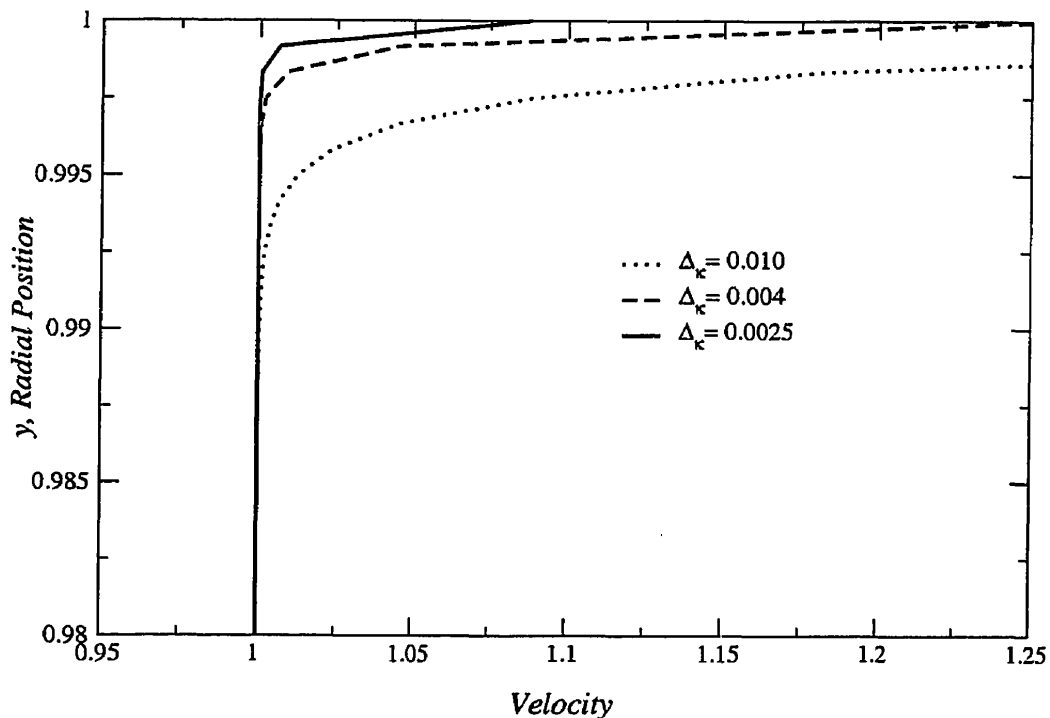


Figure 6.6: Near wall velocity at $x = 0$ for $\Delta_\kappa = 0.010$, 0.004 and 0.0025

It seems apparent from the results shown in Figure 6.6 that using a smaller vortex spacings could further improve the accuracy near the tube wall. In theory that is correct; however, the limiting factor affecting vortex spacing becomes the availability of computer memory. In the test case above, a tube of length 10 with $\Delta_\kappa = 0.0025$ corresponds to $N = 4001$ vortex rings. This in turn means there will be 4001 equations with 4001 unknowns resulting in 16,008,001 elements that need to be stored in memory. If each element requires 8 bytes of memory (assuming double precision), our simple example will use 128MB of memory. If we doubled the length

of our tube, the required memory would quadruple.

With all this in mind we can certainly see the difficulty Acton (1980) faced in trying to model the tube flow. We can see that the resolution attainable now would not have been possible with the computational resources of 1980 and that based on our tests, Acton's spacing of 0.100 would not have come close to approximating the exact solution.

Following directly from determining the vortex spacing is the consideration of the tube length, L_t , for the model. For the tube geometries shown in Figure 6.5, the changing radius of the tube, not surprisingly, results in variations in vortex strength. These variations can be seen, in the neighborhood of the pulse, even once the tube has returned to a constant radius. Therefore, in choosing a tube length our primary concern is to ensure that the vortex strength has become constant at the inflow and outflow boundaries so that the no-change boundary condition may be properly enforced. Additionally, a section of tube with constant vortex strength also ensures the appropriate conditions for specifying the free stream velocity.

After running several initial tests, the length of the tube selected for use in these simulations was $-20 \leq x \leq +20$, an overall length of $L_t = 40$. This tube length ensured that both the vortex strength and the fluid velocity were uniform for at least $x = 9.5$ from the inflow and outflow boundaries. This axial range was adopted for all tube geometries.

A tube of length $L_t = 40$ with $\Delta_\kappa = 0.0025$ would correspond to $N = 16001$ unknown circulations, which following the calculation above, requires a minimum of 2GB of memory. As a result, all numerical simulations were run on a Compaq ES40 4-CPU, 667 MHz EV67 Alpha, with 4GB of memory. This resource was made

available by the MACI Alpha Cluster at the University of Calgary. The average processing time for the full tube geometry with $\Delta_\kappa = 0.0025$ was approximately 55 hours.

6.3.3 Bounding Vortices

The number of bounding vortices needed to satisfy the inflow and outflow no-change boundary conditions was evaluated, after several initial trials, using numerical tests on a uniform tube of radius $y = 1$ and length $L_t = 40$, with $U_{fs} = 1$ at $x = 0$ and $y = 0.5$. Tests were performed for $M = 0, 2N$ and $4N$, where the number of bounding vortices is referred to the number of tube vortices. The outcomes were evaluated by examining the resulting vortex strengths. Figure 6.7 shows the effect of bounding vortices on the calculated vortex strengths near the outflow boundary for each test case. Figure 6.7 shows that when using $M = 0$ or $M = 2N$ bounding vortices, the vortex strengths near the outflow (and identically at the inflow) boundary are not constant, compromising the zero-change boundary condition. However, we also see that when using $M = 4N$ bounding vortices the vortex strength is constant at the inflow/outflow boundary and consequently the zero-change boundary condition can be satisfied. Based upon these results, $M = 4N$, or $M = 64,004$, bounding vortices were used for all simulations.

The free stream velocity was assigned the appropriate value for each tube geometry at the axial position $x = -15$ and the radial position $y = 0.5$ for all simulations. The velocity profile at this location was uniform, which was verified by the results of the simulation.

An issue also arose concerning the precision of the calculations performed in the

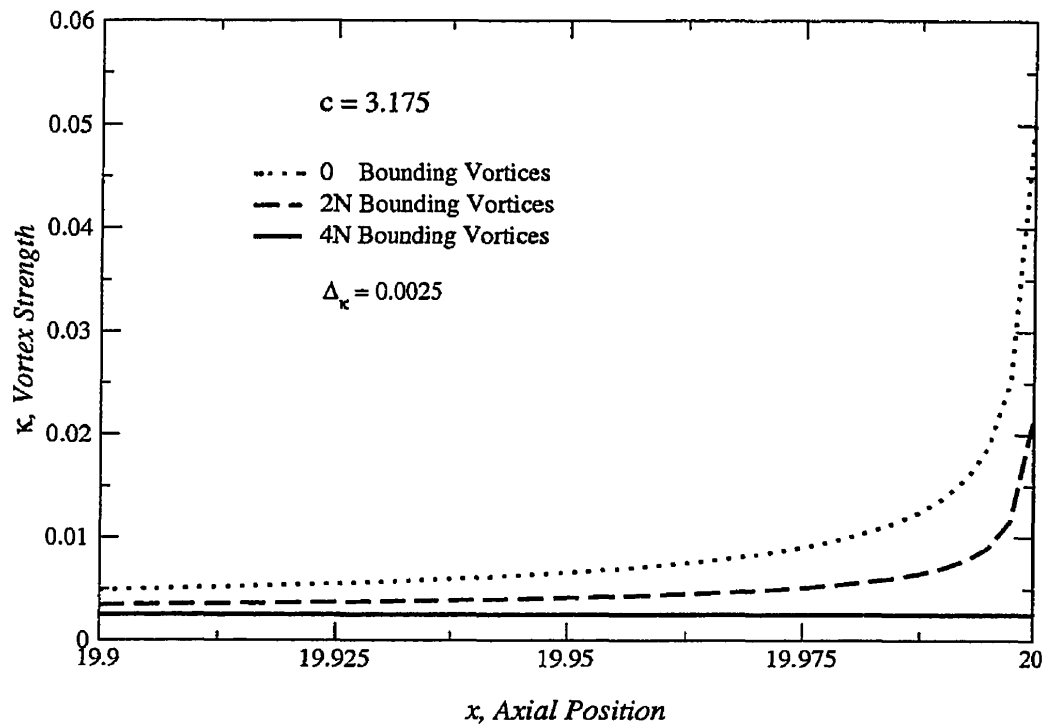


Figure 6.7: Effect of bounding vortices on the calculated vortex strength near the outflow boundary using $M = 0$, $2N$ and $4N$

simulation. Originally, all calculations were performed using single precision floating point. This appeared to provide excellent results when using $\Delta_{\kappa} = 0.004$. However, when calculations were performed using $\Delta_{\kappa} = 0.0025$ an interesting instability appeared. Figure 6.8 shows the appearance of this instability for the $c = 3.175$ tube geometry. The source of this sinusoidal instability is uncertain, but is resolved when double precision calculations are used. As a consequence of this, all results were obtained using double precision calculations.

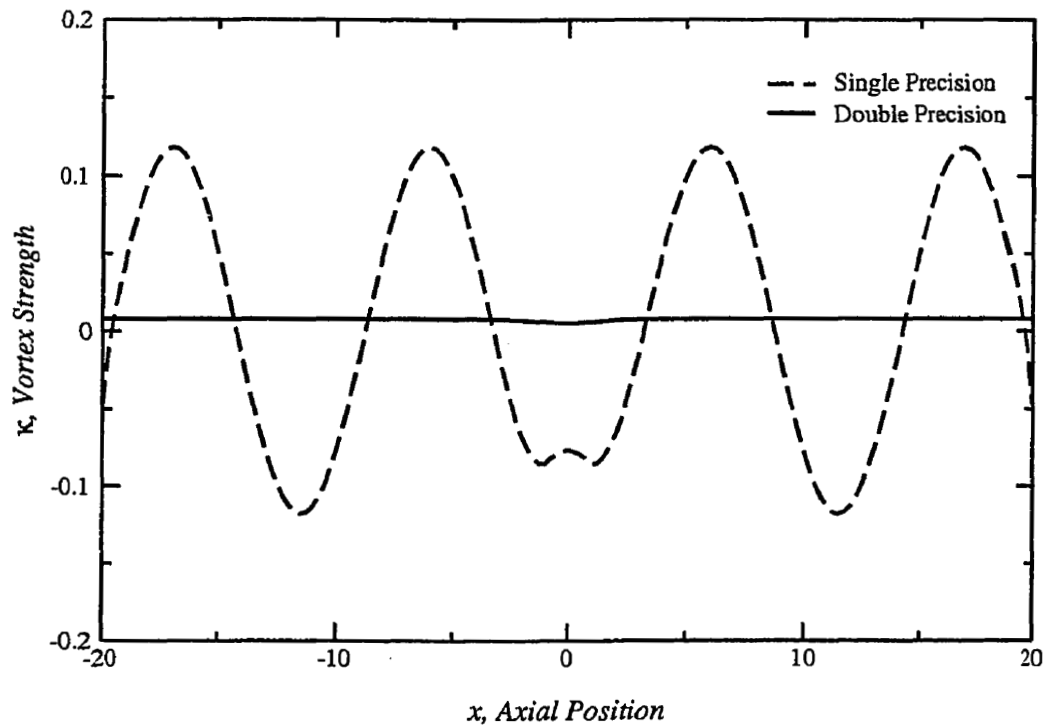


Figure 6.8: Vortex strengths determined using single and double precision calculations for $c = 3.175$ tube geometry

6.4 Simulation Results

Simulations were run for the tubes geometries shown in Figure 6.5 using the parameters specified in §6.3 for $\Delta\kappa$, L_t , and M . The resulting vortex strengths were determined for each tube geometry and are shown in Figure 6.9.

The effect of the increase in tube radius, resulting from the solitary wave, produces a decrease in vortex strength. This variations in the vortex strength appear to extend no further than $x = \pm 10$ from the tube center and confirms our selection

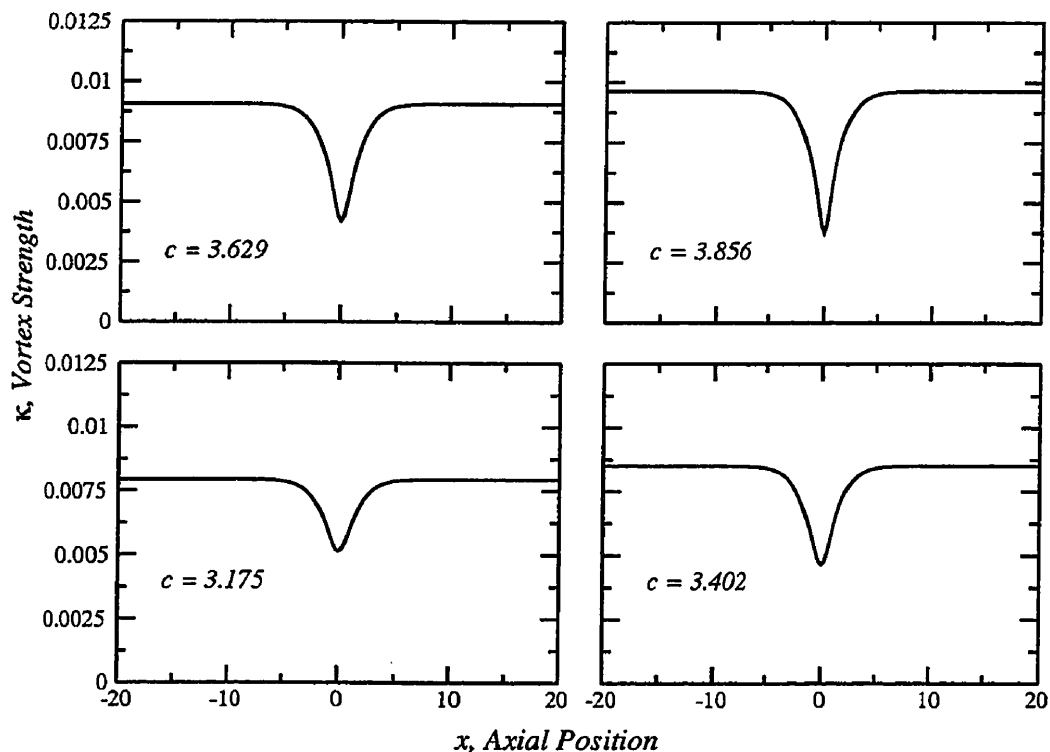


Figure 6.9: Vortex strengths determined using discrete-vortex model for for tube geometries corresponding to $c = 3.175$, 3.402 , 3.629 and 3.856

of tube length. Not surprisingly, the cases with larger free stream velocities have greater vortex strength over the entire tube.

Having calculated the vortex strengths for the four tube geometries, the velocity at any point in the flow field can now be calculated. Visualization of the flow in the tube was provided by incorporating streaklines. Virtual particles were introduced into the flow at the inflow boundary and were allowed to move in the induced velocity field of the tube. The resulting streaklines corresponded identically to streamlines

for the steady tube flow. Eleven equally spaced streamlines were determined for each tube geometry. The particle paths were determined using a second-order Ralston RK method (global error $O(h^2)$), with a time step of 0.0025. The resulting streamlines for two representative tube geometries ($c = 3.175$ and $c = 3.856$) are shown in Figure 6.10.

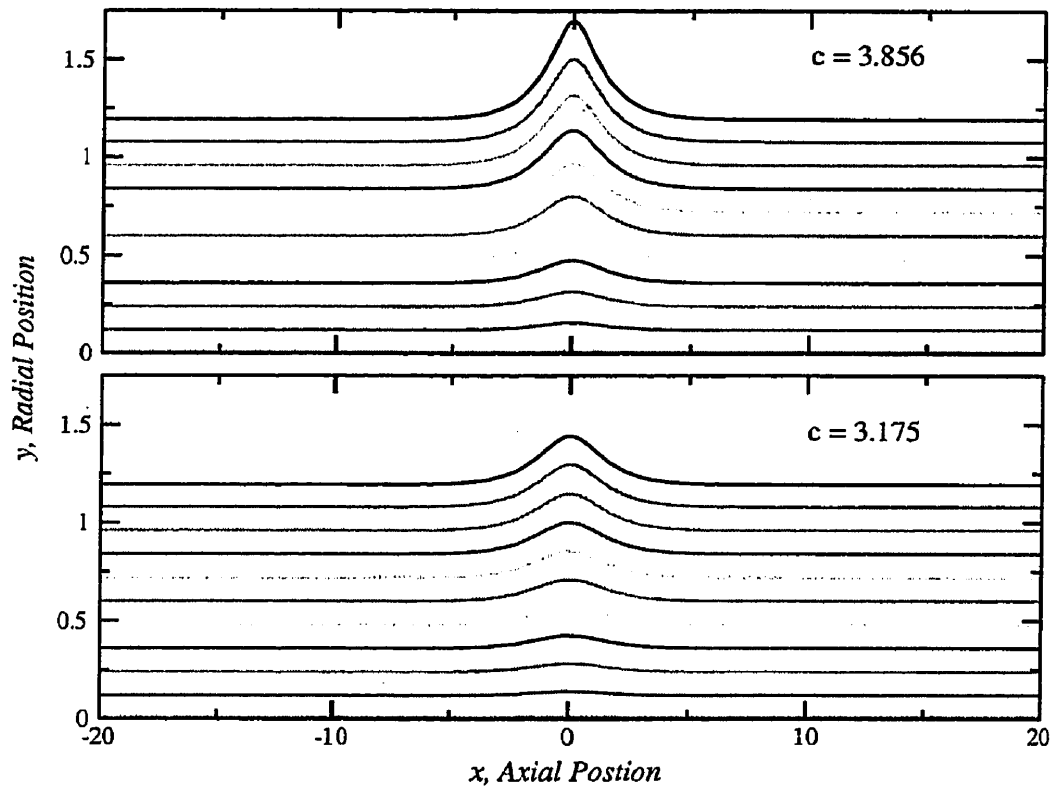


Figure 6.10: Streamlines determined for tube geometries corresponding to $c = 3.175$ and 3.856

Because our interest is in the effects at the tube wall, we shall focus our attention on the streamline nearest the tube wall. However, as we have seen in Figure 6.6, the

Table 6.1: Comparison of velocities at two positions 0.006 and 0.012 below the tube wall for $c = 3.175$ tube geometry

Axial Position	Total Velocity		Error
	0.006 below wall	0.012 below wall	
0	2.0482	2.0506	0.12%
2	2.7918	2.7912	0.02%
4	3.1052	3.1050	0.01%
6	3.1635	3.1635	0.00%
8	3.1732	3.1732	0.00%
10	3.1750	3.1750	0.00%

vortex spacing limits how close to the tube wall we can calculate the velocity of the fluid. Consequently, the top streamline resolvable for our model is approximately 0.006 below the tube wall. The question we therefore have is how much will the velocity, and subsequently the pressure, differ between the tube wall and the top resolvable streamline.

Figure 6.11 shows the velocity profile over the tube radius for the axial position $x = 0$ for each of the tube geometries. As we might expect, this plot shows that the velocity varies smoothly over the tube radius at this position. With inviscid flow, the velocity at the wall should continue to follow this profile. Therefore, the close proximity of the top streamline to the tube wall suggests that there would be little deviation between the velocity at the two locations. As additional confirmation of this, Table 6.1 shows, for several downstream distances, a comparison of the total velocity $(u_T^2 + v_T^2)^{\frac{1}{2}}$ calculated at 0.006 and 0.012 below the tube wall for the $c = 3.175$ tube. This separation was used to approximate the separation between the tube wall and the top streamline.

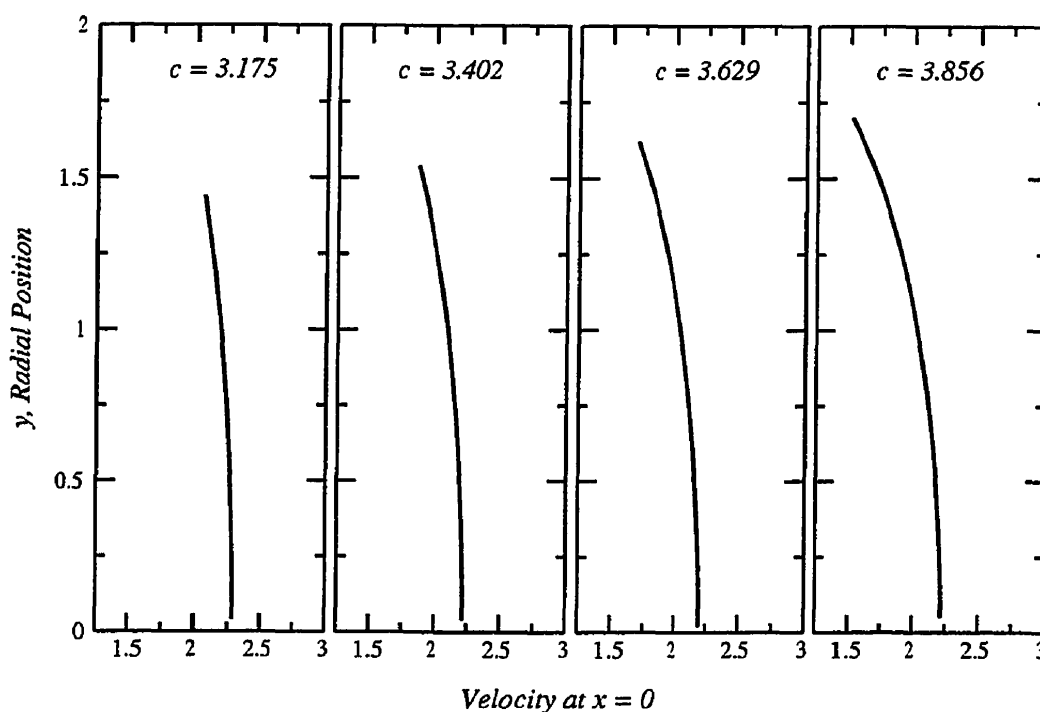


Figure 6.11: Velocity profiles at axial position $x = 0$ for tube geometries corresponding to $c = 3.175$, 3.402 , 3.629 , and 3.856

We can see from Table 6.1 that the maximum error in total velocity between the two positions is 0.12%, which not unexpectedly occurs at $x = 0$. The small difference in velocity at these radial position indicates, based on the smooth velocity profile and inviscid flow, that the difference in velocity between the tube wall and the top streamline will also be small. We can, therefore, use the top streamline to provide an excellent approximation to the tube wall streamline.

We can now apply Bernoulli's equation at points along the top streamline to determine an estimate of the pressure distribution at the tube wall. We begin by

writing Bernoulli's theorem (Batchelor, 1967) for an incompressible, inviscid fluid, such that

$$\frac{p}{\rho_f} + \frac{V^2}{2} + gy = H \quad (6.22)$$

where H is constant along any streamline of a steady flow and $V^2 = u_T^2 + v_T^2$. For the tube geometries we have considered, we can assume that the variation of gy along the streamline will be small as compared to the velocity and can therefore be neglected.

If we can identify a position with known conditions, for example the inflow boundary, then we can write the explicit values for V_∞ and p_∞ . Since H is constant along a streamline we can easily re-write Eq. (6.22), taking advantage of the definitions at ∞ so that

$$\frac{p_\infty}{\rho_f} + \frac{V_\infty^2}{2} = \frac{p}{\rho_f} + \frac{V^2}{2} \quad (6.23)$$

where p and V are determined at any other point along the streamline. Grouping the pressure and velocity terms we find

$$\frac{p}{\rho_f} - \frac{p_\infty}{\rho_f} = \frac{V_\infty^2}{2} - \frac{V^2}{2} \quad (6.24)$$

We will find it useful to re-write the left-hand side of Eq. (6.24) as $p^* = p - p_\infty$ leaving

$$\frac{p^*}{\rho_f} = \frac{1}{2}(V_\infty^2 - V^2) \quad (6.25)$$

At this point we non-dimensionalize Eq. (6.25) using the expressions given in §4.6, leaving

$$\bar{p}_{2D}^* = \frac{1}{2}(\bar{V}_\infty^2 - \bar{V}^2) \quad (6.26)$$

Eq. (6.26) permits us to calculate the pressure at any point along a streamline.

We recall from §4.6 the non-dimensionalized pressure determined using the one-dimensional, inviscid fluid model, given by Eq. (4.58). Re-writing Eq. (4.58) in terms of \bar{p}^* , \bar{V} and y , leaves us with

$$\bar{p}_{1D}^* = \frac{1}{2}((1 + U')c - \bar{V}_\infty)^2 \left[1 - \left(\frac{y_\infty}{y} \right)^4 \right] \quad (6.27)$$

where V_∞ and y_∞ are the velocity and radius at the inflow boundary. The value of y will be the radial position of any other point on the tube wall streamline.

If we now consider the top streamline for each tube geometry, we can calculate the approximate pressure at the tube wall using Eq. (6.26) and compare it to Eq. (6.27). Figure 6.12 shows the pressure exerted on the tube wall predicted by the one-dimensional and two-dimensional fluid models.

The two pressure distributions, for each tube geometry, shown in Figure 6.12 appear to agree quite closely, with the greatest difference occurring for the peak pressure at the maximum tube radius. The difference in peak pressure between Eq. (6.27) and Eq. (6.26) is found to be 9.8%, 10.2%, 10.8% and 11.9%, for each of the tube geometries respectively. It is not surprising that the difference in peak pressure increases with an increase in maximum tube radius owing primarily to the increasing contribution of the radial velocity.

The reasonably close agreement of the pressure between the two models suggests that we could anticipate little difference between solitary wave profiles determined using the one-dimensional and two-dimensional fluid models. In fact, there is other evidence to support such a claim.

If we examine the studies that have included the radial velocity in the fluid

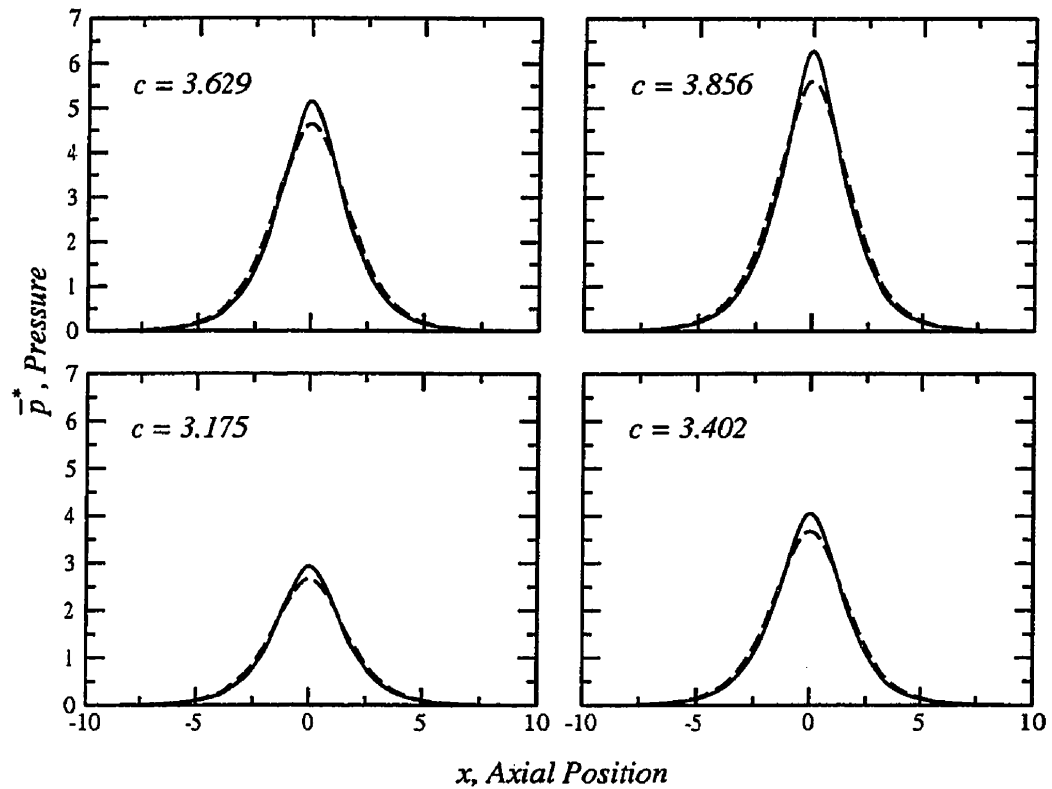


Figure 6.12: Tube wall pressures predicted using Eq. (6.26) (—) and Eq. (6.27) (---)

model (Hashizume, 1985; Demiray and Dost, 1998a; Demiray, 1998a; Antar and Demiray, 1999; Demiray, 1999d), we find that only one study makes any comparison to the results for a one-dimensional fluid model. The study by Demiray (1998a) considers a one-dimensional membrane (neglect axial displacements) with both a one-dimensional and two-dimensional fluid model. The reductive perturbation technique is used and coefficients are determined for the KdV equation using each fluid model. Using the D1 constitutive equation used in the earlier chapters, Demiray

(1998a) calculates the shape of solitary waves for each of the fluid models. The results of this comparison indicate that the shape of the waves predicted using the one-dimensional fluid model are not significantly different from the waves predicted using the two-dimensional fluid model. This certainly supports our contention that the close agreement in the pressures predicted using the one-dimensional and two-dimensional fluid models would lead to the prediction of similar solitary wave profiles.

It is surprising that more studies have not made this same comparison. Nevertheless, the results of Demiray (1998a) offers clear support of the results of this chapter. As a result, it appears that the extra effort that would be required to include the two-dimensional fluid model may not provide greater accuracy in the predicted solitary wave profile.

6.5 Conclusions

In this chapter we have addressed the final area of interest for solitary waves: the fluid model. The physical existence of solitary waves has been attributed to the inertia of the fluid moving in the tube and the restoring force applied by the tube wall. Clearly, the key is in the interaction at the tube wall.

In this chapter a novel discrete vortex model is derived, based on the discrete vortex model used for simulating axisymmetric jets and the panel method. In this model, discrete axisymmetric vortex rings are placed at equal intervals on the tube wall. By specifying locations of zero-flow and a free stream velocity, the strength of the discrete vortices can be determined. Once the vortex strengths are known the velocity at any point in the flow can be calculated. This model was used to

simulate the steady two-dimensional flow in tubes with geometries corresponding to the solitary wave profiles for $c = 3.175, 3.402, 3.629,$ and 3.856 .

Using Bernoulli's equation the pressure at the tube wall was approximated for each of the four tube geometries. This pressure was then compared to the one-dimensional pressure derived in Chapter 4. The results of this chapter suggest that for the tube geometries considered the one-dimensional fluid model approximates closely the pressure predicted using the two-dimensional fluid model. Based on this result, the use of the one-dimensional fluid model appears to provide a good approximation of the two-dimensional flow for the range of tube geometries we have considered and that the solitary waves predicted using either fluid model would be comparable.

Chapter 7

Conclusions and Recommendations

7.1 Conclusions Drawn from the Study

The goal of this study was to investigate solitary waves in fluid-filled elastic tubes by applying a technique that operates directly on the governing field equations to determine the exact solution. Using this technique we were able to consider a number of problems and comment on the accuracy of the commonly used reductive perturbation technique.

In Chapter 2 we presented a method for determining solitary wave solutions for fluid-filled elastic tubes that considers the governing equations exactly without resorting to using approximate methods. This approach permits the determination of the speed and amplitude of the solitary waves by merely determining the roots of a simple algebraic equation. A numerical example was considered for a thin membrane, allowing only radial displacements. The results using the exact approach were compared to the results determined using the reductive perturbation technique and it was shown that the error in the RPT can become as large as 20% for displacements up to 25% of the tube radius.

Chapter 3 illustrated the broader application of our proposed technique through an investigation of a problem in plasma physics, specifically ion-acoustic waves. The purpose of presenting this problem was to illustrate how the analysis could be extended further than in the first example and to compare our approach to results that

include higher order terms in the approximation. Our comparison showed that using our approach resulted in more accurate results with much less effort.

In Chapter 4, we began by deriving the exact shell equations for the tube, including both axial and radial displacements. We then showed that by applying the calculus of variations to our system of equations, conserved quantities could be found that allowed us to determine the first integrals of our governing equations. The first integrals then allowed us to determine the speed, amplitude and shape of the resulting solitary wave ‘exactly’. The results showed that the amplitude calculated using both displacements was an order of magnitude greater than was found for the example in Chapter 2. Based upon a less complex, closed-form example it was shown that the axial strain u' is of the same order as the magnitude of the radial displacement w . Consequently, the practice of neglecting the axial displacement is shown to have inherent limitations.

In Chapter 5, based upon the results of the previous chapter, we examined a procedure for considering the axial displacement approximately to reduce the governing equations to one dependent variable. Exploiting the approximately linear relationship between the \bar{u}' and \bar{w} in the prestressed reference configuration, we suggest that the first integral of the axial governing equation be used to determine a linear function $\bar{u}' = K_c \bar{w}$, which is then substituted into the radial governing equation thus reducing it to a function of w alone. Using this procedure the amplitude and shape are determined for two wave speeds and compared to the exact solution. With proper tuning the error in the approximate technique was found to be about 3%. The effect of neglecting the slope-squared terms was also considered and was found to increase the error in the predicted amplitude to approximately 10%. In either of these cases,

the error is an order of magnitudes less than the error resulting from neglecting the axial displacement.

Finally, in Chapter 6 the potential error resulting from using a one-dimensional fluid model is examined. To accomplish this, a two-dimensional potential flow model, referred to as the modified discrete-vortex method, is developed using axisymmetric-vortex rings placed on the tube boundary to model the pressure for tube geometries corresponding to the shape of solitary waves with wave speeds $c = 3.175, 3.402, 3.629$ and 3.856 . The approximation of the tube wall streamline is used to calculate the pressure along the wall of the tube for each tube geometry. It is shown that the predicted pressures from our existing one-dimensional model compare very well with the two-dimensional flow, with a maximum error of 12% occurring at the maximum tube radius. Based upon this, the solitary waves predicted using both models are expected to be in close agreement.

Therefore, we have presented a method by which an exact solitary wave solution is determined directly from the governing field equations.

7.2 Recommendations for Future Work

There are several areas that should be considered in future work in this area:

- A direct comparison to experimental data should provide even further verification of the results of our proposed direct approach. Therefore, any future studies should include the development of a series of experiments aimed at generating solitary waves in fluid-filled elastic tubes and measuring their speed, amplitude and shape.

- The minimal effort required to find the exact solution using our proposed method could be applied to examining more complex tube models. In this regard, the tube could be considered as thick-walled (so the tube resistance to shear force is included) or anisotropic (so the response of the tube is direction specific) or viscoelastic.
- It would also be useful to further develop the fluid model to account for both the axial and radial velocities. While our results have shown that the one-dimensional fluid model should provide very similar results, it would be beneficial to be able to determine the solitary wave solutions for the different fluid models and to undertake a direct comparison between them.

Bibliography

- Ablowitz, M. J. and Clarkson, P. A. (1999) Solitons and symmetries. *J. Eng. Math.*, **36**, 1–9.
- Acton, E. (1980) A modelling of large eddies in an axisymmetric jet. *J. Fluid Mech.*, **98**, 1–31.
- Adlam, J. H. and Allen, J. E. (1958) The structure of strong collision-free hydro-magnetic waves. *Philos. Mag.*, **3**, 448–454.
- Allen, J. E. (1998) The early history of solitons (solitary waves). *Physica Scripta*, **57**, 436–441.
- Antar, N. and Demiray, H. (1999) Weakly nonlinear waves in a prestressed thin elastic tube containing a viscous fluid. *Int. J. Eng. Sci.*, **37**, 1859–1876.
- Arnold, V. I. (1978) *Mathematical Methods of Classical Mechanics*. Springer–Verlag, New York.
- Batchelor, G. K. (1967) *An Introduction to Fluid Dynamics*. Cambridge University Press.
- Bathe, M. and Kamm, R. D. (1999) A fluid-structure iteration finite element analysis of pulsatile blood flow through a compliant stenotic artery. *ASME J. Biomech. Eng.*, **121**, 361–369.
- Bhatnagar, P. L. (1979) *Nonlinear waves in one-dimensional dispersive systems*. Oxford University Press.

- Bhattacharyya, S. and Roychoudhury, R. (1988) Effect of ion temperature on ion-acoustic solitary waves in a two-ion plasma. *Can. J. Phys.*, **66**, 467–470.
- Budiansky, B. (1968) Notes on nonlinear shell theory. *J. Appl. Mech.*, **June**, 393–401.
- Chatterjee, P. and Roychoudhury, R. (1994) Effect of ion temperature on large-amplitude ion-acoustic solitary waves in relativistic plasma. *Phys. Plasma*, **1**, 2148–2153.
- Chung, J. N. and Troutt, T. R. (1988) Simulation of particle dispersion in an axisymmetric jet. *J. Fluid Mech.*, **186**, 199–222.
- Das, G. C. and Tagare, S. G. (1975) Propagation of ion-acoustic waves in a multi-component plasma. *Plasma Phys.*, **17**, 1025–1032.
- Davidson, R. C. (1972) *Methods in Nonlinear Plasma Theory. Pure and Applied Physics* Academic Press, New York.
- Demiray, H. (1972) On the elasticity of soft biological tissue. *J. Biomech.*, **5**, 309–311.
- Demiray, H. (1996) Solitary waves in prestressed elastic tubes. *Bull. Math. Biol.*, **58**, 939–955.
- Demiray, H. (1997a) The effect of shear stress on solitary waves in arteries. *Bull. Math. Biol.*, **59**(5), 993–1012.
- Demiray, H. (1997b) Nonlinear waves in an inviscid fluid contained in a prestressed viscoelastic tube. *Z. angew. Math. Phys.*, **48**, 325–340.

- Demiray, H. (1997c) Small but finite amplitude waves in a prestressed viscoelastic thin tube filled with an inviscid fluid. *Int. J. Engng. Sci.*, **35**(4), 353–363.
- Demiray, H. (1997d) Solitary waves in initially stressed thin elastic tubes. *Int. J. Non-Linear Mechanics*, **32**(6), 1165–1176.
- Demiray, H. (1998a) On the propagation of solitary waves in prestressed thin elastic tubes. *Z. angew. Math. Phys.*, **49**, 538–557.
- Demiray, H. (1998b) Slowly varying solitary waves in an elastic tube filled with a viscous fluid. *ARI*, **51**, 98–102.
- Demiray, H. (1999a) Dressed solitary waves in fluid-filled elastic tubes. *Int. J. Nonlinear Mech.*, **34**, 185–196.
- Demiray, H. (1999b) Dressed solitary waves in thick-walled elastic tubes. *ARI*, **51**, 228–234.
- Demiray, H. (1999c) A modified reductive perturbation method as applied to non-linear ion-acoustic waves. *J. Phys. Soc. Japan*, **68**(6), 1833–1837.
- Demiray, H. (1999d) Propagation of weakly nonlinear waves in a fluid-filled thin elastic tube. *Trans. CSME*, **23**(2), 253–265.
- Demiray, H. (2000a) A method for higher-order expansion in non-linear in-acoustic waves. *Int. J. Nonlinear Mech.*, **35**, 347–353.
- Demiray, H. (2000b) On the contribution of higher order terms to solitary waves in fluid filled elastic tubes. *ZAMP*, **51**, 75–91.

- Demiray, H. (2001a) Solitary waves in elastic tubes filled with a layered fluid. *Int. J. Eng. Sci.*, **39**, 629–639.
- Demiray, H. (2001b) Solitary waves in fluid-filled tubes: weakly dispersive case. *Int. J. Eng. Sci.*, **39**, 439–451.
- Demiray, H. and Akgün, G. (1997) Wave propagation in a viscous fluid contained in a prestressed viscoelastic thin tube. *Int. J. Engng. Sci.*, **35**(10/11), 1065–1079.
- Demiray, H. and Dost, S. (1998a) Axial and transverse solitary waves in prestressed thin elastic tubes. *ARI*, **50**, 201–210.
- Demiray, H. and Dost, S. (1998b) Solitary waves in a thick walled elastic tube. *Appl. Math. Model.*, **22**, 583–599.
- Epstein, M. and Johnston, C. (1999) Improved solution for solitary waves in arteries. *J. Math. Biol.*, **39**, 1–18.
- Erbay, H. A., Erbay, S., and Dost, S. (1992) Wave propagation in fluid-filled nonlinear viscoelastic tubes. *Acta Mech.*, **95**, 87–102.
- Fung, Y. C. (1997) *Biomechanics: Circulation*. Springer, New York, 2nd edition.
- Guckenheimer, J. and Holmes, P. (1986) *Nonlinear oscillations, dynamical systems and bifurcations of vector fields*. Springer-Verlag, New York.
- Hashizume, Y. (1985) nonlinear pressure waves in a fluid-filled elastic tube. *J. Phys. Soc. Japan*, **54**(9), 3305–3312.

- Hess, J. L. and Smith, A. M. O. (1966) Calculation of potential flow about arbitrary bodies. *Progress in Aeronautical Science*, **8**, 1–138.
- Ikezi, H. (1973) Experiments on ion-acoustic solitary waves. *Phys. Fluids*, **16**, 1668–1675.
- Ishihara, A., Hashizume, N., and Tabibana, M. (1951) Statistical theory of rubber-like elasticity. IV: Two-dimensional stretching. *J. Chem. Phys.*, **19**, 1508–1511.
- Jeffrey, A. and Kawahara, T. (1982) *Asymptotic Methods in Nonlinear Wave Theory*. Pitman Advanced Publishing, Boston.
- Johnston, C. R. and Epstein, M. (2000) On the exact amplitude, speed and shape of ion-acoustic waves. *Phys. Plasmas*, **7**, 906–910.
- Korteweg, D. J. (1878) Ueber die fortpflanzungsgeschwindigkeit des schalles in elastischen rohren. *Annalen der Physik and Chemie*, **5**, 525–542.
- Korteweg, D. J. and de Vries, G. (1895) On the change of form of long waves advancing in a rectangular canal, and on a new type of long stationary waves. *Phil. Mag.*, **39**, 422–443.
- Kuiken, G. D. (1984) Wave propagation in a thin-walled liquid-filled initially stressed tube. *J. Fluid Mech.*, **141**, 289–308.
- Lamb, H. (1945) *Hydrodynamics*. Dover, 6th edition.
- Leonard, A. (1980) Vortex methods for flow simulation. *Journal of Computational Physics*, **37**, 289–335.

- Lovelock, D. and Rund, H. (1975) *Tensors, Differential Forms, and variational Principles*. Pure & Applied Mathematics. John Wiley & Sons, New York.
- Malfliet, W. and Hereman, W. (1996) The tanh method: I. Exact solutions of nonlinear evolution and wave equations. *Physica Scripta*, **54**, 563–568.
- Malfliet, W. and Ndayirinde, I. (1998) Dressed solitary waves in an elastic tube. *Physica D*, **123**, 92–98.
- Malfliet, W. and Wieers, E. (1996) The theory of nonlinear ion-acoustic waves revisited. *J. Plasma Physics*, **56**, 441–450.
- Miles, J. (1980) Solitary waves. *Ann. Rev. Fluid. Mech.*, **12**, 11–43.
- Moodie, T. B. and Haddow, J. B. (1977) Waves in thin-walled elastic tubes containing an incompressible inviscid fluid. *Int. J. Non-linear Mechanics*, **12**, 223–231.
- Morgan, G. W. and Kiely, J. P. (1954) Wave propagation in a viscous liquid contained in a flexible tube. *J. Acous. Soc. America*, **26**(3), 323–328.
- Pedley, T. J. (1980) *The Fluid Mechanics of Large Blood Vessels*. Cambridge Monographs on Mechanics and Applied Mathematics. Cambridge University Press, Cambridge, England.
- Popel, S. I., Vladimirov, V., and Shukla, P. K. (1995) Ion-acoustic solitons in electron-positron-ion plasmas. *Phys. Plasma*, **2**, 716–719.
- Rosenhead, L. (1932) The formation of vortices from a surface discontinuity. *Proc. Roy. Soc. Lond. A*, **134**, 323–347.

- Russell, J. S. (1837) *Report of the Committee on Waves*, Meeting of the British Association for the Advancement of Science, 7th John Murray, London.
- Saffman, P. G. (1992) *Vortex Dynamics*. Cambridge University Press.
- Sarioglu, M. T. (1999) Dressed solitary waves in a fluid filled then elastic tube. *Int. J. Eng. Sci.*, **37**, 527–540.
- Sawatzky, R. P. and Moodie, T. B. (1988) On the propagation of pressure pulses through a viscous fluid contained in a viscoelastic tube. *Q. J. Mech. Appl. Math.*, **41**, 33–50.
- Shimizu, S. (1995) Simulation of axisymmetric jet issuing from a nozzle with collar. *JSME International Journal*, **38**(1), 39–44.
- Skalak, R. (1966) Wave propagation in blood flow In Fung, Y. C., editor, *Biomechanics, Proc. Symp. Appl. Mech. Div. ASME*, pages 20–46, New York. ASME.
- Su, C. H. and Gardner, C. S. (1969) Korteweg-de Vries equation and generalizations. III. Derivation of the Korteweg-de Vries equation and burgers equation. *J. Math. Phys.*, **10**(3), 536–539.
- Sun, S. M. and Shen, M. C. (1995) Existence of solitary pressure pulses in a cylindrical fluid-filled elastic tube. *J. Diff. Equations*, **115**, 224–256.
- Taniuti, T. (1974) Reductive perturbation method and far fields of wave equations. *Prog. Theor. Phys. Supp.*, **55**, 1–35.
- Taniuti, T. and Wei, C. (1968) Reductive perturbation method in nonlinear wave propagation. I. *J. Phys. Soc. Japan*, **24**(4), 941–946.

- Verheest, F. (1988) Ion-acoustic solitons in multi-component plasmas including negative ions at critical densities. *J. Plasma Phys.*, **39**, 71–79.
- Washimi, H. and Taniuti, T. (1966) Propagation of ion-acoustic solitary waves of small amplitude. *Phys. Rev. Letters*, **17**(19), 996–998.
- Whitham, G. B. (1974) *Linear and Nonlinear Waves*. Pure and Applied Mathematics. John Wiley & Sons, New York.
- Womersley, J. R. (1955) Oscillatory motion of a viscous liquid in a thin-walled elastic tube-i: The linear approximation for long waves. *Phil. Mag.*, **46**, 199–219.
- Yomosa, S. (1987) Solitary waves in large blood vessels. *J. Phys. Soc. Japan*, **56**, 506–520.
- Young, T. (1808) Hydraulic investigations subservient to an intended Croonian lecture on the motion of the blood. *Phil. Trans. Roy. Soc.*, **98**, 164–186.
- Young, T. (1809) On the functions of the heart and arteries. *Phil. Trans. Roy. Soc.*, **99**, 1–31.
- Zabusky, N. J. and Kruskal, M. D. (1965) Interaction of solitons in a collisionless plasma and the recurrence of initial states. *Phys. Rev. Letters*, **15**, 240–243.